
Theses and Dissertations

2006

Spatial and temporal evolution of the photoinitiation rate in thick polymer systems

Nicole Lynn Kenning
University of Iowa

Follow this and additional works at: <https://ir.uiowa.edu/etd>

 Part of the [Biochemical and Biomolecular Engineering Commons](#)


Copyright 2006 Nicole Lynn Kenning

This dissertation is available at Iowa Research Online: <https://ir.uiowa.edu/etd/76>

Recommended Citation

Kenning, Nicole Lynn. "Spatial and temporal evolution of the photoinitiation rate in thick polymer systems." PhD (Doctor of Philosophy) thesis, University of Iowa, 2006.
<https://doi.org/10.17077/etd.cilsbax0>

Follow this and additional works at: <https://ir.uiowa.edu/etd>

 Part of the [Biochemical and Biomolecular Engineering Commons](#)

SPATIAL AND TEMPORAL EVOLUTION OF THE PHOTOINITIATION RATE IN
THICK POLYMER SYSTEMS

by

Nicole Lynn Kenning

An Abstract

Of a thesis submitted in partial fulfillment of the
requirements for the Doctor of Philosophy
degree in Chemical and Biochemical Engineering
in the Graduate College of
The University of Iowa

May 2006

Thesis Supervisor: Professor Alec B. Scranton

ABSTRACT

It was once thought either impossible or inefficient to photopolymerize a thickness greater than a thin film because of the optical attenuation of light into the depth of the sample. However, if several considerations are allowed, it is indeed possible. Three particular modifications are essential to enhance light penetration into the depth of the system. An initiator that absorbs in a region of the spectrum where no other components absorb maximizes the incident light intensity for photolysis of the initiator. Concentration and/or molar absorptivity of the initiator lower than typically used in thin films enhance light penetration. Finally, photobleaching initiators exhibit decreased absorbance upon photolysis and thus allow light to penetrate more deeply into the system with time.

A need to model these systems is born out of the desirability to use light to initiate polymerizations of all sorts, including thicker systems. In this project, a set of differential equations describing the spatial and temporal evolution of the light intensity gradient, photoinitiator concentration gradient, and the photoinitiation rate profile are developed for a thick polymer system. The generalized model accounts for the consumption of initiator, evolution of the products of photolysis, diffusion of the initiator and photolysis products, and absorbance by all system components. The purpose of these studies was to characterize further these systems so that results accurately capture the photoinitiation process. Several key objectives have been accomplished, including the effects of illumination with polychromatic incident light, various illumination schemes, and verification of the predicative ability of the model.

The ultimate goal of this project was two fold; first, to build a tool that models photopolymerization systems well, and second, to develop a means for choosing reaction components for photopolymerization applications. To understand and predict how these systems work contributes significantly to the photopolymerization field because it allows the user to predict system behavior accurately and to choose system components appropriate for a particular application.

Abstract Approved: _____

Thesis Supervisor

Title and Department

Date

SPATIAL AND TEMPORAL EVOLUTION OF THE PHOTOINITIATION RATE IN
THICK POLYMER SYSTEMS

by

Nicole Lynn Kenning

A thesis submitted in partial fulfillment of the
requirements for the Doctor of Philosophy
degree in Chemical and Biochemical Engineering
in the Graduate College of
The University of Iowa

May 2006

Thesis Supervisor: Professor Alec B. Scranton

Graduate College
The University of Iowa
Iowa City, Iowa

CERTIFICATE OF APPROVAL

PH.D. THESIS

This is to certify that the Ph.D. thesis of

Nicole Lynn Kenning

has been approved by the Examining Committee for the thesis requirement for the Doctor of Philosophy degree in Chemical and Biochemical Engineering at the May 2006 graduation.

Thesis Committee:

Alec B. Scranton, Thesis Supervisor

Gregory Carmichael

Chris Coretsopoulos

Julie L. P. Jessop

Johna Leddy

To mom, dad, and ian

ACKNOWLEDGMENTS

I would like to express my sincere gratitude to a number of people who have played essential roles during my graduate career.

First and foremost, I would like to thank my advisor, Dr. Alec B. Scranton for his exceptional guidance, and without whom, I would be on a different course in life. I can not imagine a more supportive, encouraging, creative person to have advised me through this process.

I would also like to thank Professors Carmichael, Coretsopoulos, Jessop, and Leddy for serving on my committee and making valuable suggestions. I am also grateful to Dr. Mohamed El-Maazawi for getting me interested and started on this project. His always enthusiastic assistance in orienting me to the project and in the laboratory was vital to my success with this work.

I am also grateful to past and present research group members – Vishal Sipani, DongKwan Kim, Kaveri Jain, Lijing Gou, Peter Ganahl, Beth Ficek, and Leroy Magwood. Each has provided valuable input and ideas, as well as many great conversations. I would particularly like to thank Dane Kriks for conducting various experiments that I have presented in my dissertation. He has assisted me in numerous ways throughout the course of my research and has always performed simulations and experiments with great care and interest.

I would also like to thank the NSF Industry/University Cooperative Research Center and the Department of Chemical and Biochemical Engineering of University of

Iowa for giving me financial support, and Linda Wheatley and Jill Gerot for all of their assistance with any questions of problems that I have had throughout the years.

Finally, I would like to thank my parents, who have always been my greatest supporters and whom I love so dearly. I would not be where I am without them. I would especially like to thank my husband, Ian, for his tremendous support, advice, patience, and love. I dedicate my work to these three people who have been my constants throughout.

TABLE OF CONTENTS

| | |
|---|------|
| LIST OF TABLES | vii |
| LIST OF FIGURES | viii |
| CHAPTER | |
| 1. INTRODUCTION AND BACKGROUND | 1 |
| 1.1. Introduction..... | 1 |
| 1.2. Background and Significance | 2 |
| 1.3. Motivation for this Research..... | 8 |
| 2. OBJECTIVES | 12 |
| 3. SPATIAL AND TEMPORAL EVOLUTION OF THE PHOTOINITIATION RATE FOR THICK POLYMER SYSTEMS WITH MONOCHROMATIC LIGHT | 14 |
| 3.1. Introduction..... | 14 |
| 3.2. Governing Equations | 15 |
| 3.3. Results and discussion | 17 |
| 3.3.1. Modeling the Optimum Concentration of Initiator | 17 |
| 3.3.2. Thick Film..... | 20 |
| 3.3.2.1 Initiator Concentration | 20 |
| 3.3.2.2 Initiator Molar Absorptivity..... | 21 |
| 3.3.2.3 Intensity..... | 21 |
| 3.4. Conclusions..... | 22 |
| 4. SPATIAL AND TEMPORAL EVOLUTION OF THE PHOTOINITIATION RATE FOR THICK POLYMER SYSTEMS ILLUMINATED ON BOTH SIDES | 32 |
| 4.1. Introduction..... | 32 |
| 4.2. Governing Equations | 33 |
| 4.3. Results and discussion | 36 |
| 4.3.1. Effect of Illumination on Both Sides | 36 |
| 4.3.2. Effect of Photoinitiator Concentration and Molar Absorptivity | 41 |
| 4.3.3. Effect of Monomer Absorption..... | 45 |
| 4.3.4. Reflective Boundary Condition | 46 |
| 4.3.5. Perpendicular Illumination..... | 48 |
| 4.4. Conclusions..... | 50 |

| | | |
|--------|---|-----|
| 5. | SPATIAL AND TEMPORAL EVOLUTION OF THE PHOTOINITIATION RATE FOR THICK POLYMER SYSTEMS ILLUMINATED WITH POLYCHROMATIC LIGHT | 72 |
| 5.1. | Introduction..... | 72 |
| 5.2. | Governing Equations | 74 |
| 5.3. | Results and Discussion | 77 |
| 5.3.1. | Initiation Rate Profiles for Simultaneous Illumination by Two Wavelengths | 78 |
| 5.3.2. | Initiation Rate Profiles for Simultaneous Illumination by Multiple Wavelengths..... | 85 |
| 5.3.3. | Initiation Rate Profiles for Polychromatic Illumination | 87 |
| 5.4. | Conclusions..... | 90 |
| 6. | MODELING OF THE PHOTOINITIATION RATE IN REAL THICK POLYMER SYSTEMS ILLUMINATED WITH POLYCHROMATIC LIGHT | 104 |
| 6.1. | Introduction..... | 104 |
| 6.2. | Governing Equations | 105 |
| 6.3. | System Under Investigation: Selection of Photoinitiators and Light Sources | 109 |
| 6.4. | Results and Discussion | 110 |
| 6.4.1. | Initiation with BAPO | 110 |
| 6.4.2. | Initiation with TPO | 111 |
| 6.4.3. | Initiation with BDMB..... | 112 |
| 6.4.4. | Initiation with DMPA | 113 |
| 6.5. | Conclusions..... | 114 |
| 7. | CONCLUSIONS AND RECOMMENDATIONS | 130 |
| 7.1. | Summary of research | 130 |
| 7.2. | Recommendations for Future Work..... | 137 |
| | APPENDIX A..... | 139 |
| | REFERENCES | 145 |

LIST OF TABLES

| | | |
|------------|--|----|
| Table 3.1. | Characteristics of the initiation wave front of BAPO at four concentrations. | 25 |
| Table 3.2. | Properties of the photoinitiation wave front modeled with different concentrations. | 27 |
| Table 3.3. | Properties of the photoinitiation wave front modeled with different initiator absorptivities. | 29 |
| Table 3.4. | Properties of the photoinitiation wave front modeled with different intensities. | 31 |
| Table 4.1. | Maximum rates achieved and the time necessary to reach these rates at the top, middle, and bottom of samples illuminated on one or two sides. | 58 |
| Table 5.1. | Values used for modeling a perfectly bleaching multi-wavelength illumination system including incident wavelength; intensity; initiator quantum yield, and the Napierian molar absorptivities..... | 97 |

LIST OF FIGURES

| | | |
|-------------|---|----|
| Figure 1.1. | Concentration and intensity gradients as function of depth and time. | 10 |
| Figure 1.2. | Effect of initiator absorptivity on initiation rate at 5, 25, and 50 s. | 11 |
| Figure 3.1. | Experimental determination of optimum BAPO initiator concentration from cure time and maximum temperature. | 23 |
| Figure 3.2. | Profiles of the photoinitiation wave front as a function of depth and time for BAPO with initiator concentration 0.2 wt%. | 24 |
| Figure 3.3. | Photoinitiation rate in a 1000 μm thick sample at several illumination times for a system with initiator concentrations (a)1.0, (b)1.5, and (c)2.0 wt%. | 26 |
| Figure 3.4. | Photoinitiation rate of a 1000 μm thick sample at several illumination times for a system with initiator molar absorptivity of (a) 1000, (b) 10000, and (c) 20000 L/mol-cm. | 28 |
| Figure 3.5. | Photoinitiation rate of a 1000 μm thick sample at several illumination times for a system with incident intensities of (a) 50, (b)75, and (c)100 mW/cm^2 | 30 |
| Figure 4.1. | Rate of initiation as a function of sample depth and time for a system with initiator concentration 0.01 mol/L | 52 |
| Figure 4.2. | Initiation rate variation with time at top, middle, and bottom of a system with initiator concentration 0.01 mol/L | 53 |
| Figure 4.3. | Rate of initiation as a function of sample depth and time for a system with initiator concentration 0.01 mol/L. | 54 |
| Figure 4.4. | Initiation rate variation with time at top, middle, and bottom of a system with initiator concentration 0.01 mol/L | 55 |
| Figure 4.5. | Rate of initiation as a function of sample depth and time for a system with initiator concentration 0.01 mol/L | 56 |
| Figure 4.6. | Initiation rate variation with time at top, middle, and bottom of a system with initiator concentration 0.01 mol/L. | 57 |

| | | |
|--------------|--|----|
| Figure 4.7. | Percent variation as a function of time for one ($I(z=0)=100$ mW/cm^2 , $\epsilon=525$ L/mol-cm) and two ($I(z=0)=I(z=1)=50$ mW/cm^2 , $\epsilon_{i1}=\epsilon_{i2}=525$ L/mol-cm) sided illumination schemes with initiator concentration 0.01 mol/L and $z=1$ cm. | 58 |
| Figure 4.8. | Rate of initiation as a function of sample depth and time for a system with initiator concentration 0.02 mol/L | 60 |
| Figure 4.9. | Rate of initiation as a function of sample depth and time for a system with initiator concentration 0.04 mol/L..... | 61 |
| Figure 4.10. | Rate of initiation as a function of sample depth and time for a system with initiator concentration 0.03 mol/L | 62 |
| Figure 4.11. | Rate of initiation as a function of sample depth and time for a system with initiator concentration 0.01 mol/L | 63 |
| Figure 4.12. | Rate of initiation as a function of sample depth and time for a system in which the monomer absorbs. | 64 |
| Figure 4.13. | Rate of initiation as a function of sample depth and time for a system with initiator concentration=0.01 mol/L, $I_{(z=0)}=100$ mW/cm^2 , $z=1$ cm, $\epsilon_i=525$ L/mol-cm . A. One-sided illumination with no reflection. B. One-sided illumination with reflective barrier at $z=1$ cm..... | 65 |
| Figure 4.14. | Rate of initiation as a function of time for a system with initiator concentration=0.01 mol/L..... | 67 |
| Figure 4.15. | Two-dimensional model schematic with incident light on two perpendicular sides..... | 68 |
| Figure 4.16. | Light intensity profile at the instant the light sources are turned on for a two-dimensional sample in which light is incident on two perpendicular sides..... | 69 |
| Figure 4.17. | Concentration profile for a two-dimensional sample in which light is incident on two perpendicular sides. | 70 |
| Figure 4.18. | Initiation rate profile for a two-dimensional sample in which light is incident on two perpendicular sides. | 71 |
| Figure 5.1. | Photoinitiation rate profiles for three different cases: two cases of monochromatic illumination at wavelengths λ_1 and λ_2 , and the case of simultaneous illumination at both wavelengths..... | 93 |

| | | |
|-------------|--|-----|
| Figure 5.2. | Intensity (—) and concentration (---) gradients of monochromatic (●,○) and multi-wavelength (no marker) illumination after 100 seconds of illumination for (a) λ_1 and (b) λ_2 wavelengths..... | 94 |
| Figure 5.3. | Photoinitiation rate profiles after 100 seconds of illumination for three different cases: (a) equal photon flux, (b) λ_1 with twice the photon flux of λ_2 , and (c) λ_1 with three times the photon flux of λ_2 (7.3×10^{-4} Einsteins/m ² •s)..... | 95 |
| Figure 5.4. | Photoinitiation rate profiles after 100 seconds of illumination for three different cases: (a) equal photon flux, (b) λ_1 with twice the photon flux of λ_2 , and (c) λ_1 with three times the photon flux of λ_2 | 96 |
| Figure 5.5. | Photoinitiation rate profiles for simultaneous multi-wavelength illumination for the system described in Table 5.1..... | 98 |
| Figure 5.6. | Photoinitiation rate profiles for simultaneous multi-wavelength illumination for the system described in Table 5.1..... | 100 |
| Figure 5.7. | Molar Absorptivity of TPO (—) and its photolysis products (---), 0.013% in methanol. | 101 |
| Figure 5.8. | Photoinitiation of a system initiated with TPO using a medium pressure 200 W Hg-Xe arc lamp..... | 102 |
| Figure 5.9. | Photoinitiation of a system initiated with TPO using a medium pressure 200 W Hg-Xe arc lamp..... | 103 |
| Figure 6.1. | Chemical structures of photoinitiators modeled. | 118 |
| Figure 6.2. | Napierian molar absorptivity of initiator (—) and its respective photolysis products (---), 0.013% in methanol. | 119 |
| Figure 6.3. | Normalized intensity as a function of wavelength for a medium pressure 200W Hg-Xe arc lamp and an LED lamp with emission centered around 400 nm..... | 121 |
| Figure 6.4. | Photoinitiation of a system initiated with BAPO using a medium pressure 200 W Hg-Xe arc lamp..... | 122 |
| Figure 6.5. | Photoinitiation of a system initiated with BAPO using the LED light source..... | 123 |
| Figure 6.6. | Photoinitiation of a system initiated with TPO using a medium pressure 200 W Hg-Xe arc lamp..... | 124 |
| Figure 6.7. | Photoinitiation of a system initiated with TPO using the LED light source..... | 125 |

| | | |
|--------------|---|-----|
| Figure 6.8. | Photoinitiation of a system initiated with BDMB using a medium pressure 200 W Hg-Xe arc lamp..... | 126 |
| Figure 6.9. | Photoinitiation of a system initiated with BDMB using the LED light source..... | 127 |
| Figure 6.10. | Photoinitiation of a system initiated with DMPA using a medium pressure 200 W Hg-Xe arc lamp..... | 128 |
| Figure 6.11. | Photoinitiation of a system initiated with DMPA using the LED light source..... | 129 |

CHAPTER 1

SPATIAL AND TEMPORAL EVOLUTION OF THE PHOTOINITIATION RATE FOR THICK POLYMER SYSTEMS

1.1. Introduction

Photoinitiation is the process by which visible or ultraviolet radiation produces active centers that initiate a polymerization reaction. In this project, free-radical, as opposed to ionic, photoinitiation is investigated. Generally, it is not efficient for light to directly produce radical monomers, so photoinitiators are added to produce the radical species.¹ Radical production can only occur when photons are absorbed, and the extent to which an initiator absorbs light is termed the absorptivity (ϵ). Not all photons that are absorbed induce radicals, however, and the probability that an absorbed photon will cause photolysis is the quantum yield (ϕ).

Photopolymerization is widely used in many industrial applications from photolithography to dental restorations to a range of electronic applications² and is established as the primary method for web processes and fiber optic coatings where fast reactions and high production rates are critical. Photopolymerization is well suited for these applications because of its many advantages. Light-induced polymerizations are environmentally friendly, since they are generally solvent free, and use less energy than typical thermally initiated polymerizations. In addition, the reaction may also be controlled both spatially and temporally.³⁻⁵ A variety of authoritative reviews of photopolymerization of films and coatings are available.⁶⁻⁸ To date photopolymerizations are primarily restricted to the production of films and coatings on the order of 100 μm , because of attenuation of light into the depth of the

sample. Only recently have photopolymerizations of thick systems become commercially important, including relining of municipal drainage pipes and production of flexographic printing plates. A number of investigators have shown that light may also be used to polymerize thick polymers and composites if the initiating wavelength and initiator systems are carefully selected.^{6,9-11} For example, the initiating wavelength should not be strongly absorbed by the monomer, and the initiator concentration is typically lower than commonly used for photopolymerizations of thin films and coatings. In addition, many photoinitiators exhibit photobleaching in which the absorbance decreases with illumination time when exposed to light of the proper wavelength. This occurs because the absorption characteristics of the photolysis products are different than the original initiator molecule. Two classes of α -cleavable photoinitiators for which photobleaching is particularly pronounced are aryl phosphine oxides in the 365 nm region of the spectrum and substituted titanocenes in the 450 nm region.¹²⁻¹⁴ Photobleaching is particularly important for photopolymerization of thick polymer parts and pigmented coatings. In thick systems, a significant light intensity gradient may exist which leads to an exceptionally complex photoinitiation profile. Therefore, the effects of a host of variables on the resulting photoinitiation rate are needed in order to effectively design reaction systems. This project models the behavior of photoinitiation in thick polymer systems to obtain a fundamental understanding of the mechanisms involved.

1.2 Background and Significance

A number of investigators have recently reported theoretical descriptions of photoinitiation of thick systems illuminated with monochromatic light and have found that the rate of photobleaching is non-uniform and resembles a wave front.¹⁵⁻¹⁷ For example, Terrones and Pearlstein¹⁵ recently presented a complete and accurate unsteady state model describing perfectly photobleaching systems (those in which only the initiator absorbs the wavelength of interest and then becomes non-absorbing upon photolysis) illuminated with monochromatic light. This model considered the initiator consumption and optical attenuation for free-radical photopolymerizations, but neglected diffusion of the initiator through the sample, as well as absorption of light by any species other than the initiator. These authors demonstrated that for these assumptions, as well as the condition of the initiator becoming completely non-absorbing upon photolysis, the resulting differential equations could be solved analytically. Terrones and Pearlstein showed that for high initiator absorptivity, the local initiation rate becomes non-uniform, and assumes the form of a wave front that moves through the sample depth. Although the model was effective within its assumptions, the important conditions of light absorbance by photolysis products, monomer, and/or additives, and diffusion of the initiator, which are likely important occurrences in photocured systems, were not considered.

Similarly, in a report by Ivanov and Decker,¹⁶ perfect photobleaching and monochromatic incident light were assumed, and diffusion of the initiator was neglected. Again, because of these assumptions, the coupled differential equations were able to be solved analytically. These authors linked the initiation kinetics to the

polymerization kinetics by assuming steady-state bimolecular radical termination. Ivanov and Decker determined that the amount of light that is able to pass through a thick sample is dependent on the initiator absorptivity and concentration. They also showed that increasing the thickness of a sample causes the concentration profile to change from exponential decay to linear decay. The authors discovered that, because the initiation proceeds through the sample in a wave-like manner, the portion of the sample that is furthest from the incident light will not polymerize at the same time as the layers near the surface of the sample. These surface layers must first photobleach before light can reach the deeper layers.

In these analyses of the monochromatic illumination of perfectly bleaching systems the governing equations could be written in dimensionless form to yield generalized correlations. For example, Ivanov and Decker expressed the dimensionless depth as the distance from the illuminated surface multiplied by the optical density (which is equal to the molar absorptivity times the initiator concentration and has dimensions of inverse length), and the dimensionless time as the product of the initiator quantum yield, initiator molar absorptivity, incident light intensity, and the time of illumination.⁴ Based on these definitions, the governing differential equations were written in dimensionless form, and generalized correlations were provided for the normalized light intensity (I/I_0) or normalized initiator concentration (C_i/C_{i0}) as functions of dimensionless distance and dimensionless time. Note that the characteristic distance (inverse optical density) and the characteristic time (product of the initiator quantum yield, initiator molar absorptivity and incident light intensity) do not have natural, meaningful physical

values, and therefore the dimensionless variables do not have specific meaningful values (for example, a dimensionless distance or time of unity is not especially significant) and are even unbounded. Indeed, Ivanov and Decker included charts with values of dimensionless distance ranging from 0 to 20 and dimensionless time from 0 to 14, and for many physical systems these values are too low. More importantly, the dimensionless analysis is only valid for monochromatic illumination (a single intensity and single molar absorptivity) of a perfectly bleaching system with no absorption by other components (and no diffusion). For polychromatic illumination, a unique intensity and molar absorptivity are required for each incident wavelength, and the governing equations do not reduce to a dimensionless form since no single characteristic distance or characteristic time emerge.

The current research project continues the work of Miller *et al.* who studied the effects of initiator concentration, initiator absorptivity, initiator quantum yield, photolysis product absorptivity, monomer absorptivity, and initiator diffusion on the photoinitiation rate profile using monochromatic illumination.¹⁷ The authors built upon the work done by Terrones and Pearlstein¹⁶ and Ivanov and Decker¹⁶ by generalizing the governing differential equations to include the effects of photolysis product absorptivity, monomer absorptivity, and diffusion of the initiator. Because of the complexity of the resulting equations, the model was solved numerically using the method of finite differences. Figure 1.1 shows plots of the concentration and initiation gradients as functions of time and depth.

The initiation rate is proportional to the product of concentration and intensity, and as expected, this model showed that the photoinitiation rate propagates through

the depth of a sample as a wave front. Miller *et al.* showed that initiator concentration and initiator absorptivity must be measured separately due to the continuous change of optical density in the sample. Also, the authors demonstrated that absorption by any species other than the initiator leads to an initiation wave front that decreases rapidly and disappears completely without having propagated into the sample, as shown in Figure 1.2. These authors did not, however, take into account illumination by more than one incident wavelength, which is important to consider since single wavelength illumination is not an industry standard; indeed, it is rarely used. More complex illumination schemes also were not studied.

Goodner and Bowman developed a model to incorporate the effects of heat and mass transfer on free radical photopolymerizations.¹⁸ The model included the effects of spatial variation of light intensity, primary radical termination, and both diffusion and reaction controlled kinetics along with heat generation, heat transfer, and mass transfer to predict conversion, rate, and temperature. Here, Goodner and Bowman assumed monochromatic light and a non-photobleaching initiator. These authors found that the maximum polymerization rate would be four times higher at the surface of the sample than in the deeper layers and that the time to reach polymerization in the deeper layers would be delayed by approximately the same ratio. They also showed the importance of including the effects of heat transfer and light intensity. The authors found that when these effects were not considered, the cure time necessary to reach a specified conversion was much below that needed when the effects were taken into account, leading to a sample that would not meet desired specifications if the former model was used to predict cure time. Goodner and

Bowman demonstrated that, in thick samples, retention of heat could allow conversion in the sample of almost 100%. This paper includes a very comprehensive model of photopolymerization that is important to the current research of polychromatic initiation.

In other reports by Terrones and Pearlstein, the effects of kinetics and chain length distributions on monomer conversion are studied in detail.¹⁹⁻²⁰ When studying kinetics, the authors use a steady-state approximation for radical concentrations and again neglected diffusion and convection.¹⁹ Here, the authors find that the non-uniform initiation rate discussed previously can lead to non-uniform conversion profiles. They also found that to increase conversion and decrease thermal nonuniformity, the ratio of initiator concentration to light intensity needed to be increased. This resulted in the negative outcomes of increased use of photoinitiator and increased processing time. The authors also concluded that monomer concentration has no effect on fractional conversion of monomer. In a subsequent paper, Terrones and Pearlstein determined that the spatial nonuniformity of chain length distributions is much greater than the nonuniformity of monomer conversion.²⁰ Chain length distributions are important in determining material properties. While the concentration of monomer was found to have no effect on monomer conversion in the former paper, this report found the chain length distribution is dependent on monomer concentration.

In addition to modeling general systems, several researchers modeled specific polymerization schemes. For example, Cramer *et al.* studied the mechanism of thiol-ene photopolymerization.²¹ In their research, a model of thiol-ene polymerization was

created using a step-growth scheme, and this model was used to interpret results obtained experimentally. In another publication, Cramer *et al.* expand upon the previously mentioned model to include a number of vinyl functional groups.²² Here the model developed successfully predicts the kinetics and rate limiting steps of various functional groups. Finally, in a report by Lovestead *et al.*, the kinetics of multivinyl free radical polymerizations were modeled.²³ The systems studied are complex, and so is the resulting model. This model was developed to determine the polymerization kinetics for a range of cure specifications. Although the modeling effort discussed in this proposal is focused on the initiation step of the photopolymerization reaction, there is clearly a desire to have model results match experimental results. These reports show that it is possible to model accurately very specific systems of interest, though a more general model, of the type this project is trying to obtain, would be of use to many.

1.3. Motivation for this research

The review of current and active research presented above illustrates the interest and need for a more complete, fundamental model of photoinitiation in thick systems. While a number of recent researchers have noted the importance of this topic, and have presented models which advance the field, all research to date has been based on monochromatic illumination (indicated by a single initiator molar absorptivity) and there has been very little investigation of absorption by the photolysis products. Indeed, monochromatic illumination is a drastic simplification of photoinitiation since the overwhelming majority of light sources are polychromatic,

and a monochromatic model does not accurately describe initiation behavior. In this thesis, the fundamental description of photoinitiation in thick systems is expanded to include illumination with polychromatic light. Any combination of initiator/monomer/light source can be readily investigated with this advanced model as long as the absorption and emission data are known.

The format of this thesis is to build in intricacy from the simplest modeling cases of monochromatic light to the most complex cases of real systems. This thesis begins by stating the objectives of the research in Chapter 2. Monochromatic illumination of selected systems is discussed in Chapter 3, and a more complex design variable (two light sources) is presented in Chapter 4. The coupled effects that occur with polychromatic illumination are studied in detail in Chapter 5, and Chapter 6 uses the polychromatic model to investigate real systems. Finally, Chapter 7 will give conclusions of this research and recommendations for future directions.

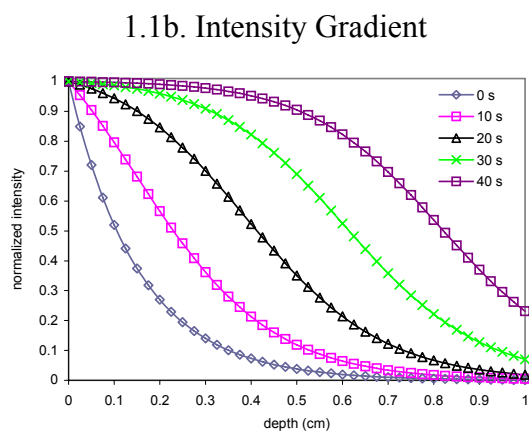
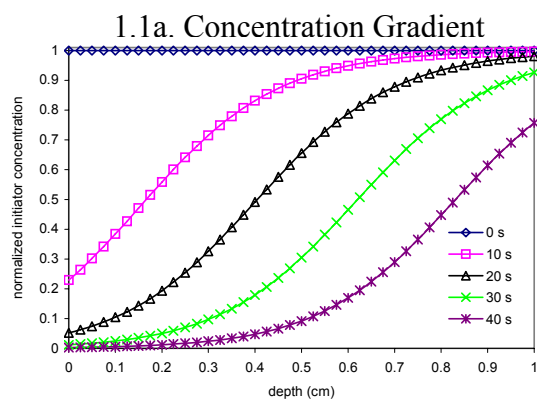
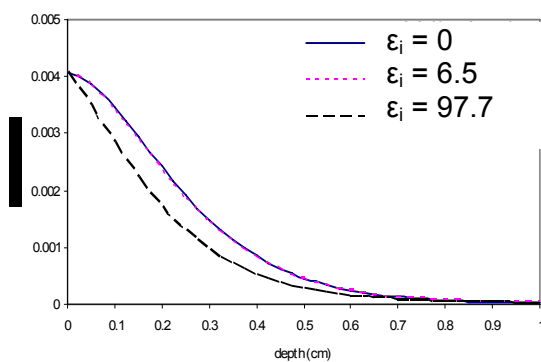
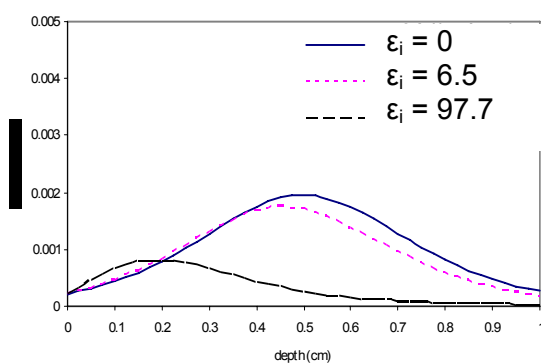


Figure 1.1. Concentration and intensity gradients as function of depth and time.

1.2a. 5 Seconds of Illumination



1.2b. 25 Seconds of Illumination



1.2c. 50 Seconds of Illumination

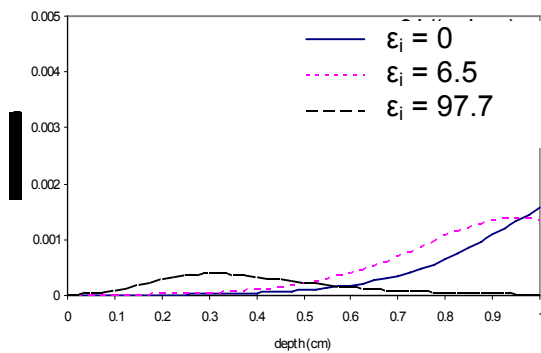


Figure 1.2. Effect of initiator absorptivity on initiation rate at 5, 25, and 50 s. Absorptivity units (ϵ_i) are L/(mol-cm).

CHAPTER 2 OBJECTIVES

The previous chapter illustrates that there is a compelling motivation and need for the development of a complete, fundamental model of photoinitiation in thick systems. In a number of recent publications, several investigators have presented models for the simplest case of monochromatic illumination with perfectly bleaching photoinitiators. Since the overwhelming majority of photopolymerization is done with polychromatic light sources, and photoinitiators rarely exhibit complete photobleaching, a monochromatic model of this sort does not accurately describe the photoinitiation behavior of real systems. This research addresses these shortcomings and adds significantly to the fundamental understanding of initiation behavior in these complex systems.

The broad objective of this research is to develop a set of differential equations that accurately describe the spatial and temporal evolution of the light intensity gradient, photoinitiator concentration gradient, and ultimately the photoinitiation rate profile in thick polymer systems. The ultimate goal of this project is to build a model that adds to the fundamental understanding of initiation behavior, and thus is useful in choosing photopolymerization system components. This broad objective is approached by completing the following specific goals:

1. To advance state-of-the-art modeling of photoinitiation in thick systems by accounting for illumination with polychromatic light; specifically, to account for the unique light intensity and molar absorptivity corresponding to each wavelength active in initiation;

2. To illustrate the effects of polychromatic illumination through simulations that include varying degrees of photobleaching and the following important conditions: illumination with two incident wavelengths (to clarify the coupled nature of the governing equations) with varying relative and absolute intensities, illumination with five incident wavelengths at two initiator concentrations, and continuous spectrum illumination;
3. To compare and contrast the photoinitiation of commercial initiator/light source/monomer systems using light source emission spectra, as well as initiator and monomer absorbance spectra obtained in the lab;
4. To investigate the nature of the photoinitiation rate profile for a variety of illumination configurations.

CHAPTER 3 SPATIAL AND TEMPORAL EVOLUTION OF THE PHOTOINITIATION RATE FOR THICK POLYMER SYSTEMS WITH MONOCHROMATIC LIGHT

3.1. Introduction

As illustrated in the previous chapter, the primary focus of this thesis is a detailed, fundamental description of photoinitiation in thick systems using polychromatic light, and chapters 5 and 6 are dedicated to this topic. As a prelude to these complex systems, in this chapter the relatively simple case of monochromatic illumination is considered, and simulation results are compared with experimental data. The model for this simplest case of monochromatic illumination of perfectly bleaching systems is equivalent to those reported by Miller, *et al.*¹⁷ The models describing more complex systems described in chapters 4-6 (two-sided illumination, and polychromatic illumination) have not been previously reported in the literature.

To effectively and efficiently photoinitiate a thick system, the concentration of initiator must be optimized to allow both sufficient initiation rates and deep penetration of light. This optimum may be determined experimentally, but in order to determine this concentration from the model, either a minimum initiation rate for sufficient production of radicals or a maximum initiation time for efficient production must be set. To demonstrate this, a model was created to match the experimental determination of optimum concentration.

The process of photopolymerization is most widely used in curing films and coatings (usually $\leq 1000 \mu\text{m}$). To demonstrate that the model can be used for these situations, the effect of initiator concentration, light intensity, and initiator molar

absorptivity on the photoinitiation rate is examined in a 0.1 cm thick system. The resulting photoinitiation rate profiles are compared by maximum rate, width at half height, rate of wave front propagation, and time for the peak rate to move through the sample depth. For thinner systems, higher initiator concentrations can be used than in thick samples, but the general trends for thick films are the same as those for a thick sample. For example, as the intensity is increased, the initiation rate increases, as well as the rate of wave propagation through the sample depth. This chapter illustrates these general trends.

3.2. Governing Equations

To investigate the optimum concentration of initiator for thick systems, the following model system was selected: a thick polymerization system (typically 1 cm thick) of rectangular cross-section subject to uniform monochromatic illumination normal to the top surface. To investigate photoinitiation in thin systems, the following model system was selected: a thin polymerization system (typically 1 mm thick) of rectangular cross-section subject to uniform monochromatic illumination normal to the top surface. The set of differential equations that describe the evolution of the light intensity gradient, the initiator concentration gradient, and the local photoinitiation rate for these conditions are shown below, and were solved by method of finite differences for these studies.

$$\frac{\partial C_i(z,t)}{\partial t} = -\varepsilon_i \phi_i \left(\frac{I(z,t)}{N_A h\nu} \right) C_i(z,t) + D_i \frac{\partial^2 C_i(z,t)}{\partial z^2} \quad (1)$$

$$\frac{\partial C_p(z,t)}{\partial t} = \varepsilon_i \phi_i \left(\frac{I(z,t)}{N_A h \nu} \right) C_i(z,t) + D_p \frac{\partial^2 C_p(z,t)}{\partial z^2} \quad (2)$$

$$\frac{\partial I(z,t)}{\partial z} = -(\varepsilon_i C_i(z,t) + A_m + \varepsilon_p C_p(z,t)) I(z,t) \quad (3)$$

Here, $C_i(z,t)$ represents the initiator molar concentration at depth z and time t ; $C_p(z,t)$ represents the photolysis product molar concentration at depth z and time t ; $I(z,t)$ represents the incident light intensity at depth z and time t , with dimensions of energy/(area·time); ε_i is the Napierian initiator molar absorptivity with dimensions of volume/(length·mole); ε_p is the Napierian photolysis product molar absorptivity, with dimensions of volume/(length·mole) and accounts for the photon absorption by all fragmentation species; N_A is Avogadro's number; h is Planck's constant; ν is the frequency of light, with dimensions of inverse time; ϕ_i is the quantum yield of the initiator, defined as the fraction of absorbed photons that lead to fragmentation of the initiator; D_i is the diffusion coefficient for the initiator with dimensions of length²/time; D_p is the diffusion coefficient for the photolysis products; and A_m is the absorption coefficient of the monomer and the polymer repeat unit. Note that in this study the Napierian molar absorptivity was adopted because it is most natural for the differential version of the absorption equation (equation 3). In the literature the decadic (base 10) molar absorptivity is commonly reported and should be converted to the Napierian value before using the model.

The following boundary and initial conditions apply:

$$C_i(z,0) = C_o \quad (4)$$

$$C_p(z,0) = 0 \quad (5)$$

$$\frac{\partial C_{i,p}(z,t)}{\partial z} = 0 \text{ at } z = 0 \text{ and } z = z_{\max} \text{ (the thickness of the sample)} \quad (6)$$

$$I(0,t) = I_o \quad (7)$$

Here, Equation 4 indicates that the initiator concentration is initially uniform through the depth of the sample. Equation 5 accounts for the fact that photolysis product concentration is initially equal to zero throughout the sample, while Equation 6 represents the no-flux boundary condition at the ends of the sample for both the initiator and the fragments; this boundary condition is necessary due to the diffusional terms in the governing equations. Equation 7 indicates that the light intensity at the exposed surface is equal to the respective incident light intensity at all times.

Finally, Equation 8 defines the instantaneous local rate of production of free radicals, $R_i(z,t)$, if two active centers are produced upon fragmentation of the initiator molecule.

$$R_i(z,t) = 2C_i(z,t)I(z,t)\phi_i\varepsilon_i \quad (8)$$

3.3. Results and Discussion

3.3.1. Modeling the Optimum Concentration of Initiator

The optimum concentration of bisacylphosphineoxide (BAPO) initiator was determined experimentally to be 0.2 wt% for a 0.9 cm sample.²⁴ A temperature probe was placed at the bottom of a 0.9 cm sample, and a polymerization reaction was performed. The experiment was conducted under adiabatic conditions, and because

polymerization is exothermic, the temperature change could be monitored on the dark side of the sample (opposite the illumination source). The temperature increased as the polymerization progressed, and the reaction was finished when the temperature remained constant. The concentration of 0.2 wt% was determined to be the optimal because it is the concentration at which the cure time is the shortest, as shown in Figure 3.1. The concentration that exhibited the shortest cure time also attained the highest final temperature. Because the experiments were carried out under adiabatic conditions, a higher temperature denotes that more heat was released during polymerization, implying that more double bonds were reacted. This suggests that not only is the cure time minimum at the optimum concentration, but also that the degree of conversion is maximum.

To match the conditions for the experimental studies, the model used a monochromatic illumination wavelength of 366 nm, light intensity of 65 mW/cm², BAPO concentrations of 0.1, 0.2, 0.3 and 0.4 wt%, and the initiator molar absorptivity was estimated to be approximately 20,000 L/mol·cm. The simulation results provided profiles of the photoinitiation rate as a function of depth beneath the illuminated surface for different times, as shown in Figure 3.2 for the case of 0.2 wt% BAPO. Figure 3.2 illustrates that the photoinitiation rate is not uniform, but rather resembles a photoinitiation wave that begins on the illuminated surface of the sample and moves through the sample as a photoinitiation front. The simulation results for the other concentrations all revealed similar frontal propagation.

The characteristics of the polymerization front can be completely described using the following parameters: 1) the maximum, or peak, initiation rate (which

corresponds to the height of the reaction peak); 2) the width of the peak (at half height); 3) and the rate at which the front moves through the sample. A summary of the simulation results for all BAPO concentrations is shown in Table 3.1. The modeling results show a dependence of the propagation rate of the initiation wave front on the photoinitiator concentration. As the concentration of BAPO increases, the maximum rate of initiation (taken at the peak of the initiation rate curve) also increases. On the other hand, the average rate at which the front moves through the sample shows the opposite trend and decreases as the concentration of the photoinitiator increases. The interplay of these two competing effects is what leads to the occurrence of an optimum concentration. The maximum initiation rate must be high enough to produce enough active centers to complete the polymerization in a reasonable time; therefore, at low concentrations, the time to polymerize the thick sample decreases with increasing initiator concentration. However, if the initiator concentration is too high, the light is not able to penetrate into the depth efficiently, and the initiation wave does not move through the sample at a high enough propagation rate to complete initiation throughout the depth in a reasonable time. For example, if it is desired to complete the cure of the thick sample in less than 3 minutes, the simulation results indicate that the samples containing 0.3 and 0.4 wt.% initiator are not appropriate choices. The optimum concentration predicted by the model for cure in less than 3 minutes is 0.2 wt%. This is in good agreement with that established experimentally, with the slight difference in the predicted cure time likely arising from the fact that monochromatic light and a perfectly bleaching photoinitiator were used in the model. Table 3.1 also illustrates that the breadth of the

photoinitiation front decreases as the initiator concentration is increased, making the initiation profile less uniform across the depth of the sample.

3.3.2 Thick Films

3.3.2.1 Initiator Concentration

Because the sample thickness is decreased in these simulations, the initiator concentration is able to be increased to values typical of thicker films, here, between 1-2 wt%. Figure 3.3 shows the photoinitiation rate at several illumination times. Similar to thick system initiation,¹⁷ the initiation wave of the system with the lowest concentration moves through the sample the most rapidly, while the system with the highest concentration has the highest maximum initiation rate. These systems waves were characterized by 1) the maximum, or peak, initiation rate (which corresponds to the height of the reaction peak); 2) the width of the peak at half height; 3) the rate at which the front moves through the sample; and 4) the time for the initiation wave front to pass through the sample depth. These results are shown in Table 3.2. As concentration is increased, the maximum photoinitiation rate is increased, while the breadth of the wave front is decreased. The rate at which the wave front moves through the sample, and the total time for the wave to pass through also increases with increasing concentration. Indeed this again indicates that there is an optimum photoinitiator concentration that produces a sufficient photoinitiation rate, but that also efficiently initiates throughout the depth of the sample.

3.3.2.2 Initiator Molar Absorptivity

Three initiator molar absorptivities were chosen to model initiation with a low, medium, and high initiator molar absorptivity. Here, 1000, 10000, and 20000 L/mol-cm absorptivities were simulated, and the resulting photoinitiation rate profiles are shown in Figure 3.4. As shown in the similar thick polymer simulations,¹⁷ a low molar absorptivity leads to the initiation wave penetrating deep into the sample depth, while a high absorptivity leads to a very high maximum initiation rate. This illustrates the benefit of using polychromatic illumination, where these effects can be combined by having multiple incident wavelengths, each corresponding to different (high and low) values of absorptivity. Table 3.3 shows the analysis of the wave fronts. As the initiator molar absorptivity is increased, the maximum rate increases and the peak breadth decreases. Interestingly, the dramatic change in molar absorptivity does not lead to a large change in the time it takes for the peak of the wave front to pass through the depth of the sample.

3.3.2.3 Intensity

The effect of incident intensity on the resulting photoinitiation rate was also modeled using incident intensities of 50, 75, and 100 mW/cm². Figure 3.5 shows the resulting photoinitiation rates at several illumination times for these three cases. Table 3.4 shows the analysis of these initiation wave profiles. This table illustrates that increasing intensity leads to both increased maximum rates of initiation and decreased peak breadth. However, increasing intensity has the benefit of higher rates of wave propagation through the sample depth that leads to the case corresponding to the

highest intensity having the initiation wave that passes through the sample in the least amount of time. Each illumination source will have a specific intensity, so the choice of intensity for a system is directly coupled to choice of illumination source. Higher intensities can mean higher energy costs, so lamp intensity is another design variable that must be optimized.

3.4. Conclusions

A fundamental understanding of the effects of a host of variables is needed to ensure proper selection of reaction components and design of the reaction system. This chapter illustrates that there is an optimum concentration of initiator that results in high initiation rates and efficient progression of the initiation wave front throughout the sample. The model reveals that as in thicker systems, for thick films with complete photobleaching, increasing the initiator concentration leads to an increase in both the photoinitiation rate and the time required to cure throughout the depth of the sample. Also, an initiator with a high molar absorptivity leads to a narrowing of the initiation rate profile which moves as a sharp front from the illumination surface toward the center of the sample. Finally, increasing the intensity has a positive effect on both the maximum rate of photoinitiation, as well as the rate at which the wave front moves through the sample, however, other considerations such as energy costs may prevent this from being a practical implementation.

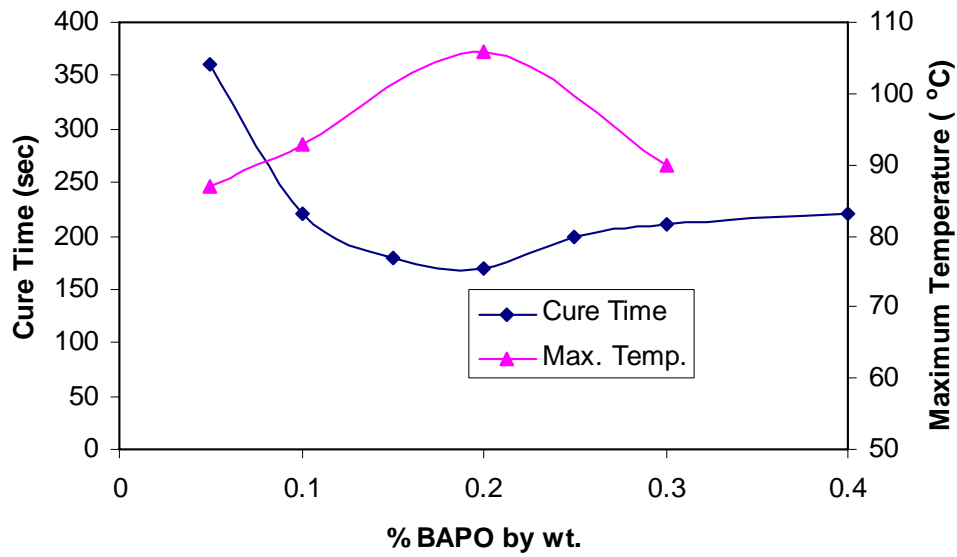


Figure 3.1. Experimental determination of optimum BAPO initiator concentration from cure time and maximum temperature.

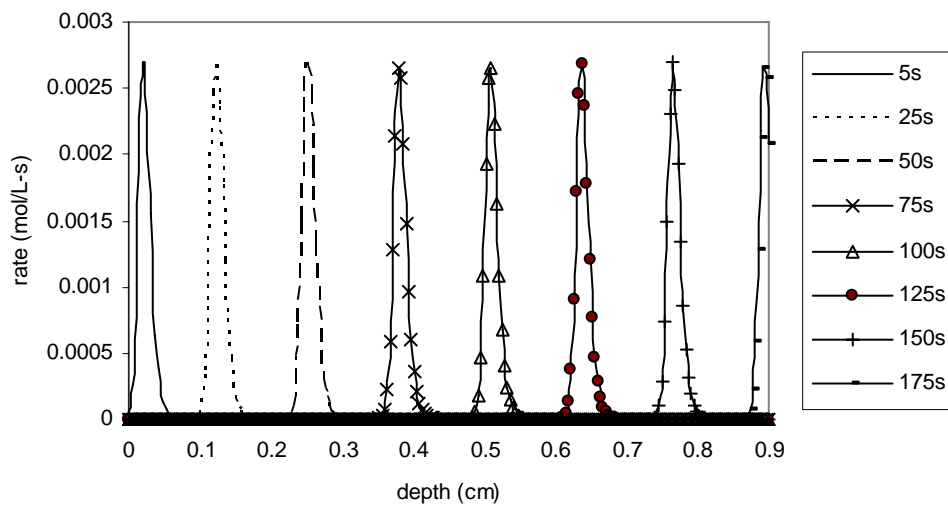


Figure 3.2. Profiles of the photoinitiation wave front as a function of depth and time for BAPO with initiator concentration 0.2 wt%.

$$I_0=65 \text{ mW/cm}^2, \lambda=366 \text{ nm}, z=0.9 \text{ cm}, \epsilon_i=20000 \text{ L/mol cm}$$

Table 3.1: Characteristics of the initiation wave front of BAPO at four concentrations.
 $I=0.65 \text{ mW/mm}^2$, $\lambda=366 \text{ nm}$, $z=0.9 \text{ cm}$, $\epsilon=20000 \text{ L/mol cm}$

| Concentration, (wt%) | Max Rate of Initiation, (mol/L.s) | Breadth of Wave Front, WHM, (cm) | Average Rate of Wave Front Propagation, (cm/s) | Time for Wave to Propagate Through Sample Depth, (s) |
|----------------------|-----------------------------------|----------------------------------|--|--|
| 0.1 | 0.00135 | 0.045 | 0.0100 | 89 |
| 0.2 | 0.00270 | 0.021 | 0.0051 | 176 |
| 0.3 | 0.00380 | 0.015 | 0.0027 | 330 |
| 0.4 | 0.00500 | 0.008 | 0.0014 | 648 |

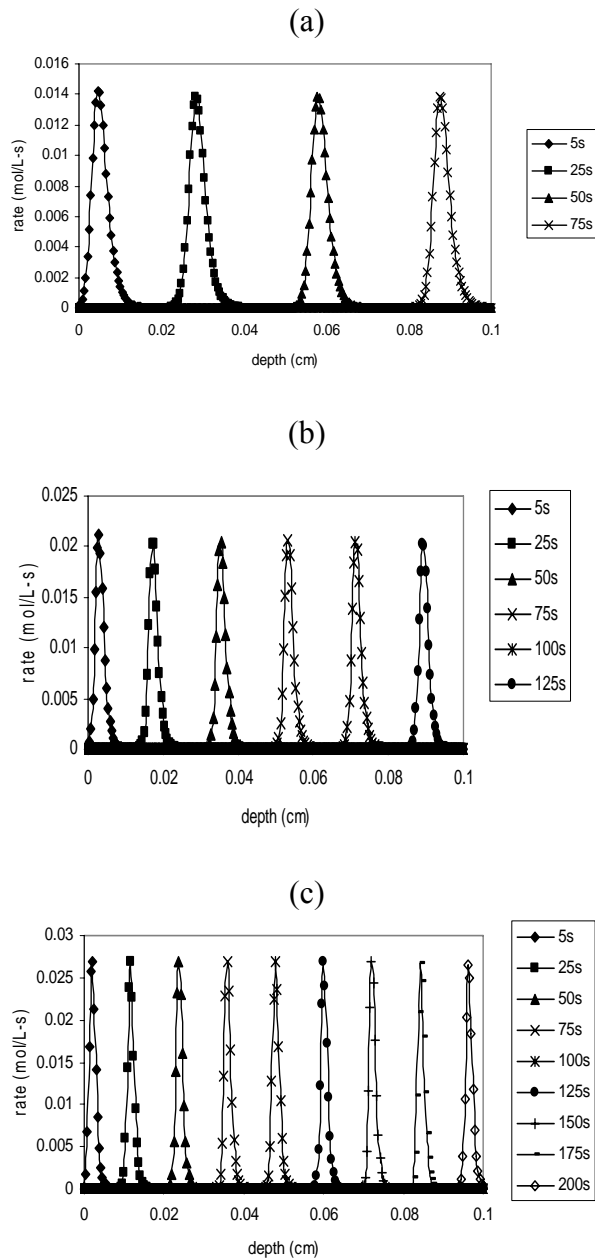


Figure 3.3. Photoinitiation rate in a 1000 μm thick sample at several illumination times for a system with initiator concentrations (a)1.0, (b)1.5, and (c)2.0 wt%.

$I_0=65 \text{ mW/cm}^2$, $\lambda=366 \text{ nm}$, $\epsilon_i=20,000 \text{ L/mol-cm}$.

Table 3.2. Properties of the photoinitiation wave front modeled with different concentrations. $I=0.65 \text{ mW/mm}^2$, $\lambda=366 \text{ nm}$, $z=0.9 \text{ cm}$, $\epsilon=20000 \text{ L/mol cm}$

| Concentration, (wt%) | Max Rate of Initiation, (mol/L-s) | Breadth of Wave Front, (mm) | Rate of Wave Front Propagation, (mm/s) | Time for Wave to Propagate Through 1mm Depth, (s) |
|-------------------------|---|-----------------------------------|---|---|
| 1 | 0.014 | 41.2 | 11.8 | 85 |
| 1.5 | 0.020 | 29.2 | 7.14 | 140 |
| 2 | 0.027 | 20.9 | 4.83 | 207 |

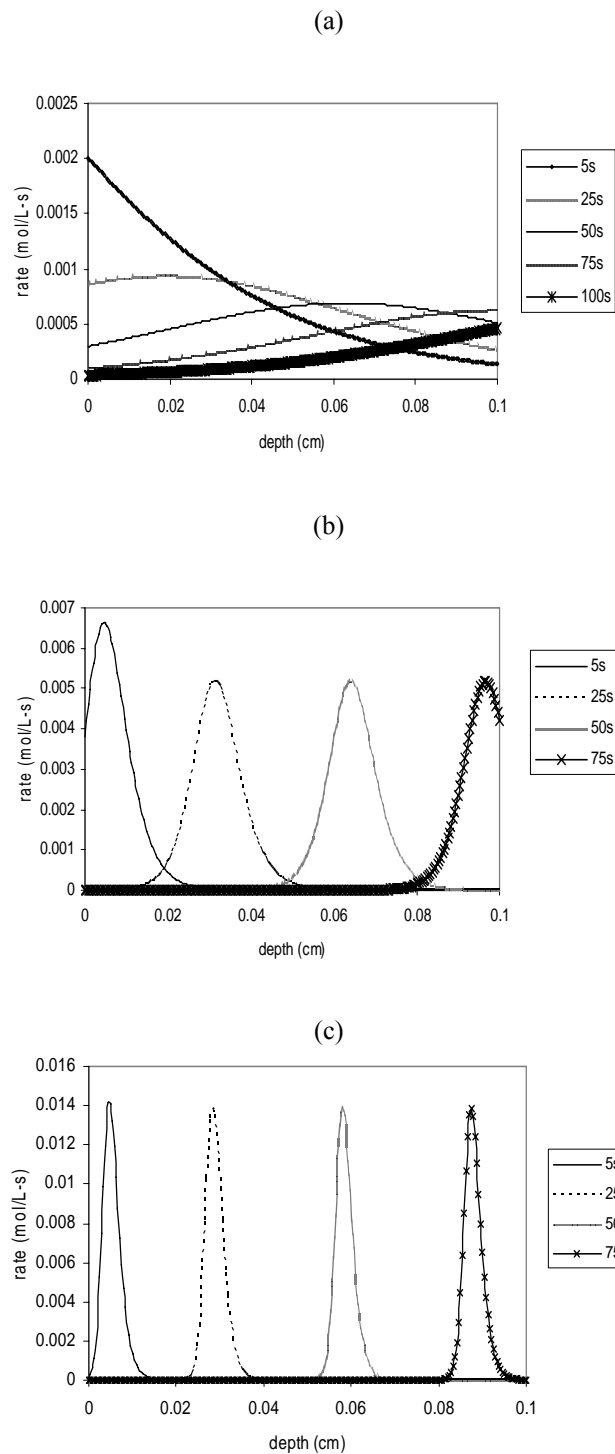


Figure 3.4. Photoinitiation rate of a 1000 μm thick sample at several illumination times for a system with initiator molar absorptivity of (a) 1000, (b) 10000, and (c) 20000 L/mol-cm.

$$I_0=65 \text{ mW/cm}^2, \lambda=366 \text{ nm}, C_{i0}=1.0 \text{ wt}\%$$

Table 3.3. Properties of the photoinitiation wave front modeled with different initiator absorptivities. $I=0.65 \text{ mW/mm}^2$, $\lambda=366 \text{ nm}$, $z=0.9 \text{ cm}$

| Molar Absorptivity, (L/mol-cm) | Max Rate of Initiation, (mol/L-s) | Breadth of Wave Front, (mm) | Rate of Wave Front Propagation, (mm/s) | Time for Wave to Propagate Through 1mm Depth, (s) |
|--------------------------------|-----------------------------------|-----------------------------|--|---|
| 1000 | 0.00069 | >1000 | 14.3 | 70 |
| 10000 | 0.00520 | 125 | 12.8 | 78 |
| 20000 | 0.01400 | 46 | 11.6 | 86 |

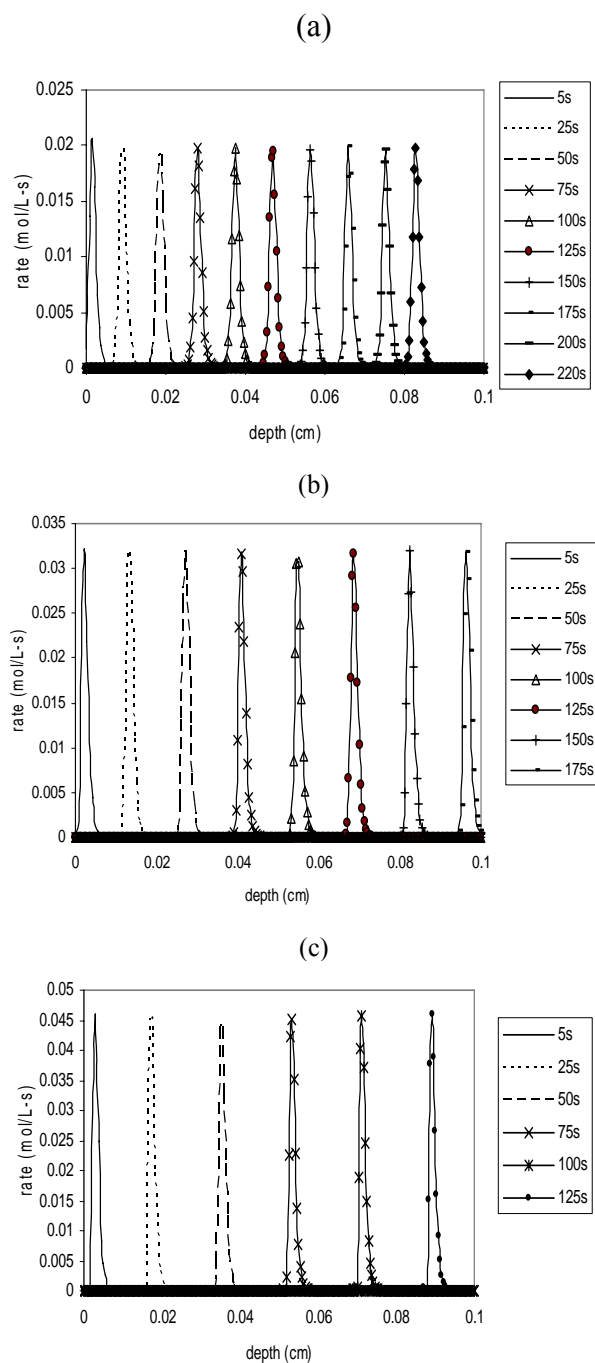


Figure 3.5. Photoinitiation rate of a 1000 μm thick sample at several illumination times for a system with incident intensities of (a) 50, (b) 75, and (c) 100 mW/cm^2 .

$\lambda=366 \text{ nm}$, $C_{i0}=1.0 \text{ wt}\%$, and $\varepsilon_i=20,000 \text{ L}/\text{mol}\cdot\text{cm}$.

Table 3.4. Properties of the photoinitiation wave front modeled with different intensities.

| Intensity, (mW/cm ²) | Max Rate of Initiation, (mol/L-s) | Breadth of Wave Front, (mm) | Rate of Wave Front Propagation, (mm/s) | Time for Wave to Propagate Through 1 mm Depth, (s) |
|-------------------------------------|---|-----------------------------------|---|---|
| 50 | 0.020 | 25 | 3.73 | 268 |
| 75 | 0.032 | 21 | 5.50 | 182 |
| 100 | 0.046 | 17 | 7.14 | 140 |

CHAPTER 4

SPATIAL AND TEMPORAL EVOLUTION OF THE PHOTOINITIATION RATE FOR THICK POLYMER SYSTEMS ILLUMINATED ON BOTH SIDES

4.1. Introduction

In this chapter, the description of a system illuminated with monochromatic light is expanded to account for a second illumination source. Due to the variation in light intensity with depth in the sample, the placement of the lamp is important, and the photoinitiation profile may be markedly affected by addition of a second light source. For example, in the case of a thin polymerization system in which the light intensity is practically uniform throughout the film, a second light source directed on the bottom of the sample will simply have an additive effect on the intensity. In contrast, for a thick polymerization system in which the light intensity varies significantly across the sample, the addition of a second light source will dramatically change the shape of photoinitiation profile. Therefore, the control and placement of multiple lamps are more complex design variables for thick systems.

In this chapter, the effect of multiple light sources on the polymerization of thick polymer systems (~1 cm) is examined by generalizing the previously reported description of the temporal evolution of the light intensity gradient and the initiator concentration gradient in photobleaching systems using monochromatic light illuminated from above.¹⁷ The effect of the addition of a second light source on the opposite side is investigated and the results are compared with those obtained for the single-side illumination case. Also presented are simulation results obtained for a system illuminated on one side with a reflective substrate on the other. The simulation

results from these cases will illustrate the effects of several system variables on the evolution of the photoinitiation rate profile.

4.2. Governing Equations

To investigate the effect of two-sided illumination on the photoinitiation rate profiles for thick systems, the following model system was selected: a thick polymerization system (typically 1 cm thick) of rectangular cross-section subject to uniform monochromatic illumination normal to the top and bottom surfaces. Note that in this system the illuminated surfaces are parallel to one another, and that this model geometry is relevant to applications such as the production of flexographic printing plates. The set of differential equations that describe the evolution of the light intensity gradient, the initiator concentration gradient, and the local photoinitiation rate for these conditions are shown below. These equations were solved by method of finite differences for these simulations.

$$\frac{\partial C_i(z,t)}{\partial t} = -\varepsilon_{i1}\varphi_i\left(\frac{I_1(z,t)}{N_A h\nu}\right)C_i(z,t) - \varepsilon_{i2}\varphi_i\left(\frac{I_2(z,t)}{N_A h\nu}\right)C_i(z,t) + D_i \frac{\partial^2 C_i(z,t)}{\partial z^2} \quad (1)$$

$$\frac{\partial C_p(z,t)}{\partial t} = \varepsilon_{i1}\varphi_i\left(\frac{I_1(z,t)}{N_A h\nu}\right)C_i(z,t) + \varepsilon_{i2}\varphi_i\left(\frac{I_2(z,t)}{N_A h\nu}\right)C_i(z,t) + D_p \frac{\partial^2 C_p(z,t)}{\partial z^2} \quad (2)$$

$$\frac{\partial I_1(z,t)}{\partial z} = -(\varepsilon_i C_i(z,t) + A_m + \varepsilon_p C_p(z,t))I_1(z,t) \quad (3)$$

$$\frac{\partial I_2(z,t)}{\partial z} = -(\varepsilon_i C_i(z,t) + A_m + \varepsilon_p C_p(z,t))I_2(z,t) \quad (4)$$

Here, $C_i(z,t)$ represents the initiator molar concentration at depth z and time t ; $C_p(z,t)$

represents the photolysis product molar concentration at depth z and time t ; $I(z,t)$ represents the incident light intensity at depth z and time t , with dimensions of energy/(area·time); ϵ_i is the Napierian initiator molar absorptivity with dimensions of volume/(length·mole); ϵ_p is the Napierian photolysis product molar absorptivity, with dimensions of volume/(length·mole) and accounts for the photon absorption by all fragmentation species; N_A is Avogadro's number; h is Planck's constant; ν is the frequency of light, with dimensions of inverse time; ϕ_i is the quantum yield of the initiator, defined as the fraction of absorbed photons that lead to fragmentation of the initiator; D_i is the diffusion coefficient for the initiator with dimensions of length²/time; D_p is the diffusion coefficient for the photolysis products; and A_m is the absorption coefficient of the monomer and the polymer repeat unit. Note that in this study the Napierian molar absorptivity was adopted because it is most natural for the differential version of the absorption equation (equation 3). In the literature the decadic (base 10) molar absorptivity is commonly reported and should be converted to the Napierian value before using the model.

The subscripts 1 and 2 correspond to the light sources on the top and bottom of the sample, respectively. For example, $I_1(z,t)$ represents the light intensity from lamp 1 at time t and depth z below the surface of the sample, ϵ_2 is the molar absorptivity of the initiator at the wavelength of lamp 2, *etc.* For the equations shown here, each lamp is assumed to be monochromatic, although these wavelengths can differ. It would also be straight-forward to generalize these equations to include multiple wavelengths.

The following boundary and initial conditions apply:

$$C_i(z,0) = C_o \quad (5)$$

$$C_p(z,0) = 0 \quad (6)$$

$$\frac{\partial C_{i,p}(z,t)}{\partial z} = 0 \text{ at } z = 0 \text{ and } z = z_{\max} \text{ (the thickness of the sample)} \quad (7)$$

$$I(0,t) = I_1 \quad (8)$$

$$I(1,t) = I_2 \quad (9)$$

Here, Equation 5 indicates that the initiator concentration is initially uniform through the depth of the sample. Equation 6 accounts for the fact that photolysis product concentration is initially equal to zero throughout the sample, while Equation 7 represents the no-flux boundary condition at the ends of the sample for both the initiator and the fragments; this boundary condition is necessary due to the diffusional terms in the governing equations. Finally, Equations 8 and 9 indicate that the light intensity at each exposed surface is equal to the respective incident light intensity at all times.

Finally, Equation 10 defines the instantaneous local rate of production of free radicals, $R_i(z,t)$, if two active centers are produced upon fragmentation of the initiator molecule.

$$R_i(z,t) = 2C_i(z,t) \sum_j [I(z,t)]_j \phi_j \epsilon_{ij} \quad (10)$$

4.3. Results and Discussion

4.3.1. Effect of Illumination on Both Sides

To illustrate the effect of two-sided illumination, it is useful to compare simulation results for the evolution of the initiation rate profile with and without the second lamp, as shown in Figures 4.1 through 4.6. Figure 4.1 contains a family of plots of the photoinitiation rate as a function of depth at 20 second intervals for a 1 cm thick polymerization system illuminated on one side (incident light intensity of 50 mW/cm², for a sample containing 0.01 moles per liter of an initiator with an extinction coefficient of 525 L/mol-cm). A wide variety of photoinitiators are available that produce free radicals upon the absorption of photons of the appropriate energy (typically in the ultraviolet or visible regions of the spectrum).²⁵⁻²⁷ This relatively low value of the extinction coefficient is characteristic of phosphine oxide initiators at 366 nm. Since a single extinction coefficient is used to describe the system, monochromatic illumination is implied. In addition, for these simulations, it is assumed that no components other than the initiator (including the monomer, polymer, and initiator fragments) absorb at the initiating wavelength. The figure illustrates at the instant that the sample is first illuminated (time zero), the initiation rate is maximum at the illuminated surface and decreases through the depth of the sample in accordance with the absorption equation. As time increases, the rate at the illuminated surface decreases due to consumption of the photoinitiator, and the photoinitiation rate profile exhibits a maximum value at an intermediate depth (at high depths the rate is low due to a low light intensity). For example, the profile that corresponds to 60 seconds of illumination exhibits a maximum polymerization rate of

1.5×10^{-4} moles/liter-second at a depth of 0.1 cm. Therefore, a photoinitiation wave front slowly progresses through the sample (the peak rate has only passed 22.5% through the sample after 100 seconds). At longer times, as shown in Figure 4.1b, the photoinitiation rate front continues to pass through the system until all of the initiator is consumed.

Figure 4.2 shows how the initiation rate changes with time at the top, middle, and bottom of the sample (depths of 0, 0.5, and 1 cm, respectively). The maximum rate at the top of the sample occurs at the instant the sample is illuminated and is 3.67×10^{-4} moles/L-s. In the center of the sample, a maximum rate of 9.51×10^{-5} moles/L-s arises after 203 seconds of illumination, and at the bottom, a maximum rate of 9.17×10^{-5} moles/L-s occurs after 410 seconds of illumination. The effects of a number of variables on the evolution of the photoinitiation rate profiles for thick polymerization systems subject to monochromatic illumination are described in detail in reference 6.

Figure 4.3 illustrates the effect of adding a second light source of equal intensity to simultaneously illuminate the opposite surface of the system described above. Figure 4.3a illustrates that, at the instant of illumination, the rate is highest at each of the illuminated surfaces, and falls off into the middle of the sample according to the absorption equation (since the lamps have equal intensity, the minimum rate occurs at the center of the sample). Note that for the low to moderate extinction coefficient and initiator concentrations considered here, the light from each lamp penetrates past the middle of the sample and the light intensity profiles overlap, even at the instant of illumination. In addition, since the incident light intensities on either

side of the sample are equal to one another, the photoinitiation rate profiles are symmetric with respect to the center of the sample at all times. Figure 4.3b shows that as time progresses, the initiation rate at the two illuminated surfaces of the sample decreases due to the consumption of initiator, and a symmetric, bimodal photoinitiation rate profile is established. For example, the profile that corresponds to 100 seconds of illumination exhibits a maximum polymerization rate of 1.5×10^{-4} moles/L-s at a depth of 0.1 cm. It is interesting to note that at 100 seconds the initiation rate is relatively uniform with a value of $(9.85 \pm 2.39) \times 10^{-5}$ mol/L-s throughout the sample. When the peaks of the initiation wave fronts meet in the center of the sample (154 seconds), the overall photoinitiation rate profile becomes unimodal, and the rate in the center reaches its maximum. From this time on, the maximum photoinitiation rate occurs at the center of the sample, and at all depths the rate decreases as the initiator is consumed.

Figure 4.4 illustrates the variation of photoinitiation rate with time for the top, middle, and bottom of a sample illuminated on both the top and bottom. In this symmetric case, the top and bottom surfaces of the sample experience the same evolution of initiation rate, where the maximum rate occurs at the instant of illumination, and is 3.67×10^{-4} moles/L-s. Note that initiation occurs in the center of the sample at the instant of illumination, but the maximum does not arise until 154 seconds later, when a rate of 1.36×10^{-4} moles/L-s is achieved.

While comparison of Figures 4.1 and 4.3 illustrates the effect of the addition of a second light source, it is notable that the total flux of photons into the sample is twice as high for Figure 4.3 when compared to Figure 4.1. Therefore, it is instructive

to compare the results in Figure 4.3 to the single-sided illumination case that has the same total photon flux. Figure 4.5 contains simulation results for this system and illustrates that the photoinitiation profile is again non-uniform, and that the peak initiation rate passes only 0.475 cm into the sample's depth in 100 seconds, though the peak initiation rate is higher than the double-sided case.

Figure 4.6 illustrates the time evolution of the photoinitiation rate at the top, middle, and bottom of the sample for single-sided illumination with an incident light intensity of 100 mW/cm^2 . The effect of doubling the incident light intensity for single-sided illumination is illustrated by comparing Figure 4.6 to Figure 4.2. First, examination of the photoinitiation rate at the illuminated surface as a function of time reveals that the rate at time zero is directly proportional to the intensity, but that the rate decreases more rapidly for the higher incident intensity. For example, the rate has decreased to zero in approximately 150 seconds for an intensity of 100 mW/cm^2 , and is still above zero after 250 seconds for an intensity of 50 mW/cm^2 , all other variables held constant. Examination of the curves for the photoinitiation rate at the center and the bottom of the sample reveals that the higher incident photon flux leads to a higher maximum rate that is achieved in a shorter period of time (in fact for the lower light intensity, the maximum rate at the bottom of the sample is not achieved with the 250 seconds shown in this figure).

Comparison of Figures 4.4 and 4.6 illustrates the effect of illumination of both sides under the condition of constant total photon flux (two 50 mW/cm^2 lamps for two-sided illumination compared to one 100 mW/cm^2 lamp for the single-sided illumination). For the single-sided illumination case the maximum initiation rate

passes through the center of the sample in 102 seconds compared to 154 seconds for two-sided illumination. This is due to the fact that the initiator concentration near the illuminated surface is depleted more rapidly, thereby allowing the light to penetrate to the center of the sample in a shorter time. However, the time to initiate completely through the entire sample is shorter when two lamps are used.

Table 1 summarizes some of the notable values from Figures 4.1 through 4.6 to allow a more quantitative comparison of the three illumination conditions. Specifically the table shows the maximum initiation rates achieved at the top, middle, and bottom of the sample as well as the time required to reach these maximum rates for each of the cases described above. Note that Case 1 (one-sided illumination with $I_{(z=0)}=50 \text{ mW/cm}^2$) and Case 2 (two-sided illumination with $I_{(z=0)}=I_{(z=1)}=50 \text{ mW/cm}^2$) have the same maximum initiation rate at the top of the sample due to identical local conditions of intensity and initiator concentration at time zero. Case 2 exhibits a higher maximum rate at the bottom of the sample than either Cases 1 or 3 (one-sided illumination with $I_{(z=0)}=100 \text{ mW/cm}^2$) due to the high light intensity and high initiator concentration present when the light illuminates that area. It is also interesting to compare the values of the maximum rates. At the top of the sample, the maximum rate for Case 3 is twice as high as Cases 1 and 2 for obvious reasons. At the center of the sample, the maximum initiation rate for Case 3 is nearly twice that of Case 1, and 28% higher than Case 2. At the bottom of the sample, by far the highest rate is observed for the two-sided illumination case (Case 2).

For some applications, the uniformity of the photoinitiation as a function of depth may be an important consideration. As described above, single-sided

illumination leads to an inherently non-uniform initiation front that passes from the illuminated surface through the depth of the sample. For quantitative comparison of the uniformity of initiation for different illumination schemes, the percent variation of the initiation rate at a given time was defined as the range of the initiation profile divided by the maximum initiation rate. Representative values for an illumination time of 100 seconds by are shown in column 5 of Table 1. These values illustrate that two-sided illumination leads to a considerably more uniform photoinitiation rate as a function of depth in the sample. Specifically, at 100 seconds of illumination, the variation for Case 1 is 2.5 times that of Case 2, and the variation of Case 3 is 2.25 times that Case 2.

Table 1 illustrates that the percent variation at a particular point in time is much lower for the system illuminated from both sides. It is interesting to note that the percent variation in the two-sided system is in fact lower at every point in time, as shown in Figure 4.7. The two systems in this figure have the same total intensity, 100 mW/cm^2 , but the variation through the sample is dramatically different. The two-sided case starts out with a lower percent variation than the one-sided case, which then decreases rapidly over a 90 second time period before the system starts to move towards a unimodal profile.

4.3.2. Effect of Photoinitiator Concentration and Molar Absorptivity

Initiator concentration is of particular interest in thick photopolymerization, because it has a pronounced impact on the photoinitiation rate profile. For single-sided illumination of thick systems with complete photobleaching, increasing the

initiator concentration leads to an increase in both the photoinitiation rate and the time required to cure throughout the depth of the sample. For two-sided illumination, the situation is more complex due addition of the second light source. For high initiator concentrations, each light source may lead to a sharp photoinitiation front that moves from the illumination surface toward the center of the sample, independent of the second light source. In contrast, for low initiator concentrations, the light intensity gradients from the two lamps may overlap immediately upon illumination, leading to more uniform initiation rate profiles and a less frontal behavior. To investigate the effects of increasing concentration quantitatively, a series of simulations were performed for photopolymerization systems with concentrations of 0.02 and 0.04 mol/L of an initiator with an extinction coefficient of 525 L/mol-cm (incident light intensity of 50 mW/cm²).

Figure 4.8 shows a series of profiles of the photoinitiation rate as a function of depth for a system with initiator concentration of 0.02 mol/L. Comparison of Figure 4.8 to Figure 4.3 reveals that the doubling of the initiator concentration has a dramatic effect on the resulting photoinitiation rate profiles. At this higher concentration, the photoinitiation front on each illuminated side is relatively narrow, therefore the system is much less uniform from the beginning of the reaction, and there is no overlap of the two light intensity gradients at time zero. In addition, little improvement in the uniformity of the profile is observed with increasing time, although after 100 seconds of illumination considerable initiation has occurred throughout the depth of the sample. These results clearly illustrate that the initiator

concentration has a marked effect on the time-evolution of the photoinitiation rate profile.

As the initiator concentration is increased further, the light intensity gradient at each illuminated surface becomes sharper, and the breath of the photoinitiation front becomes narrower. These trends are illustrated by comparing Figure 4.9 (which corresponds to an initiator concentration of 0.04 mol/L) to Figure 4.3 and Figure 4.8. At this concentration, there is no overlap of intensity in the middle of the sample even after 260 seconds of illumination, and the photoinitiation progresses as two independent fronts moving from the illuminated surfaces toward the center of the sample. Note that eventually the two sharp fronts meet in the center of the sample.

For photopolymerizations of thin systems such as films and coatings, the optical density (the product of the initiator molar absorptivity and the initiator concentration) is often used to select the initiator concentration. It is common practice to choose an initiator concentration that is proportional to the inverse of the molar absorptivity to keep the optical density constant when changing from one photoinitiator to another. This rule of thumb arises from the fact that two systems that have the same optical density have the same initial light intensity gradient. This generally works well for photopolymerizations of coatings, however photopolymerizations of thick systems are more complex, especially when the molar absorptivity of the products are considerably different than that of the original initiator. Figure 4.10 shows a system with the same initial optical density as shown in Figure 4.3 (they both have an initial optical density of 5.25), but with a higher initiator concentration of 0.03 mol/L and a lower initiator absorptivity of 175 L/mol-

cm. Comparison of Figure 4.10 to Figure 4.3 reveals that two systems with the same initial optical density behave very differently as the illumination time is increased. In general, for two systems with the same initial optical density, the photoinitiation rate profile of the system with higher initiator concentration and lower initiator absorptivity will evolve more slowly. In this specific case, the photoinitiation profile for the case with the high molar absorptivity (Figure 4.3) has become unimodal (due to merging of the two fronts) in less than 140 seconds, and the reaction is nearly complete (the initiator nearly consumed) in approximately 260 seconds. In contrast, the system with the higher concentration has is not even close to the unimodal profile after 260 seconds, and does not reach unimodality until 347 seconds. For these thick systems, the optical density of the two cases is the same only the instant at which the illumination is begun. Once the photoinitiation reaction has started, the system with the higher molar absorptivity and lower concentration will have the initiator depleted more rapidly, and will therefore have a lower optical density (averaged over the depth of the sample) than the high concentration case. Once the photoinitiation reaction has begun, an initiator concentration gradient as a function of depth is established in the sample, therefore the local optical density changes with depth. For this reason the optical density is not a particularly useful value for describing the time evolution of photobleaching systems.

Figure 4.11 illustrates the influence of a relatively high initiator molar absorptivity (20,000 L/mol-cm) on the initiation rate profile when the sample is illuminated from two sides. In comparison to Figure 4.3, Figure 4.11 illustrates that an initiator with a high molar absorptivity leads to a narrow the initiation rate profile

which moves as a sharp front from the illumination surface toward the center of the sample (the arrows indicate the direction each of the initiation peaks is moving; ultimately they will meet in the middle and initiation will be complete). While this condition leads to an inherently non-uniform photoinitiation profiles (indeed the percent variation is 100% at all times), there are situations in which a sharp initiation front is desired, such as flexographic printing where backside illumination may be used to create a substrate of specific depth, and topside illumination through a mask needs to create defined surface features.

4.3.3. Effect of Monomer Absorption

Since the monomer is the predominant component in most photopolymerization systems (typically more than 90% of the total system), it is important for the monomer absorption coefficient to be as small as possible at the effective initiation wavelength. This is especially true for photoinitiation of thick samples since even a relatively small value of the molar absorptivity will significantly attenuate the incident light. Figure 4.12 illustrates the effects of monomer absorption of the incident wavelength (all variables have the same values as in Figure 4.3 except the monomer absorption coefficient). Figure 4.12a contains results for the case of a mildly absorbing monomer, while Figure 4.12b shows simulation results for a system in which the monomer absorbs on the same order as the initiator (the molar absorptivity of the monomer is 1000 times lower than that of the initiator because the concentration is higher by the same factor). In general, absorption by the monomer leads to reduced penetration of light into the sample and therefore reduces the

photoinitiation rate at a given depth and slows the rate at which the photoinitiation profile evolves. In Figure 4.12a the monomer is only slightly absorbing at the wavelength of interest, therefore this attenuation is mild, however for the case shown in Figure 4.12b the light attenuation is more severe and the light does not reach the center of the sample. In this case, the photoinitiation rate remains zero in the center and the initiation rate closer to the illumination surfaces continuously decreases until it approaches zero. These figures illustrate why choosing an initiator/monomer/light source combination is critical to thick photopolymerizations.

4.3.4. Reflective Boundary Condition

A special case of two-sided illumination is a reflective boundary condition in which the sample is illuminated on only one side with a lamp, but any light that reaches the back surface is reflected back into the sample. In this case, the intensity of reflected light is initially low (typically zero) but increases with time as the initiator is consumed and more light is able to penetrate through the sample. For example, Figure 4.13 illustrates the effect of the reflective boundary condition on the resulting photoinitiation rate profile. This figure contains photoinitiation rate profiles for both the reflecting and non-reflecting boundary conditions for a 1 cm sample illuminated on one side with a single light source of intensity 100 mW/cm^2 and an initiator concentration of 0.01 mol/L (initiator molar absorptivity of 525 L/mol-cm). Note that initially ($t=0$), the initiation rate profiles are identical since no light reaches the back surface. With increasing time the reflective boundary leads to an increased light intensity at the back side of the sample ($z=1$) which in turn leads to an increase in the

rate at which the photoinitiator is consumed in this location. As a result, starting at approximately 120 seconds in this system, the initiation rate in the last quarter of the sample is increased. At approximately 150 seconds, the last quarter of the sample with the reflective boundary exhibits a nearly uniform initiation rate, then. Note that after 180 seconds of illumination, the reflected light causes the photoinitiation rate to increase monotonically near the back surface and the photoinitiation rate profile shows no maximum.

The effect of the reflective boundary condition is also evident by examining the photoinitiation rate at back the surface since this is the location in the sample where the difference between the reflective and non-reflective cases will generally be the largest. To illustrate this effect, Figure 4.14 contains plots of the initiation rates at the back surface ($z=1$ cm) as functions of time of the reflective and non-reflective cases under the same conditions as Figure 4.13. Figure 4.14 illustrates that for both systems the initiation rate is initially approximately zero since very little light penetrates to the back surface. As the initiator near the illuminated surface is consumed, light does reach the back surface, and the initiation rate becomes non-zero (at approximately 30 seconds for the system shown here). The light intensity at $z=1$ for the reflective case will always be twice that of the non-reflective condition, therefore for the first 160 seconds, the reflective boundary conditions results in a doubling of the photoinitiation rate at $z=1$ (up until this time the photoinitiator concentration is essentially the same for both systems). Due to this enhanced photoinitiation rate the initiator concentration at $z=1$ will decrease more rapidly for the reflective case (indeed when $t=200$ seconds, the initiator concentration at $z=1$ for

the reflective case is half that of the non-reflective case), therefore the photoinitiation rate reaches a maximum value at an earlier time for the reflective case (2.51×10^{-4} mol/L-s at $t=179$ seconds for the reflective case compared to 1.83×10^{-4} mol/L-s at $t=205$ seconds for the non-reflective case).

The simulation results shown in Figures 4.13 and 4.14 illustrate that there can be significant benefit from use of a reflective boundary condition. For the system shown in the simulation, the maximum photoinitiation rate at $z=1$ cm was increased by 37.4% while the time to achieve this maximum was decreased by 12.7%. In addition, the time to consumed 99% of the initiator at $z=1$ cm was decreased by from 347 seconds to 252 seconds. Moreover, the addition of a reflective boundary is considerably less expensive than the addition of a second light source. A reflective surface of a mold or substrate could be implemented using a variety of commercially available polished surfaces, reflective adhesive tapes, *etc.* It is important to note that the benefit derived from a reflective boundary condition is diminished as the concentration or molar absorptivity of the initiator is increased. High value of these variables may lead to sharp photoinitiation fronts (such as those shown in Figure 4.11) which would glean little benefit from the reflective boundary.

4.3.5 Perpendicular Illumination

The model was further generalized to describe the light intensity gradient, concentration gradient, and photoinitiation rate profile in a sample in which two perpendicular sides are illuminated, as illustrated by the schematic shown in Figure 4.15. The following model system was selected for this simulation: a thick

polymerization system (1 cm^2) of rectangular cross-section subject to uniform monochromatic illumination normal to two perpendicular surfaces. Illuminating two non-parallel sides could be important for photopolymerization of complex and three-dimensional parts, and is a notable addition to the capabilities of the model. Light intensity, initiator concentration, and photoinitiation rate vary in the two-dimensional plane, with the highest intensity at the doubly-illuminated corner.

Figure 4.16 shows the normalized light intensity as a function of the two spatial dimensions at the instant the sample is illuminated. Note that the arrows in this figure indicate the directions from which the light is coming. In this figure, the doubly illuminated corner has twice the intensity of a single light source. Along each of the two edges where the light is incident, the value of the intensity is that of the incident light source plus the amount of light that penetrates to each depth from the other light source. Along these edges, the intensity will be at least equal to the intensity of a single light, and build as more light penetrates from the opposing perpendicular light source.

Figure 4.17 shows the initiator concentration gradient of the same sample at the instant illumination. The arrows again indicate the directions from which the light is illuminating the sample. At this instant in time, the concentration has depleted the most in the corner that experiences double intensity. Note that at this point, the lowest concentration is approximately 90% of the initial concentration. As shown by Miller *et al.*,³ the concentration profile is coupled to the intensity, and at the corner of the sample where the intensity is the greatest, the concentration at this time is the lowest value throughout the sample.

Figure 4.18 shows the photoinitiation rate profile at the instant the lights are turned on, which is proportional to the product of the intensity and initiator concentration gradients shown in Figures 4.16 and 4.17, respectively. Here, initiation is high in the corner where both light sources are directly incident because there is both a high intensity and high concentration. At the opposite corner of the sample, there is virtually no initiation because the light intensity is very low. As time elapses, the initiation rate at the doubly-illuminated corner of the sample will decrease as the concentration depletes, and the maximum rate of initiation will move as a wave front through the sample, towards the corner that is not illuminated.

4.4. Conclusions

To investigate the effect of two-sided illumination on the photoinitiation rate profiles of 1 cm thick polymerization systems, the governing differential equations which describe the spatial and temporal evolution of the light intensity, initiator concentration, and photoinitiation rate were solved numerically. Simulation results revealed that when two lamps of equal intensity are used, the spatial and temporal evolution of the photoinitiation rate profile is indeed highly non-uniform, but is always symmetric with respect to the center of the sample and follows a characteristic progression from a bimodal distribution, to a unimodal shape with a maximum in the center of the sample. Simulation results also revealed that two-sided illumination leads to a considerably more uniform photoinitiation rate throughout the sample. Initiator concentration is of particular interest in thick photopolymerization, because it has a pronounced impact on the photoinitiation rate profile. For high initiator

concentrations, or high initiator absorptivity, each light source may lead to a sharp photoinitiation front that moves from the illumination surface toward the center of the sample, independent of each other. In contrast, for low initiator concentrations, the light intensity gradients from the two lamps may overlap immediately upon illumination, leading to more uniform initiation rate profiles and a less frontal behavior. Simulation results confirmed that absorption by the monomer leads to reduced penetration of light into the sample and therefore reduces the photoinitiation rate at a given depth and slows the rate at which the photoinitiation profile evolves. Simulation results also revealed that a reflective back surface can be beneficial in thick systems since it may lead to an increase in the initiation rate in the deep portion of the sample. Finally, illumination of two perpendicular sides of a sample leads to a photoinitiation rate wave front that progresses from the doubly-illuminated corner across the sample towards the dark corner.

This chapter has shown that either a uniform or very sharp initiation rate front can be achieved in a thick sample if the parameters of the illumination scheme are chosen appropriately for the desired initiation behavior. Many different illumination schemes can be imagined, and this model illustrates that with independently controlled light sources, as well as properly suited system variables (such as initiator concentration and molar absorptivity), a desirable initiation rate profile can be attained.

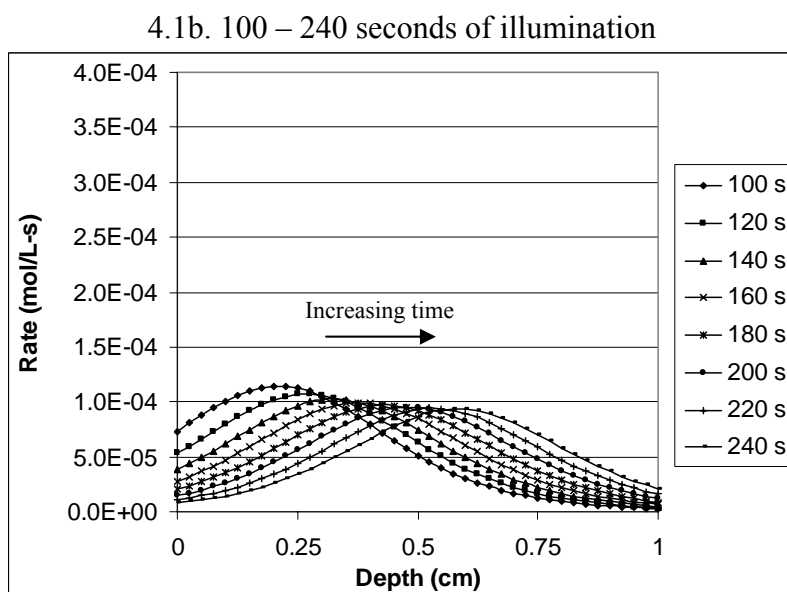
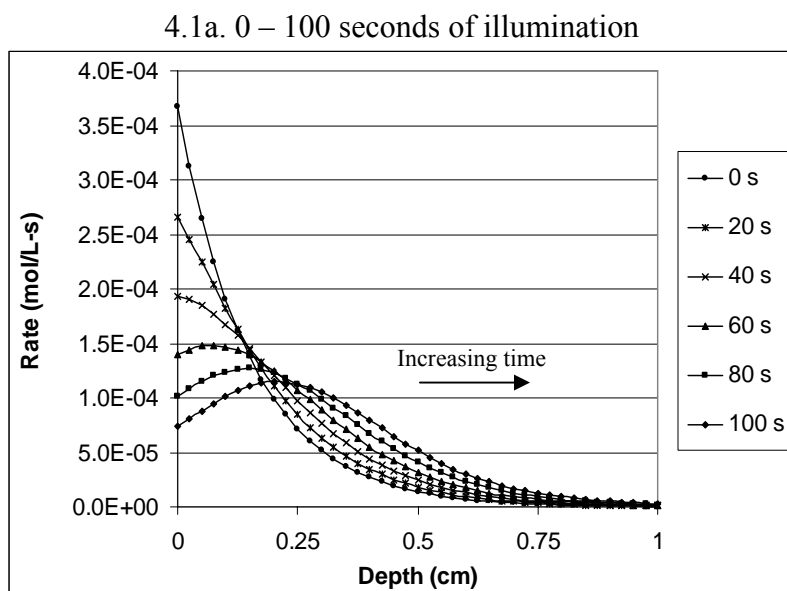


Figure 4.1. Rate of initiation as a function of sample depth and time for a system with initiator concentration 0.01 mol/L.

One-sided illumination with lamp at $z=0$ cm. $I(z=0)=50$ mW/cm², $z=1$ cm, $\epsilon_i=525$ L/mol-cm.

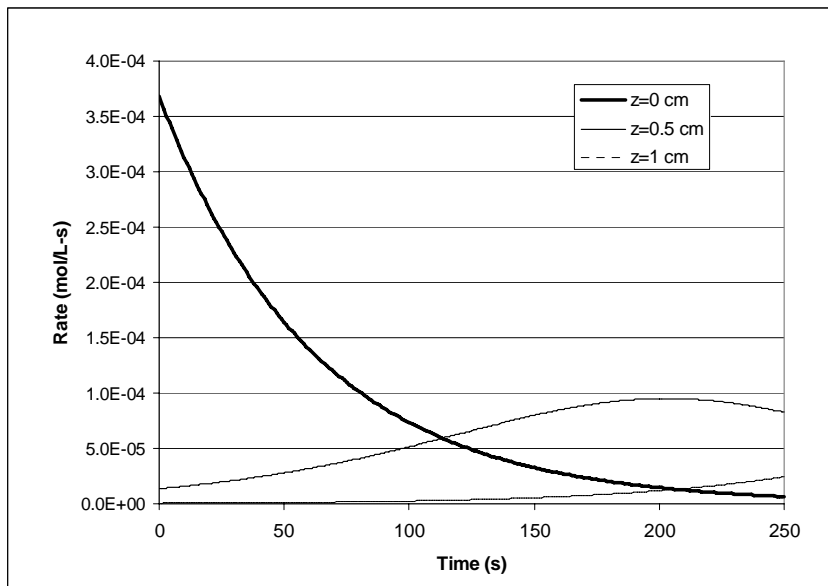
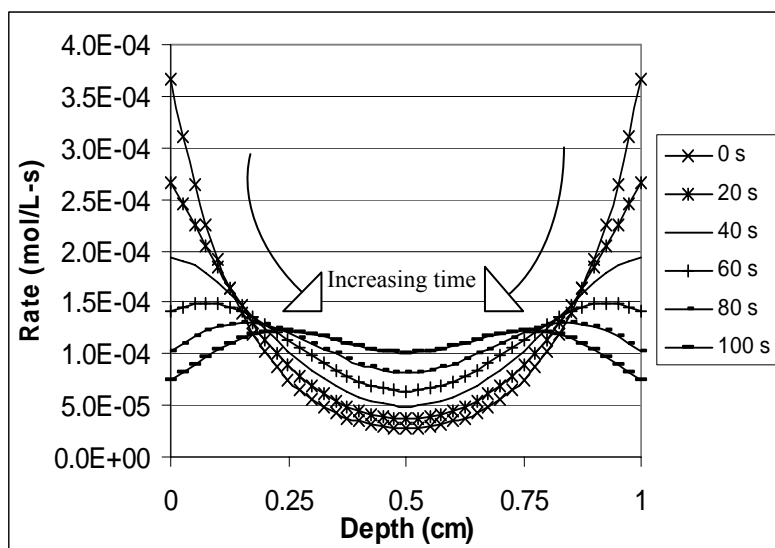


Figure 4.2. Initiation rate variation with time at top, middle, and bottom of a system with initiator concentration 0.01 mol/L.

One-sided illumination with lamp at $z=0$ cm. $I(z=0)=50$ mW/cm², $z=1$ cm, $\epsilon_i=525$ L/mol-cm.

4.3a. 0 – 100 seconds of illumination



4.3b. 100 – 240 seconds of illumination

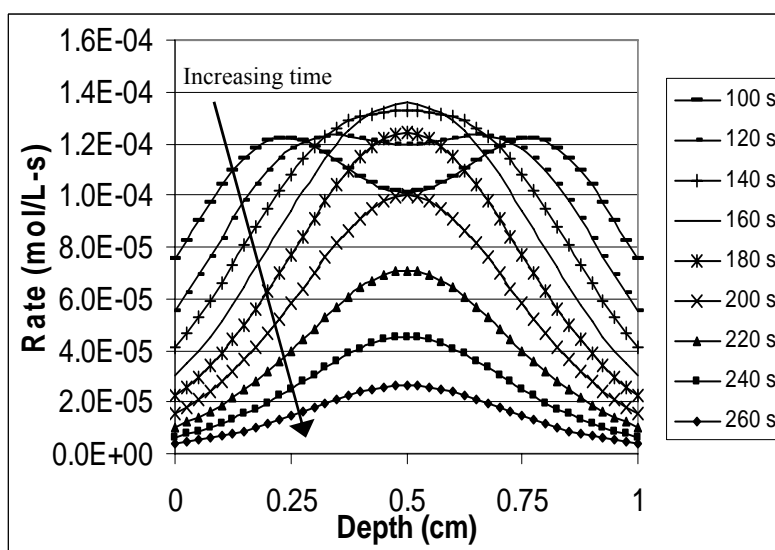


Figure 4.3. Rate of initiation as a function of sample depth and time for a system with initiator concentration 0.01 mol/L.

Two-sided illumination with lamps at $z=0$ cm and $z=1$ cm. $I_{(z=0)} = I_{(z=1)} = 50 \text{ mW/cm}^2$, $z=1$ cm, $\epsilon_{i1} = \epsilon_{i2} = 525 \text{ L/mol-cm}$.

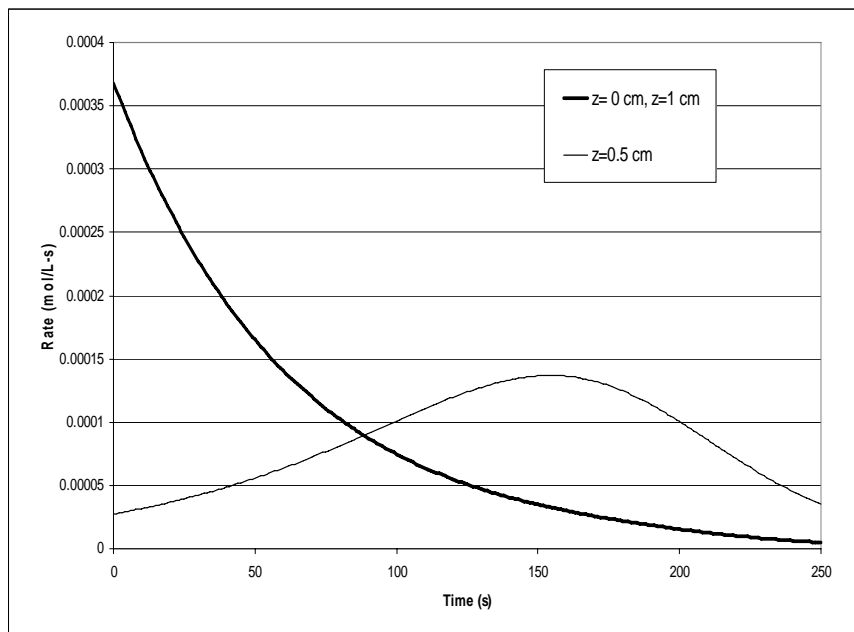


Figure 4.4. Initiation rate variation with time at top, middle, and bottom of a system with initiator concentration 0.01 mol/L.

Two-sided illumination with lamp at $z=0$ cm and $z=1$ cm. $I(z=0)=I(z=1)=50$ mW/cm^2 , $z=1$ cm, $\epsilon_{i1}=\epsilon_{i2}=525$ L/mol-cm.

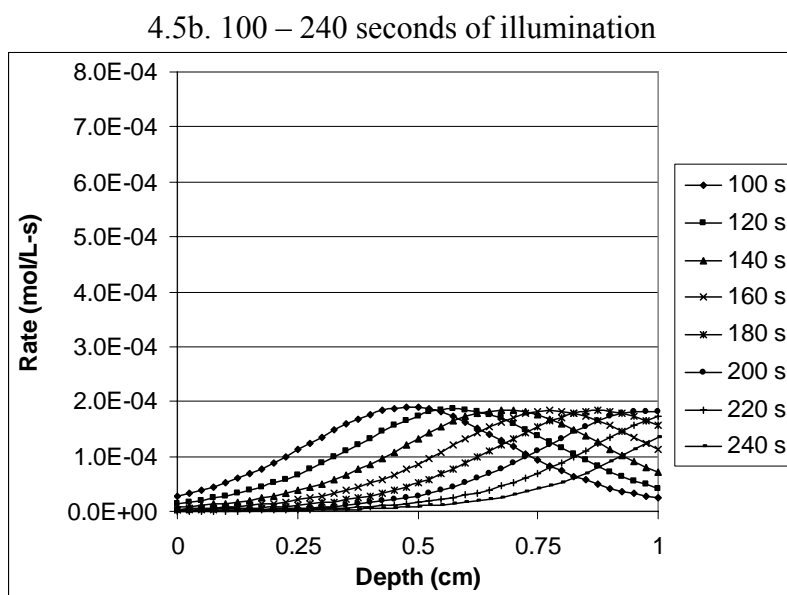
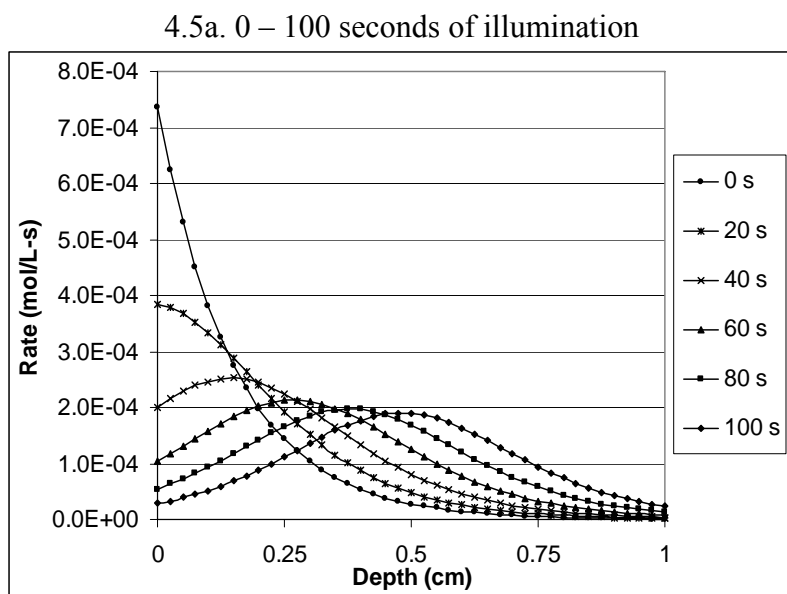


Figure 4.5. Rate of initiation as a function of sample depth and time for a system with initiator concentration 0.01 mol/L.

One-sided illumination with lamp at $z=0$ cm. $I_{(z=0)}=100$ mW/cm², $z=1$ cm, $\epsilon_i=525$ L/mol-cm.

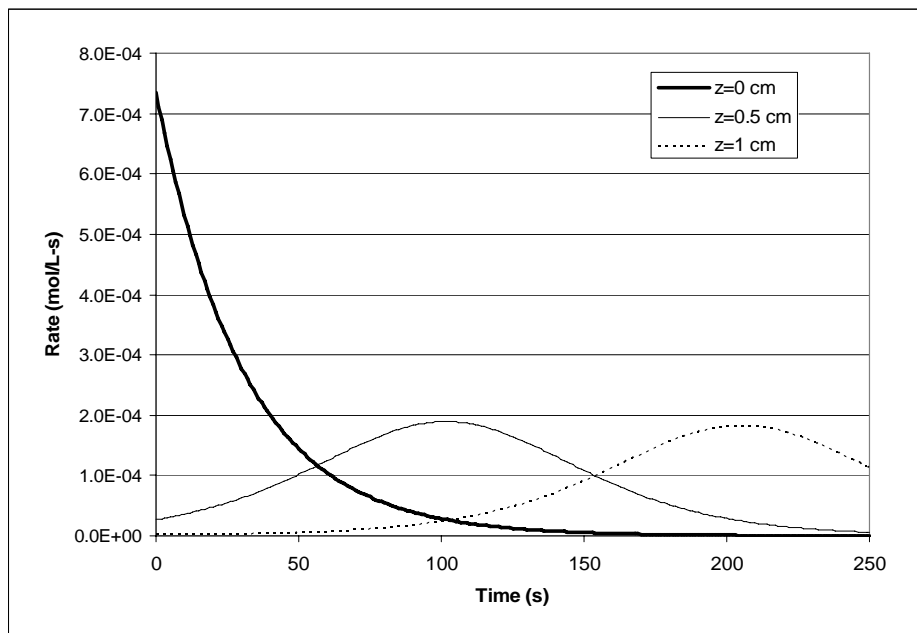


Figure 4.6. Initiation rate variation with time at top, middle, and bottom of a system with initiator concentration 0.01 mol/L.

One-sided illumination with lamp at $z=0$ cm. $I(z=0)=100$ mW/cm², $z=1$ cm, $\epsilon_1 = \epsilon_2 = 525$ L/mol-cm.

Table 4.1. Maximum rates achieved and the time necessary to reach these rates at the top, middle, and bottom of samples illuminated on one or two sides. Percent variation in initiation rate throughout the depth of each respective case is also given.

| | Max Rate at Top (0 cm) and Time to Reach Max Rate | Max Rate at Middle (0.5 cm) and Time to Reach Max Rate | Max Rate at Bottom (1 cm) and Time to Reach Max Rate | Percent Variation of initiation at 100 s of Illumination |
|---|--|--|--|--|
| Case 1. One-sided Illumination, $I_{(z=0)}=50 \text{ mW/cm}^2$ | 3.67×10^{-4} moles/L-s, 0 seconds of illumination | 9.51×10^{-5} moles/L-s, 203 seconds of illumination | 9.17×10^{-5} moles/L-s, 410 seconds of illumination | 97.8% |
| Case 2. Two-sided Illumination, $I_{(z=0)}=50 \text{ mW/cm}^2$ $I_{(z=1)}=50 \text{ mW/cm}^2$ | 3.67×10^{-4} moles/L-s, 0 seconds of illumination | 1.36×10^{-4} moles/L-s, 154 seconds of illumination | 3.67×10^{-4} moles/L-s, 0 seconds of illumination | 39.0% |
| Case 3. One-sided Illumination, $I_{(z=0)}=100 \text{ mW/cm}^2$ | 7.35×10^{-4} moles/L-s, 0 seconds of illumination | 1.89×10^{-4} moles/L-s, 102 seconds of illumination | 1.83×10^{-4} moles/L-s, 205 seconds of illumination | 87.7% |

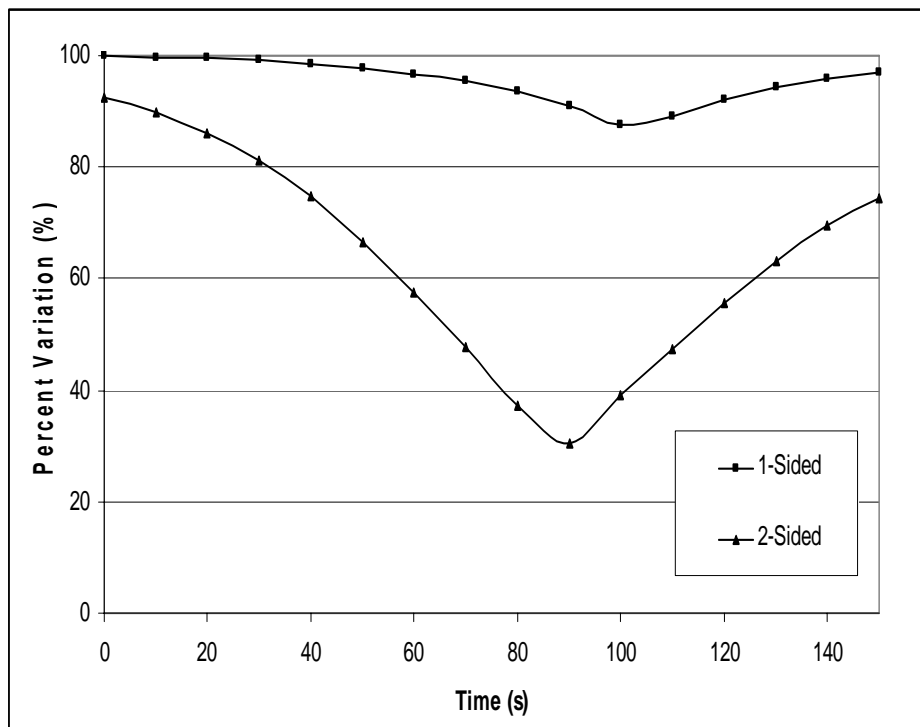


Figure 4.7. Percent variation as a function of time for one ($I_{(z=0)}=100 \text{ mW/cm}^2$, $\varepsilon=525 \text{ L/mol-cm}$) and two ($I_{(z=0)}=I_{(z=1)}=50 \text{ mW/cm}^2$, $\varepsilon_{i1}=\varepsilon_{i2}=525 \text{ L/mol-cm}$) sided illumination schemes with initiator concentration 0.01 mol/L and $z=1 \text{ cm}$.

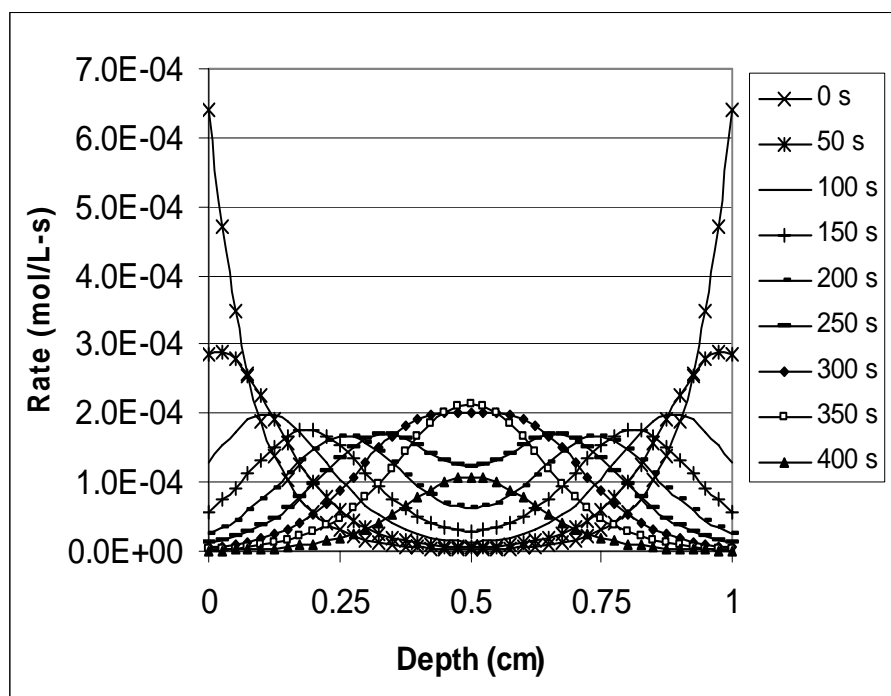


Figure 4.8. Rate of initiation as a function of sample depth and time for a system with initiator concentration 0.02 mol/L.

Two-sided illumination with lamps at $z=0$ cm and $z=1$ cm. $I_{(z=0)} = I_{(z=1)} = 50 \text{ mW/cm}^2$, $z=1$ cm, $\epsilon_{i1} = \epsilon_{i2} = 525 \text{ L/mol-cm}$.

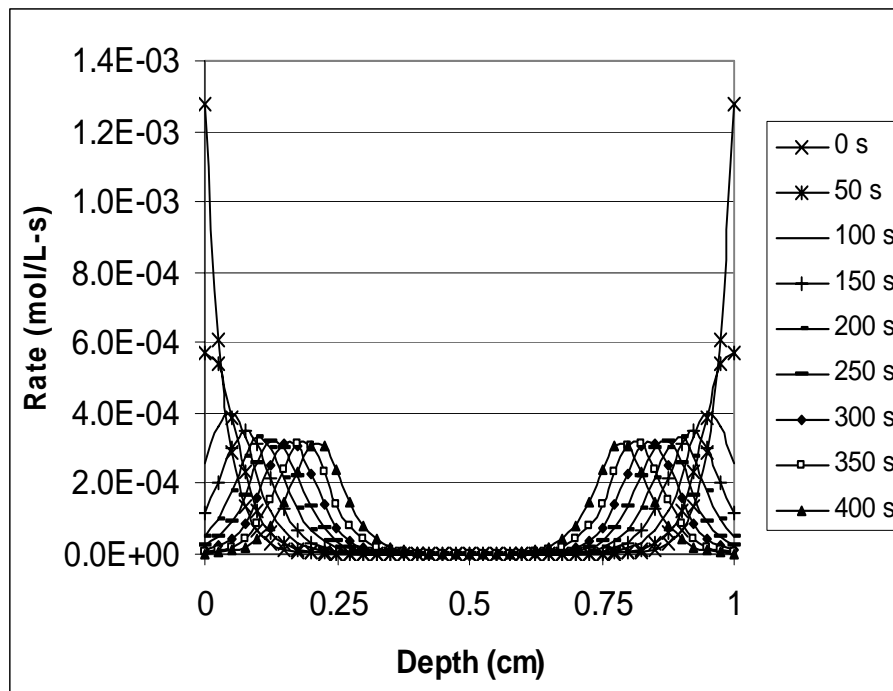


Figure 4.9. Rate of initiation as a function of sample depth and time for a system with initiator concentration 0.04 mol/L.

Two-sided illumination with lamps at $z=0$ cm and $z=1$ cm. $I_{(z=0)} = I_{(z=1)} = 50 \text{ mW/cm}^2$, $z=1$ cm, $\epsilon_{i1} = \epsilon_{i2} = 525 \text{ L/mol-cm}$.

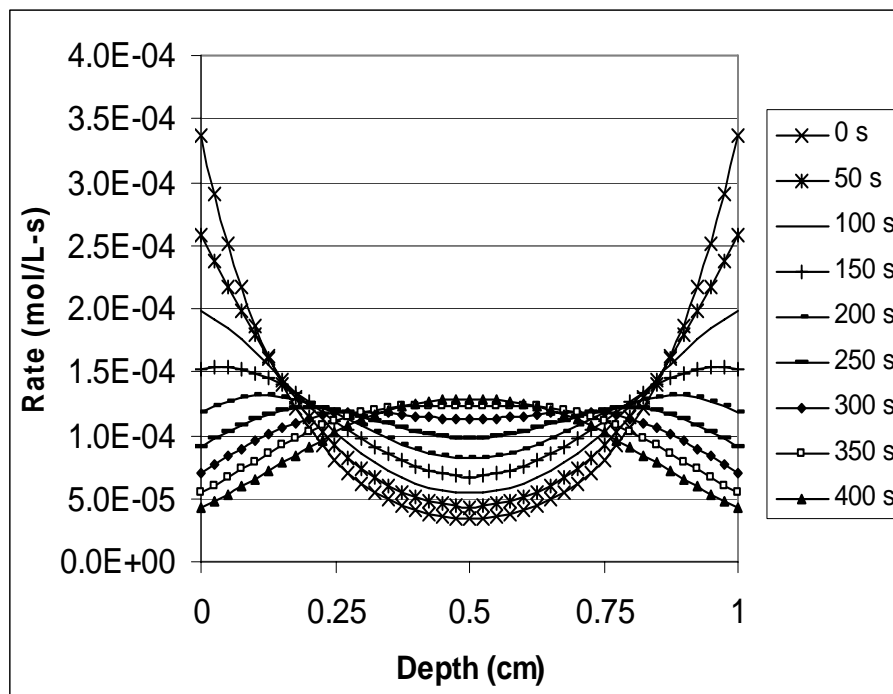


Figure 4.10. Rate of initiation as a function of sample depth and time for a system with initiator concentration 0.03 mol/L.

Two-sided illumination with lamps at $z=0$ cm and $z=1$ cm. $I_{(z=0)} = I_{(z=1)} = 50 \text{ mW/cm}^2$, $z=1$ cm, $\epsilon_{i1} = \epsilon_{i2} = 175 \text{ L/mol-cm}$.

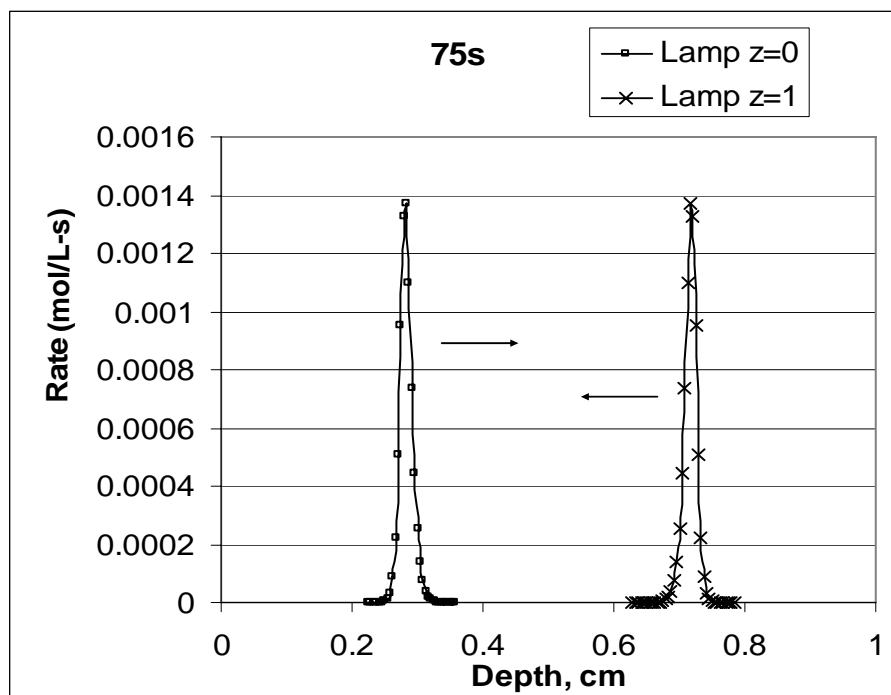


Figure 4.11. Rate of initiation as a function of sample depth and time for a system with initiator concentration 0.01 mol/L.

Two-sided illumination with lamps at $z=0$ cm and $z=1$ cm. $I_{(z=0)} = I_{(z=1)} = 50 \text{ mW/cm}^2$, $z=1$ cm, $\epsilon_{i1} = \epsilon_{i2} = 20,000 \text{ L/mol-cm}$.

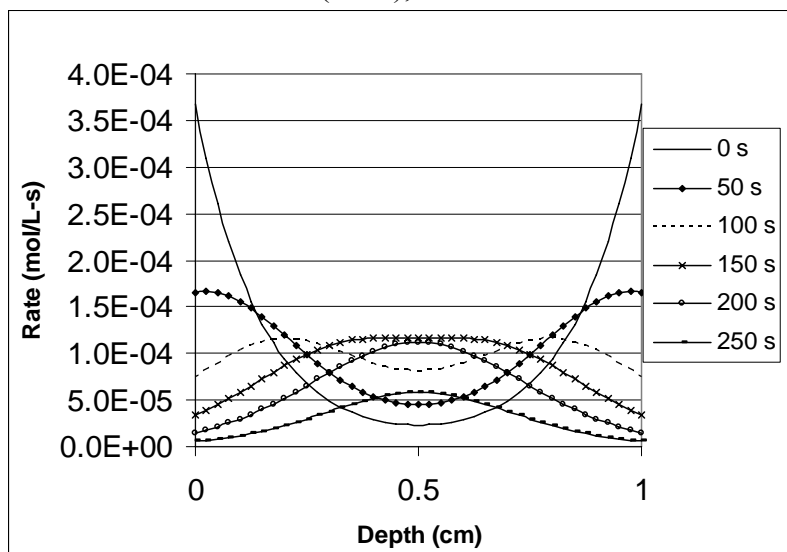
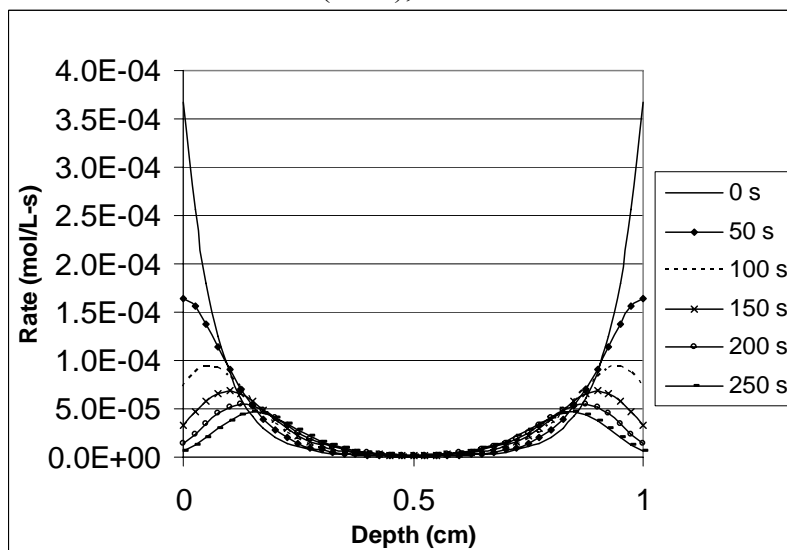
4.12a. $A_m=0.3$ (1/cm), $\epsilon_m=0.036$ L/mol-cm4.12b. $A_m=6.0$ (1/cm), $\epsilon_m=0.728$ L/mol-cm

Figure 4.12. Rate of initiation as a function of sample depth and time for a system in which the monomer absorbs.

Two-sided illumination with lamps at $z=0$ cm and $z=1$ cm. Initiator concentration = 0.01 mol/L, $I_{(z=0)} = I_{(z=1)} = 50$ mW/cm², $z=1$ cm, $\epsilon_{i1} = \epsilon_{i2} = 525$ L/mol-cm.

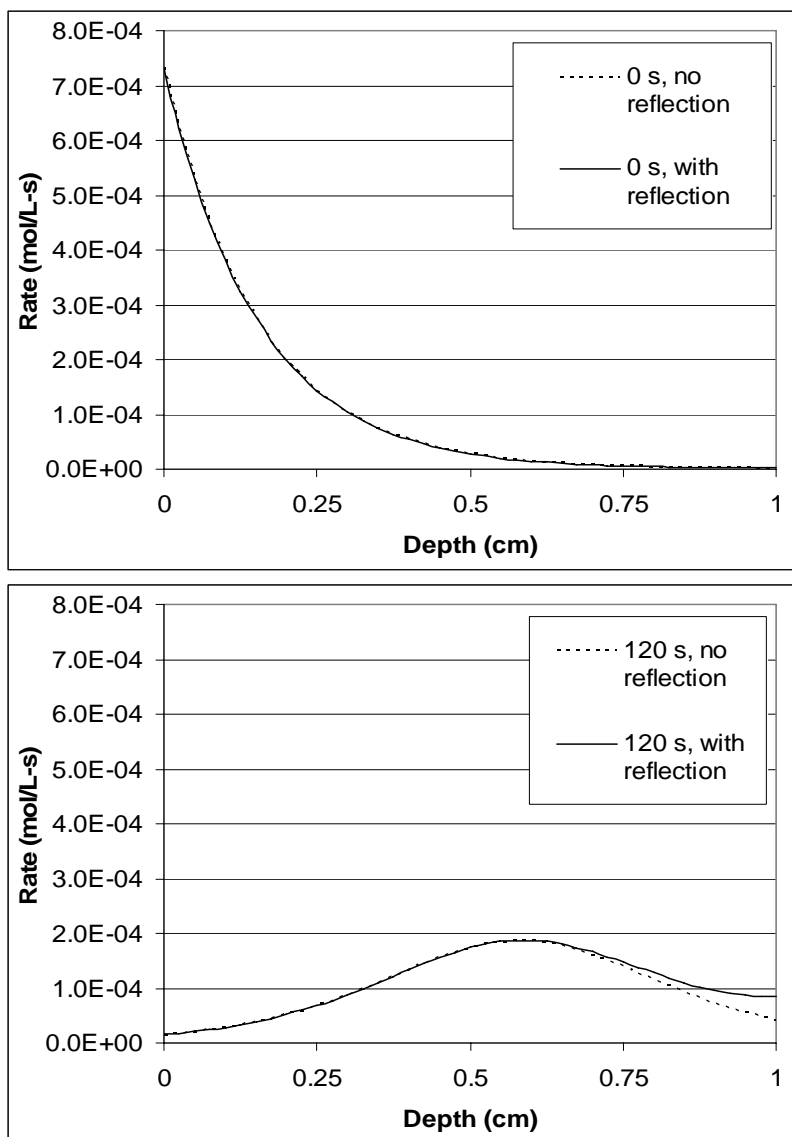


Figure 4.13. Rate of initiation as a function of sample depth and time for a system with initiator concentration=0.01 mol/L, $I_{(z=0)} = 100 \text{ mW/cm}^2$, $z=1 \text{ cm}$, $\epsilon_i=525 \text{ L/mol-cm}$. A. One-sided illumination with no reflection. B. One-sided illumination with reflective barrier at $z=1 \text{ cm}$.

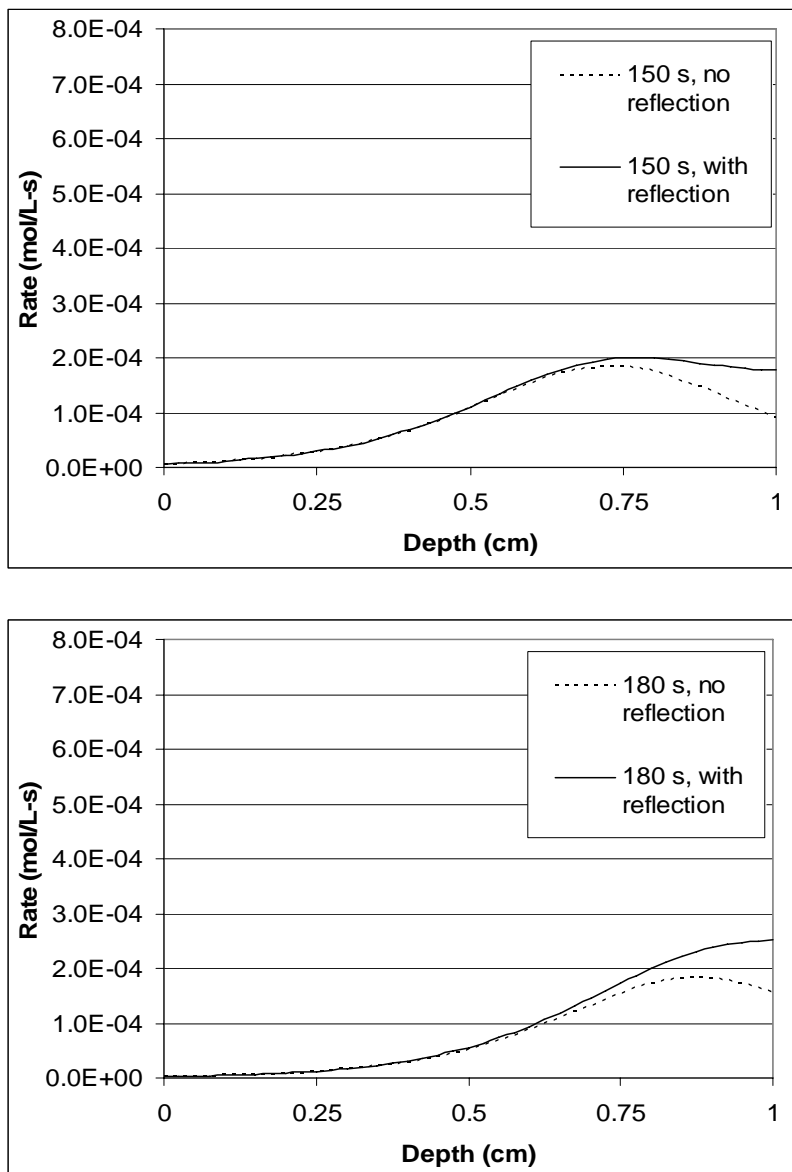


Figure 4.13. Continued.

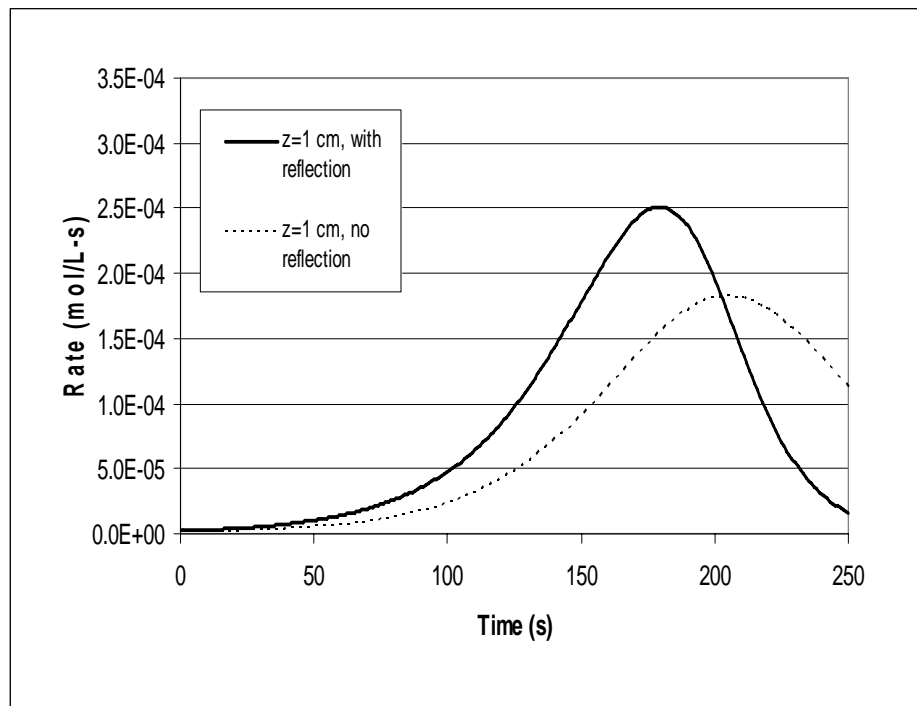


Figure 4.14. Rate of initiation as a function of time for a system with initiator concentration=0.01 mol/L.

$$I_{(z=0)} = 100 \text{ mW/cm}^2, z=1 \text{ cm}, \varepsilon_i = 525 \text{ L/mol-cm}.$$

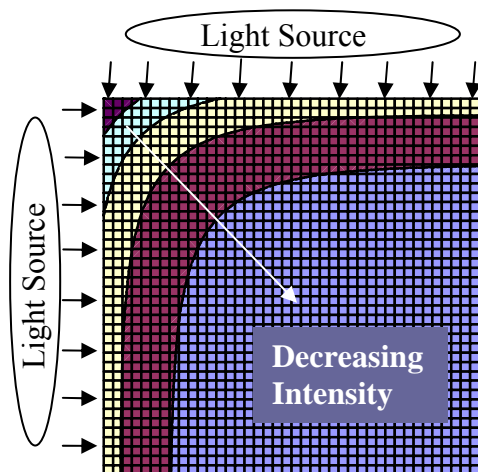


Figure 4.15. Two-dimensional model schematic with incident light on two perpendicular sides.

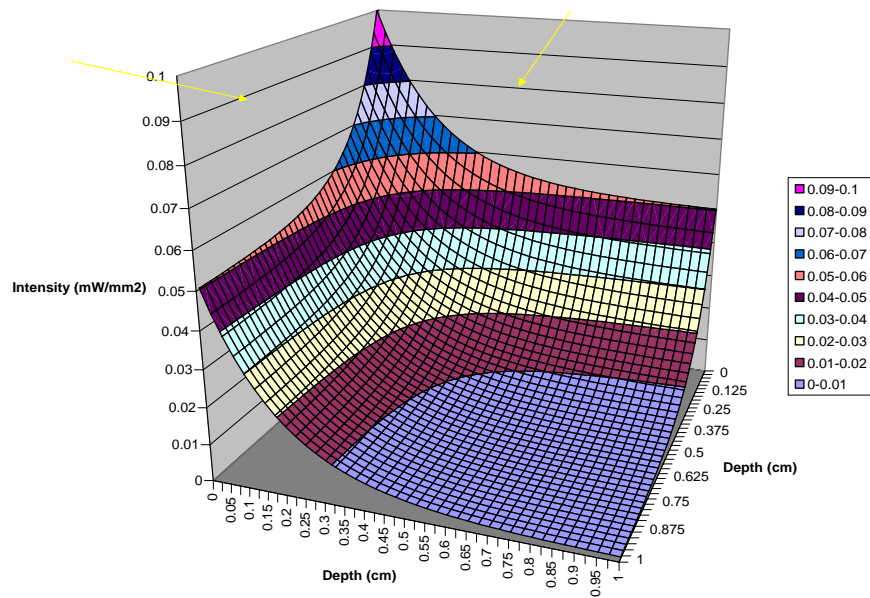


Figure 4.16. Light intensity profile at the instant the light sources are turned on for a two-dimensional sample in which light is incident on two perpendicular sides.

$C_{i0}=0.0268$ mol/L, $I=0.05$ mW/mm², $\lambda=366$ nm, $z=1.0$ cm, $\epsilon_i=20,000$ L/mol cm, $\epsilon_p=0$ L/mol-cm.

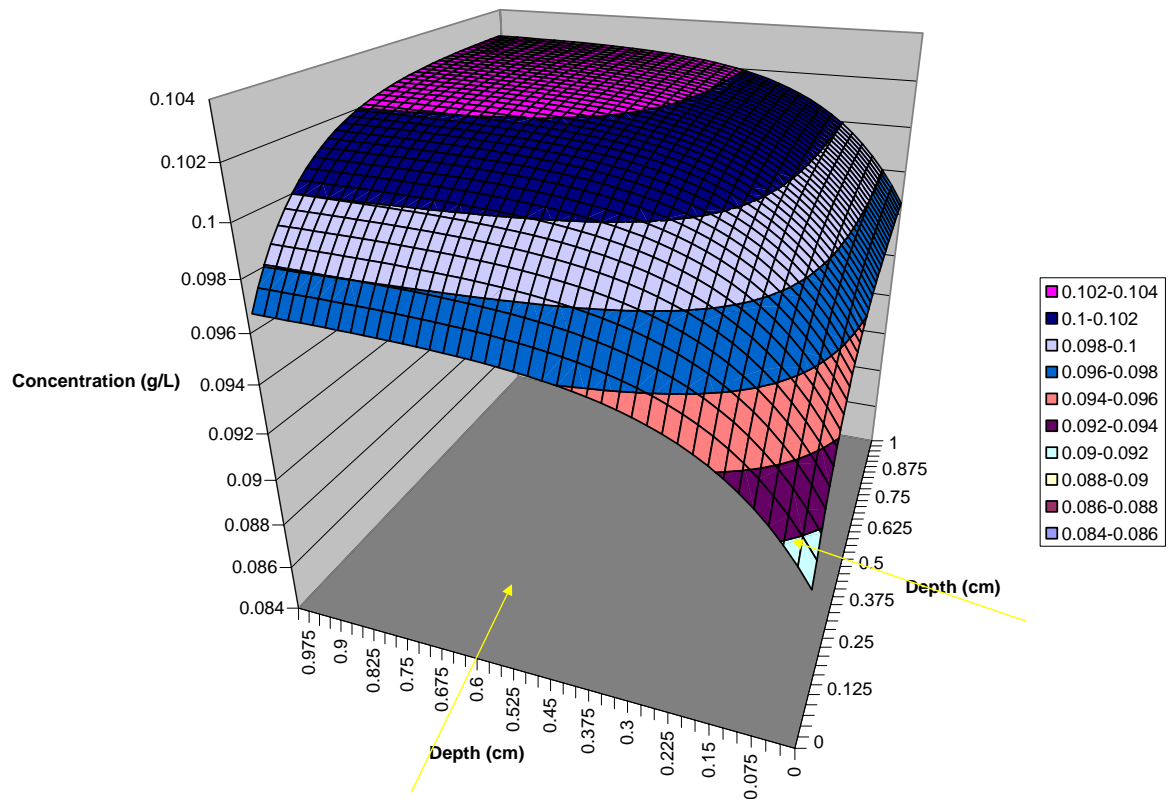


Figure 4.17. Concentration profile for a two-dimensional sample in which light is incident on two perpendicular sides.

$C_{i0}=0.0268$ mol/L, $I=0.05$ mW/mm², $\lambda=366$ nm, $z=1.0$ cm, $\epsilon_i=20,000$ L/mol cm, $\epsilon_p=0$ L/mol-cm.

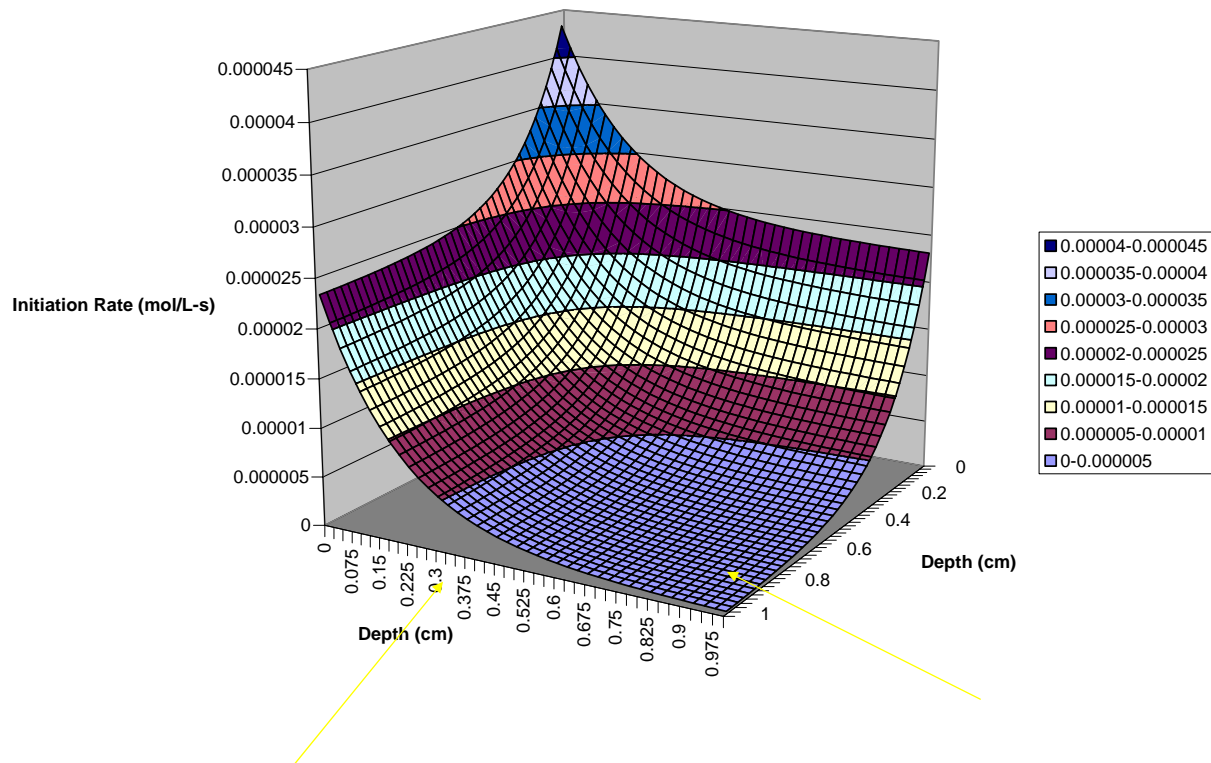


Figure 4.18. Initiation rate profile for a two-dimensional sample in which light is incident on two perpendicular sides.

$C_{i0}=0.0268$ mol/L, $I=0.05$ mW/mm², $\lambda=366$ nm, $z=1.0$ cm, $\epsilon_i=20,000$ L/mol cm, $\epsilon_p=0$ L/mol-cm.

CHAPTER 5 SPATIAL AND TEMPORAL EVOLUTION OF THE PHOTOINITIATION RATE FOR THICK POLYMER SYSTEMS ILLUMINATED WITH POLYCHROMATIC LIGHT

5.1. Introduction

As described previously, for thick systems, a significant light intensity gradient may arise which leads to an inherently non-uniform initiation rate profile that is exceptionally complex. Consequently, a fundamental understanding of the effects of a host of variables on the initiation behavior is needed in order to effectively design reaction systems. For this reason, several research groups have developed fundamental descriptions of how the rate profiles evolve with time, and have shown that the initiation rate is highly non-uniform in thick systems and resembles an initiation wave front that moves from the illuminated surface through the depth of the sample.^{15-17, 19-20} A number of contributions have revealed how variables such as initiator concentration, initiator molar absorptivity, and incident light intensity affect the height and breadth of the initiation front for perfectly bleaching systems illuminated from one side^{15-16, 19-20} as well as more general systems.^{17, 28} All of these papers have effectively considered monochromatic illumination characterized by a single absorption coefficient.

Most photopolymerizations are performed using a light source that emits over a range of wavelengths and photoinitiation with polychromatic light is considerably more complex than the monochromatic cases considered to date. For example, the most common UV light sources are medium pressure mercury-xenon (Hg-Xe) arc lamps which have prominent emissions between 200-600 nm, and the emerging light-

emitting diode (LED) sources typically emit with a significant (~ 40 nm) bandwidth. Only lasers and excimer lamps strictly emit at a single wavelength, and these sources are too costly for many applications. For the common, polychromatic light sources it is necessary accurately account for all of the incident wavelengths to understand the initiation system in a way which allows appropriate components to be selected. Modeling this case is complicated by a number of factors. For example, each incident wavelength has a unique intensity. Also, the initiator absorbs each wavelength to a different degree and photobleaches to different extents. Additionally, the contribution of one wavelength on the resulting photoinitiation rate is influenced by the intensities at all other wavelengths (due to their effect on the initiator concentration).

In this chapter, the effect of polychromatic illumination on the initiation of thick polymer systems (~ 1 cm) is examined by expanding the previously reported description of the temporal evolution of the light intensity gradient, the initiator concentration gradient, and the photoinitiation rate profile in photobleaching systems.¹⁸ The analysis reveals that the photoinitiation rate profile obtained with polychromatic illumination is considerably different than the sum of the monochromatic profiles, and that there may be a synergistic effect with some wavelengths promoting surface cure while others enhance the photoinitiation deep in the sample. This chapter begins with the presentation of the governing set of coupled differential equations, then representative simulation results are presented for three cases of increasing complexity: two incident wavelengths of similar intensity but differing initiator molar absorptivity, multiple (five) incident wavelengths approximating a mercury lamp, and polychromatic illumination from a Hg-Xe lamp

accounting for every wavelength active for initiation. The simpler illumination cases are presented since they allow important principles and trends to be clearly illustrated, while the more detailed polychromatic case will be used in the next chapter to analyze and compare photoinitiator/light source combinations.

5.2. Governing Equations

The set of differential equations which govern the evolution of the light intensity gradient and initiator concentration gradient for multi-wavelength illumination are shown below. These equations were solved by method of finite differences.

$$\frac{\partial C_i(z, t)}{\partial t} = -\frac{C_i(z, t)}{N_A h} \sum_j \left(\frac{\varepsilon_{ij} \phi_j I_j(z, t)}{v_j} \right) + D_i \frac{\partial^2 C_i(z, t)}{\partial z^2} \quad (1)$$

$$\frac{\partial C_p(z, t)}{\partial t} = \frac{C_i(z, t)}{N_A h} \sum_j \left(\frac{\varepsilon_{ij} \phi_j I_j(z, t)}{v_j} \right) + D_p \frac{\partial^2 C_p(z, t)}{\partial z^2} \quad (2)$$

$$\frac{\partial I_j(z, t)}{\partial z} = -[\varepsilon_{ij} C_i(z, t) + A_{mj} + \varepsilon_{pj} C_p(z, t)] I_j \quad (3)$$

Here, the subscript j is an index with a different value for each wavelength of light under consideration; $C_i(z, t)$ is the initiator molar concentration at depth z and time t ; $C_p(z, t)$ is the photolysis product molar concentration at depth z and time t ; $I_j(z, t)$ is the incident light intensity of a specific wavelength at depth z and time t with units of energy/(area*time); ε_i is the initiator Napierian molar absorptivity of a specific wavelength with units of volume/(length*mole); ε_p is the photolysis product Napierian molar absorptivity of a specific wavelength with units of volume/(length*mole); ϕ_i is the quantum yield of the initiator at a specific wavelength, defined as the fraction of

absorbed photons that lead to fragmentation of the initiator; N_A is Avogadro's number; h is Planck's constant; ν is the frequency of light in units of inverse seconds; D_i is the diffusion coefficient of the initiator in units of length²/time; D_p is the diffusion coefficient of the photolysis products; and A_m is the absorption coefficient of the monomer and the polymer repeat unit with units of inverse length. Note that in this study the Napierian molar absorptivity was adopted molar absorptivity because it is most natural for the differential version of the absorption equation (equation 3). In the literature the decadic (base 10) molar absorptivity is commonly reported and should be converted to the Napierian value before using the model.

Comparison of equations 1 and 2 to those used in single wavelength descriptions^{17, 29} reveals that, in the polychromatic case, the absorbance terms must be summed over all incident wavelengths. Therefore, the description of the change in initiator concentration with respect to time at a given time and depth (equation 1) contains an absorbance term for each of the "j" distinct wavelengths (these terms are negative since the initiator is consumed) plus the term that accounts for diffusion of initiator against the gradient created by the previous consumption of the photoinitiator. As in the monochromatic case, equation 2 (dependence of the photolysis product concentration on illumination time at a specific time and depth) resembles equation 1, with the exception of the opposite sign on the absorbance terms since the photolysis products are created when the initiator is consumed.

For an accurate description of initiation with polychromatic illumination, the light intensity gradient of each incident wavelength must be individually described. As shown in equation 3, the intensity of an individual wavelength is attenuated by

absorption of the initiator, monomer and polymer repeat units, and the photolysis product. Since the local initiator concentration depends upon all of the incident wavelengths, and the local light intensity of each wavelength depends upon the initiator concentration, the time-evolution of all of the light intensities are coupled to one another, and therefore the complete set of differential equations must be solved simultaneously. Therefore, the wavelength dependence of the intensity considerably increases the complexity of the model; for description of n wavelengths of incident light, $n+2$ equations must be solved simultaneously (typically a 100 nm region of the spectrum is important, therefore in excess of 100 equations must be simultaneously solved).

The following initial and boundary conditions apply to this system:

$$C_i(z,0) = C_o \quad (4);$$

$$C_p(z,0) = 0 \quad (5);$$

$$\frac{\partial C_{i,p}}{\partial z} = 0 \text{ at } z = 0 \text{ and } z = z_{\max} \quad (6);$$

$$I(0, t) = I_o \quad (7).$$

Equation 4 states that the initial initiator concentration is uniform throughout the depth of the sample. Similarly, equation 5 indicates that the initial photolysis product concentration is zero. Equation 6 is the no-flux boundary condition indicating that there is no diffusion through the ends of the sample, and equation 7 states that at any time, the intensity on the surface of the sample where the light enters is equal to the initial intensity of the light source.

The rate of production of free radicals as a function of depth was also considered in this study and is defined by equation 8.

$$R_i(z, t) = 2C_i(z, t) \sum_j [I(z, t)]_j \phi_j \varepsilon_{ij} \quad (8)$$

This defines the instantaneous local rate of production of free radicals, $R_i(z, t)$, if two active centers are produced upon fragmentation of the initiator.

Solution of this set of equations provides detailed information regarding the time-evolution of the light intensity gradient, the initiator concentration gradient, and the photoinitiation rate profile (rate of active center generation as a function of time and location). Once active centers are generated, the subsequent reaction events (propagation, termination, chain transfer, *etc*) are the same for either thick or thin polymerization systems and have been extensively investigated in literature.^{18, 30-31}

5.3. Results and Discussion

To investigate the photoinitiation rate profiles for thick systems, the following model system was selected: a thick polymerization system (typically 1 cm thick) of rectangular cross-section subject to uniform polychromatic illumination normal to the top surface. In a previous contribution,¹⁷ this polymerization geometry was examined in detail for photoinitiation using monochromatic light. In this paper, we will keep the same sample geometry and will enhance the description by characterizing the impact of multiple incident wavelengths in order to clarify the effect of coupling of the various light intensity gradients through the initiator concentration gradient. Specifically, Equation 3 illustrates that at a given location and time, for each wavelength the change in intensity with depth depends upon the local concentrations of the initiator, photolysis products, and any other light-absorbing components as well as the corresponding molar absorptivities at the wavelength under consideration. In

addition, Equation 1 shows that the instantaneous rate of consumption of the photoinitiator depends upon the local initiator concentration as well as the local light intensity and initiator molar absorptivity at each of the incident wavelengths. As a consequence of these simultaneous differential relationships, the time evolution of the light intensity gradient at one incident wavelength is dependent on the light intensities and molar absorptivities of all incident wavelengths.

5.3.1. Initiation Rate Profiles for Simultaneous Illumination by Two Wavelengths

To fully explore the impact of simultaneous illumination by more than one wavelength it is useful to examine systems of increasing complexity. Therefore the simple case of illumination by two wavelengths of similar intensity but differing initiator molar absorptivity is considered first. A series of simulations was performed to compare the photoinitiation profile for two incident wavelengths to the corresponding monochromatic cases. Figure 5.1 contains plots of the photoinitiation rate as a function of distance from the illuminated surface (depth = 0 cm), and shows profiles for three different cases: two cases of monochromatic illumination at wavelengths λ_1 and λ_2 , and the case of simultaneous illumination at both wavelengths. In all cases the photon flux at each wavelength is 7.3×10^{-4} Einsteins/m²·s (corresponding to a typical intensity of ~ 25 mW/cm² for 350 nm light) and the photoinitiation profiles are shown for 200 seconds of illumination. For this illustrative example, the initiator molar absorptivity corresponding to λ_1 was set at a relatively low value of 1,000 L/mol·cm (Napierian), while the value corresponding to λ_2 is ten times greater.

For monochromatic illumination, the effect of the initiator molar absorptivity on the resulting photoinitiation rate profile is illustrated by the dashed lines in Figure 5.1. For example, if the incident wavelength corresponds to a low initiator molar absorptivity (such as λ_1 , the thin dashed line in Figure 5.1), the photoinitiation profile is broad with a relatively low peak rate which extends deep into the sample. In contrast, if the incident wavelength corresponds to a high initiator molar absorptivity (such as λ_2 , the thick dashed line in Figure 5.1), the photoinitiation profile is sharp and slow moving with a high peak photoinitiation rate. Therefore, illuminating with monochromatic light can either lead to modest initiation deep into the sample (if the incident wavelength corresponds to low initiator molar absorptivity) or substantial initiation primarily near the illuminated surface (for high initiator molar absorptivity); however, only one of these situations is possible.

In contrast, polychromatic light may simultaneously achieve both high initiation rates near the illuminated surface and enhanced initiation deep into the sample, as illustrated by the aggregate photoinitiation rate profile in Figure 5.1 (bold solid line). The most prominent difference between the aggregate profile arising from simultaneous illumination by λ_1 and λ_2 and the two profiles arising from monochromatic illumination is the coupling that occurs with the simultaneous illumination of multiple wavelengths. In the monochromatic cases, the two different initiator absorptivities lead to distinct fronts each characterized by a unique set of values for peak rate, breadth, and rate of progression through the sample. In contrast, the aggregate profile in Figure 5.1 is a single photoinitiation front (with a single maximum) that includes the synergistic effects of the wavelengths, thereby providing

both high initiation rates near the illuminated surface and enhanced initiation deep into the sample.

The aggregate photoinitiation rate profile in Figure 5.1 is comprised of the contributions from each incident wavelength. In Figure 5.1, the contribution from λ_1 (low initiator absorptivity) is shown by the thick gray line, while the contribution from λ_2 (high initiator absorptivity) is shown by the thin solid line. Comparison of the monochromatic photoinitiation rate profiles to the corresponding contributions to the polychromatic profile reveals that the two wavelengths behave very differently. For example, the photoinitiation rate profile for the λ_2 monochromatic illumination exhibits a higher peak photoinitiation rate, a slower progression through the sample, and narrower breadth than the λ_2 contribution to the polychromatic profile. Specifically, the ratios of the peak photoinitiation rate, peak location at 100 seconds, and profile breadth for the λ_2 monochromatic profile to the corresponding values for the λ_2 contribution to the polychromatic profile are 2.00, 0.51, and 0.50 respectively. In contrast, the photoinitiation rate profile for λ_1 monochromatic illumination actually exhibits a lower peak rate (by a factor of 0.63) and a larger breadth than the λ_1 contribution to the polychromatic profile. The only trend that matches for both λ_1 and λ_2 is the progression of the photoinitiation front through the sample. In both cases the monochromatic profile progresses at half the rate of the individual contributions to the polychromatic profile.

To understand the reasons for the trends described above, it is instructive to examine the impact of both incident wavelengths on the evolution of the photoinitiator concentration gradient (which in turn impacts the light intensity

gradient at each wavelength). Figures 5.2a and 5.2b contain this information for λ_1 and λ_2 , respectively. Each figure shows both the light intensity (solid lines, left ordinate) and the initiator concentration (dashed lines, right ordinate) as functions of depth for both monochromatic (marked by circles) and two-wavelength (no marker) illumination. For example, examination of Figure 5.2a reveals that for the low initiator absorptivity wavelength (λ_1), the breadth of the initiator concentration gradient is decreased by the addition of the second wavelength. Since λ_2 corresponds to a high initiator absorptivity, it leads to more rapid consumption of the initiator near the illuminated surface thereby altering the shape of the initiator concentration gradient. Figure 5.2a also shows that the increased consumption of initiator in the simultaneous illumination case causes the increase in the progression of the initiation wave front into the sample depth. The figure also illustrates why the peak initiation rate for the λ_1 contribution to the aggregate profile is higher than the peak rate in the λ_1 monochromatic profile. In both cases, in Figure 5.2a the peak rate occurs approximately where the light intensity and initiator concentration gradients cross. The initiator consumption near the illuminated surface (by λ_2) allows this intersection to occur at both a higher light intensity and a higher initiator concentration. Both of these effects lead to a higher peak photoinitiation rate since the photoinitiation rate is proportional to the product of the initiator concentration and light intensity. Examination of Figure 5.2b reveals that for the high initiator absorptivity wavelength (λ_2) the breadth of the initiator concentration gradient is actually increased by the addition of the second wavelength. In this case, the second wavelength, λ_1 , corresponds to a low initiator absorptivity, and leads to more rapid consumption of

the initiator deep into the sample where λ_2 does not reach. This initiator consumption deep into the sample (by λ_2) causes the intersection of the light intensity gradient and initiator concentration gradient to occur at both a lower light intensity and a lower initiator concentration. Both of these effects lead to a lower peak photoinitiation rate and explain why the trend exhibited by λ_2 is opposite that of λ_1 .

For photoinitiation in thick systems, it is generally important to have both efficient deep initiation and effective surface initiation. At the surface, active centers must be produced rapidly enough to overcome oxygen inhibition, therefore a sharp peak in the photoinitiation profile near the surface may be desirable until a solid polymer is formed to prevent further oxygen diffusion. For effective deep initiation, the photoinitiation profile should be broad enough to extend through a significant fraction of the sample, and should progress through the system at an acceptable rate. The above discussion has illustrated that it is possible to achieve initiation both at the surface and deep into the sample using two incident wavelengths which correspond to different initiator molar absorptivities, however the photoinitiation rate profile obtained when both wavelengths have the same photon flux may be skewed in favor of the high initiator molar absorptivity (surface initiation). For this reason it is interesting to examine the effect of the photon flux ratio on the resulting photoinitiation rate profiles.

Figure 5.3a – 5.3c shows the photoinitiation rate profile for three systems in which the photon flux for λ_1 (corresponding to low initiator absorptivity) is equal, double, and triple that of λ_2 (7.3×10^{-4} Einsteins/m²·s). Examination of Figure 5.3a illustrates that when the photon flux is equal for the two absorptivities, the overall

peak maximum is primarily due to the λ_2 , while λ_1 produces the low, broad leading edge of the profile. Increasing the photon flux of λ_1 to twice that of λ_2 , as in Figure 5.3b, shows that λ_1 becomes more important to the peak in the overall rate, shifting it away from λ_2 , and that more initiation occurs deep in the sample due to λ_1 . Finally, as shown in Figure 5.3c, increasing the photon flux of λ_1 to three times λ_2 reveals that the peak rate of λ_1 is actually higher than the peak rate of λ_2 , again shifting the peak of the overall rate away from λ_2 . Note that as the photon flux of λ_1 is increased, the profile of the λ_1 contribution to the overall rate becomes increasingly symmetrical. In the case of Figure 5.3c, although the broad leading edge is less realized, the initiation resulting from λ_1 in the deep parts of the sample is significant, and the progression of the rate profile through the depth is more efficient due to increase consumption of initiator. This illustrative example shows how the relative photon fluxes of two wavelengths with different absorptivities can lead to very different initiation profiles by shifting the relative impact of initiation resulting from illumination by each wavelength on the aggregate photoinitiation rate profile.

The above discussion illustrates that the relative intensities of the two incident wavelengths can have a marked effect on the shape of the photoinitiation rate profile, and the observed trends provide some guidance for selection of photoinitiation light sources. For simultaneous illumination by two initiating wavelengths, it is interesting to note that the absolute incident intensity (with the relative intensity held constant) also influences the shape of the photoinitiation rate profile. For monochromatic illumination, the absolute intensity has little effect on the shape of the photoinitiation rate profile. As the incident intensity is increased, the peak photoinitiation rate in

increased and the rate of progression through the sample is enhanced, however the breadth and general shape of the profile are essentially unchanged. Figure 5.4 illustrates that the situation is very different for simultaneous illumination by two wavelengths. Figure 5.4 contains a series of profiles obtained using the same relative intensities used previously for Figure 5.3, but with an absolute photon flux that is 2.5 times lower. Comparison of Figure 5.4 to Figure 5.3 illustrates the expected results that a lower absolute photon flux leads to a lower peak photoinitiation rate and a slower progression of the photoinitiation wave through the sample. In addition, the simulation results reveal that the lower absolute photon flux results in an aggregate photoinitiation rate profile that accentuates the contribution of λ_2 (high molar absorptivity). The differences in the shapes of the profiles in Figures 5.3 and 5.4 ultimately arise from the effects of the coupling of the two light intensity gradients through the initiator concentration gradient. At the lower absolute photon flux, the rate of consumption of the photoinitiator deep into the sample (due to absorption of λ_1) is reduced, and therefore the presence of the light at wavelength λ_1 has a reduced effect on the light at wavelength λ_2 . This influence of the absolute photon flux on the shape of the photoinitiation rate profile has some interesting practical implications. For example, a single light source could be used at the beginning of a polymerization to accentuate surface initiation, then a second lamp could be added to enhance deep cure. These results also help to illustrate that the coupling that occurs during polychromatic illumination leads to complex effects that are difficult to generalize without completely solving the set of differential equations for the specific set of conditions under consideration.

5.3.2. Initiation Rate Profiles for Simultaneous Illumination by Multiple Wavelengths

The previous section illustrated trends in the photoinitiation rate profile for the relatively simple case of simultaneous illumination by two incident wavelengths of differing initiator molar absorptivity but similar photon flux. In this section, the complexity of the system is enhanced by considering multiple incident wavelengths. Specifically, simulations were performed for a hypothetical photopolymerization in which the incident light occurs at five peaks centered at the five prominent emission wavelengths of a Hg-Xe lamp (303, 313, 334, 365, and 405 nm). This illustrative example is based upon a hypothetical perfectly bleaching photoinitiator that exhibits an absorbance spectrum similar to a typical phosphine oxide photoinitiator. Table 1 provides a summary of the initiator molar absorptivities and incident light intensities used in this representative analysis.

Figures 5.5a and 5.5b show the overall initiation rate of the system described in Table 1 after 10 seconds and 100 seconds of illumination, respectively. In these plots, the ordinate corresponds to the aggregate rate of photoinitiation arising from all incident wavelengths, while the abscissa represents the depth into the sample (a depth of zero corresponds to the illuminated surface). In general, the shape of the photoinitiation rate profile is broadened due to the contributions of several different wavelengths. These contributions to the aggregate photoinitiation rate by each of the five incident wavelengths are shown in Figures 5.5c and 5.5d at 10 and 100 seconds of illumination, respectively. The most prominent contributions to the overall rate come from the wavelengths which have the highest photon flux (313 and 365 nm). The contribution from the 303 nm wavelength reinforces the 313 nm contribution,

since the molar absorptivities are nearly the same (if two wavelengths correspond to the same initiator molar absorptivity they are effectively combined in the model). Figure 5.5d also shows that although the intensity of the 405 nm wavelength is low, its contribution extends deep into the sample, and is a major contributor (>50%) to the (small) photoinitiation rate at the far side of the sample. The 334 nm wavelength corresponds to an intermediate absorptivity and therefore always overlaps with contributions from other wavelengths. The intensity of this wavelength is very low and consequentially the contribution to the overall rate is essentially negligible.

The initiator concentration plays a key role in the effectiveness of photoinitiation in thick systems. Generally, the initiator concentration for thick systems is much lower than commonly used for polymerization of films and coatings (~10 times less). For thick systems the photoinitiator concentration must be low enough to allow efficient penetration of light into the deep parts of the sample, but still must be high enough to produce sufficient active centers for effective initiation. Figure 5.6 illustrates the contributions to the aggregate photoinitiation rate of the system described in Table 1, but with a concentration 2.5 times higher than the system shown in Figure 5.5. The increased concentration accentuates the contributions of the wavelengths corresponding to high initiator molar absorptivities (303 and 313 nm). Therefore, the aggregate photoinitiation rate profile in Figure 5.6 (bold solid line) exhibits a higher peak rate, a narrower width, and a slower progression through the sample than the aggregate profile in Figure 5.5. At the higher initiator concentration the wavelengths corresponding to lower initiator molar absorptivities (365 and 405 nm) do not penetrate as far into the deep portions of the

system, therefore the leading edge of the photoinitiation profile is less pronounced (for example, after 100 seconds essentially no initiation occurs in the back half of the system). These simulation results illustrate that for each polymerization system under consideration, the initiator concentration must be optimized in order to achieve a sufficient peak rate, suitable penetration of light into the deep portions of the sample, and efficient progression of the photoinitiation rate profile through the sample depth.

5.3.3. Initiation Rate Profiles for Polychromatic Illumination

The previous sections have illustrated that photopolymerization initiated with polychromatic light is considerably more complex than the monochromatic case. The relative contribution of an individual wavelength to the photoinitiation rate profile not only depends upon the incident intensity and the initiator molar absorptivity at that wavelength, it also depends upon the intensity and initiator molar absorptivity of all other incident wavelengths. As a consequence, the shape and attributes of the aggregate photoinitiation rate profile may change markedly if any of a number of variables are changed, including the relative intensities, the absolute intensity, initiator concentration, *etc.* The simulations of the relatively simple, idealized systems shown thus far have illustrated some of these effects, and therefore provide much more information than the monochromatic descriptions available previously. However, the multi-wavelength descriptions presented thus far are still simplified representations of a continuous emission spectrum from a lamp. For example, emissions from real lamps are not a series of delta functions; in actuality, each emission peak has a breadth (perhaps ranging from 3-40 nm), and the initiator molar absorptivity may vary over the breadth of this emission. Therefore, a more complete

description of photoinitiation using polychromatic light that considers every wavelength within the region active for initiation (at 1 nm increments) is presented. This more complete model allows the incident intensity and initiator molar absorptivity at each wavelength to be independently specified. In addition, the inclusion of non-perfectly-bleaching photoinitiators will be illustrated by including the wavelength-dependent absorption by the photolysis products.

The complete, polychromatic description of photoinitiation can be applied to any combination of monomer, initiator, and light source as long as the absorption and emission properties are known. To illustrate the approach, simulation results will be presented based upon the commercially available initiator, diphenyl (2,4,6-trimethylbenzoyl)-phosphine oxide (TPO) and a medium pressure 200 Watt Hg-Xe arc lamp (Oriel). The molar absorptivity of TPO and its photolysis products was determined at one nanometer increments using an Agilent UV-Visible spectrometer, as shown in Figure 5.7. This initiator was chosen because it absorbs between 300 – 420 nm where the light source emits. Note that the absorbance of the photolysis products is significantly lower than that of photoinitiator at all wavelengths between 300 and 420 nm. This photobleaching behavior allows light to penetrate more deeply into the sample and is essential for photoinitiation in thick samples. The relative emission intensity of the Hg-Xe lamp was determined at one nanometer increments using an Ocean Optics spectrometer. For simulations of photopolymerizations initiated using the Hg-Xe lamp, an effective wavelength range of 300 to 420 nm was chosen since wavelengths shorter than 300 are generally removed by monomer absorbance (acrylate monomers generally absorb below 300 nm and recall that the

monomer is ~ 1000 times more concentrated than the initiator), and wavelengths longer than 420 are not absorbed by TPO.

Figure 5.8a shows a series of aggregate photoinitiation rate profiles at four different times for a one centimeter sample illuminated with a medium pressure 200 W Hg-Xe arc lamp (94 mW/cm^2) and initiated using a hypothetical perfectly photobleaching initiator (with the initiator molar absorptivity of TPO, but absorption by photolysis products neglected). The general shape of the photoinitiation rate profile in Figure 5.8a is similar to those shown in previous cases (Figures 5.3-5.6): non-symmetrical with a long leading edge which extends into the deeper parts of the sample; however the photoinitiation rate profile for polychromatic illumination is considerably broader due to the additive contributions of many more wavelengths. Figures 5.8b and 5.8c show the contribution to the aggregate photoinitiation rate from the 313 nm peak (effectively 308 – 318 nm) and 365 nm peak (effectively 360 – 370 nm), respectively. Just as in the simplified multi-wavelength case, the 313 nm and 365 nm emission bands account for $\sim 70\%$ of the incident light, and therefore produce the majority of the active centers near the surface (308 – 318 nm) and deeper into the sample (360 – 370 nm).

For an accurate description of photoinitiation using TPO, it is necessary to include the absorption by the initiator photolysis products (the dashed line in Figure 5.7), and these simulation results are shown in Figure 5.9 for the same conditions used previously for Figure 5.8. Figure 5.7 illustrates that the extent of photobleaching is wavelength dependent: for example, upon photolysis the molar absorptivity is decreased by $\sim 80\%$ at 313 nm, $\sim 95\%$ at 365 nm, and is essentially perfectly bleaching

for wavelengths above 375 nm. Comparison of the photoinitiation rate profiles in Figure 5.9a to those in Figure 5.8a illustrates this absorption by the photolysis products leads to a reduction in the peak photoinitiation rate at a given time, and leads to a broadening and flattening of the aggregate rate profile. It is interesting to note that the inclusion of the photolysis product absorption leads to a significant change in the shape of the photoinitiation rate profile with the greatest impact near the photoinitiation rate peak since this is where there is the largest change in the product of the local initiator concentration and light intensity (including all incident wavelengths). Comparison of Figures 5.9b and 5.9c to Figures 5.8b and 5.8c reveals that the wavelength-dependent photobleaching leads to a pronounced effect on the contribution from the 313 nm emission band (~80% bleaching) and a milder impact on the contribution from 365 nm (~95% bleaching).

5.4. Conclusions

In this contribution we have presented a mathematical description of the evolution of the photoinitiation rate profile for thick photopolymerization systems illuminated with polychromatic light. The simulations show that the photoinitiation rate profile for polychromatic illumination is much different than in systems illuminated by monochromatic light. Moreover, the results are complicated by the coupling of the light intensity gradients through the initiator concentration gradient. For this reason, we continually increase the complexity of the model from two-wavelength illumination, to five-wavelength illumination, and finally to continuous

spectrum illumination in order to fully demonstrate the effects of polychromatic illumination on the resulting photoinitiation rate profile.

Illumination with two wavelengths (high and low initiator molar absorptivity) can synergistically cause both a high rate of surface initiation and active center production in the deep portions of the sample. The presence of one incident wavelength affects all other incident wavelengths by altering the initiator concentration gradient. These simulations also illustrate that changes in either the relative and absolute incident intensities affect the relative importance of a particular wavelength to the aggregate photoinitiation profile.

Increasing the complexity of the model to include five incident wavelengths broadened the overall photoinitiation rate profile into a single, unified wave front. Wavelengths corresponding to high intensities had the largest impact on the shape of the overall rate profile, while contributions from wavelengths corresponding to similar initiator molar absorptivities essentially combined with one another. The initiator concentration has a marked effect on contributions of each wavelength to the overall photoinitiation rate profile. High initiator concentrations allow less light, regardless of absorptivity, to penetrate into the system, causing less active center generation in the deep portions of the sample, while low concentrations do not produce high rates of active center production at any depth or time.

Finally, a complete and accurate description of photoinitiation using polychromatic light was presented in which each wavelength within the region active for initiation was considered (300-420 nm) and the incident intensity and initiator molar absorptivity at each wavelength could be independently specified. Inclusion of

the continuous spectrum of incident wavelengths broadened and flattened the photoinitiation rate profile, and absorption by the photolysis products effectively filtered some incident wavelengths.

The simulation results presented here illustrated that for photoinitiation of thick systems with polychromatic light, the shape and attributes of the aggregate photoinitiation rate profile may change markedly if any of a number of variables are changed, including the relative intensities, the absolute intensity, initiator concentration, degree of photobleaching, *etc.* To optimize the selection of monomers, initiators, and light sources for thick photopolymerization systems, it is important to understand these effects. The complete, polychromatic description of photoinitiation presented here can be applied to any combination of monomer, initiator, and light source as long as the absorption and emission properties are known, and may provide an invaluable tool for design of these systems.

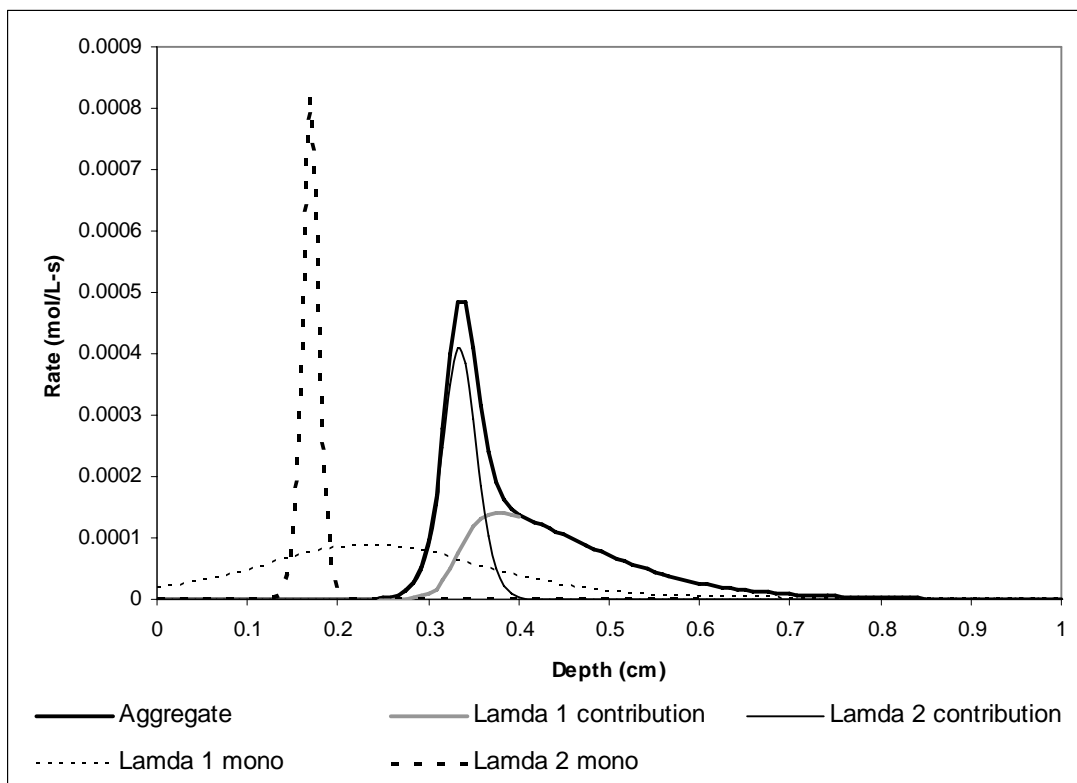


Figure 5.1. Photoinitiation rate profiles for three different cases: two cases of monochromatic illumination at wavelengths λ_1 and λ_2 , and the case of simultaneous illumination at both wavelengths.

In all cases the photon flux at each wavelength is 7.3×10^{-4} Einsteins/m²·s (corresponding to the typical intensity of ~ 25 mW/cm² for 350 nm light). The initiator molar absorptivity corresponding to λ_1 and λ_2 are 1,000 and 10,000 L/mol-cm, respectively. The initiator concentration is 0.012 mol/L, and $\epsilon_p = 0$ L/mol-cm for all cases.

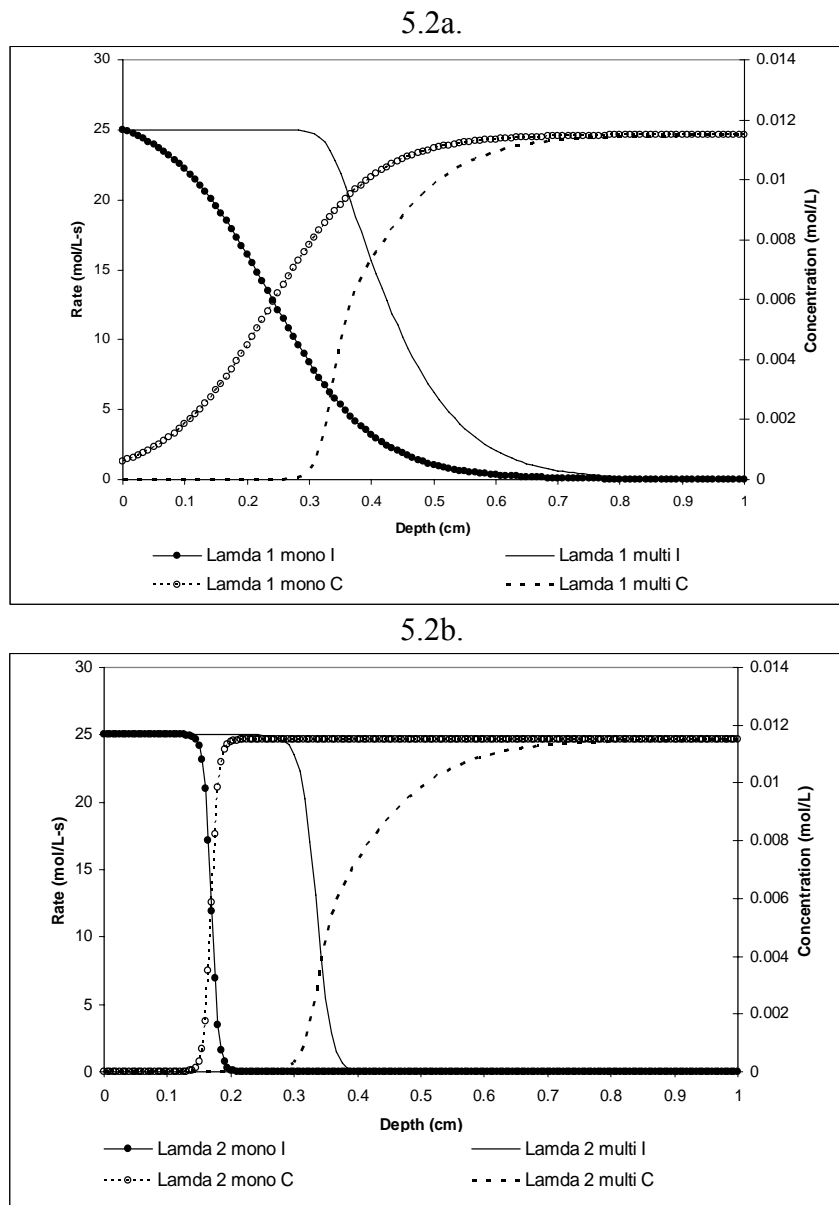
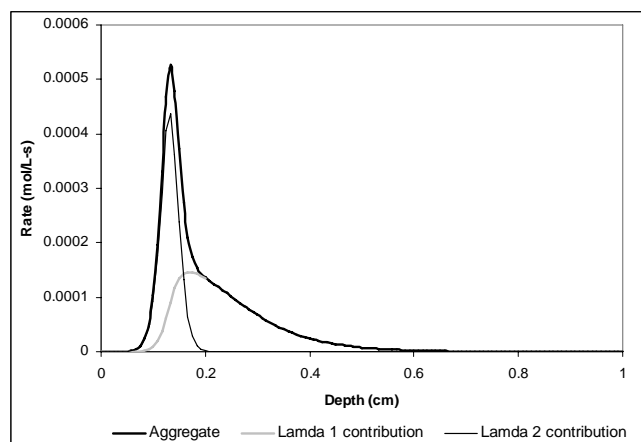
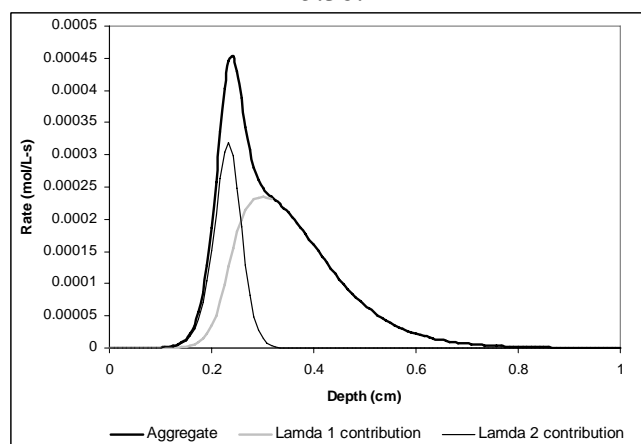


Figure 5.2. Intensity (—) and concentration (---) gradients of monochromatic (●,○) and multi-wavelength (no marker) illumination after 100 seconds of illumination for (a) λ_1 and (b) λ_2 wavelengths.

5.3a.



5.3b.



5.3c.

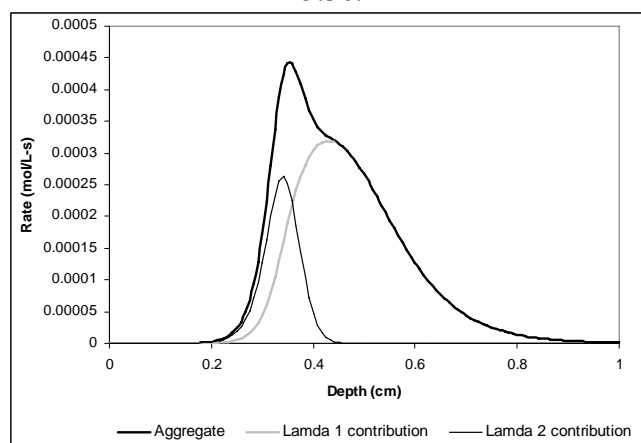
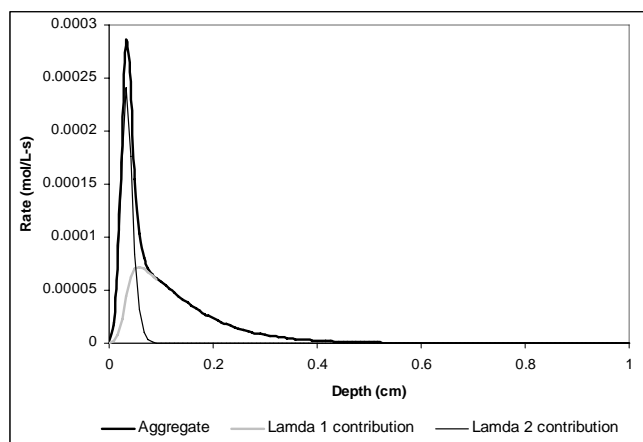


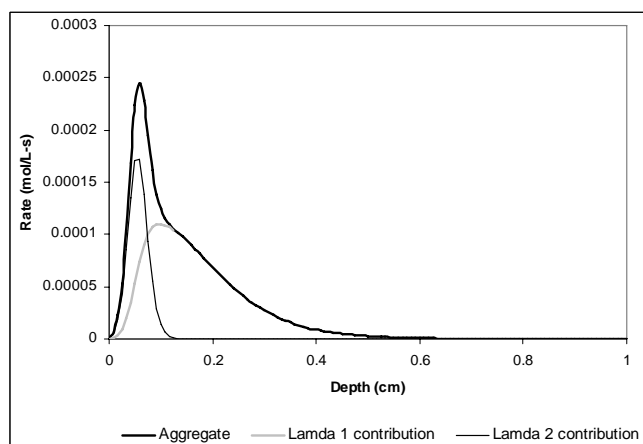
Figure 5.3. Photoinitiation rate profiles after 100 seconds of illumination for three different cases: (a) equal photon flux, (b) λ_1 with twice the photon flux of λ_2 , and (c) λ_1 with three times the photon flux of λ_2 (7.3×10^{-4} Einsteins/ $m^2 \cdot s$).

The initiator molar absorptivity corresponding to λ_1 and λ_2 are 1,000 and 10,000 L/mol-cm, respectively. The initiator concentration is 0.012 mol/L, and $\epsilon_p = 0$ L/mol-cm for all cases.

5.4a.



5.4b.



5.4c.

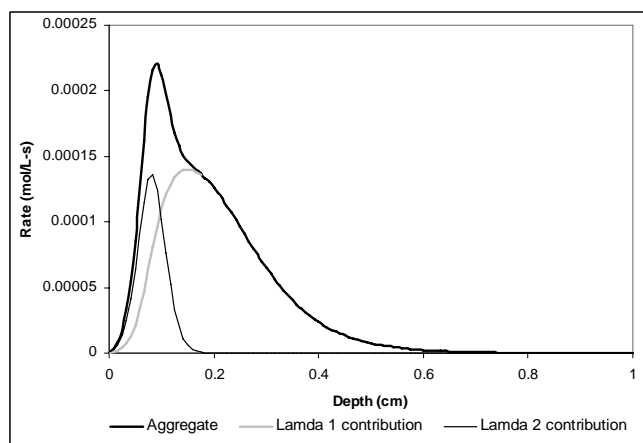


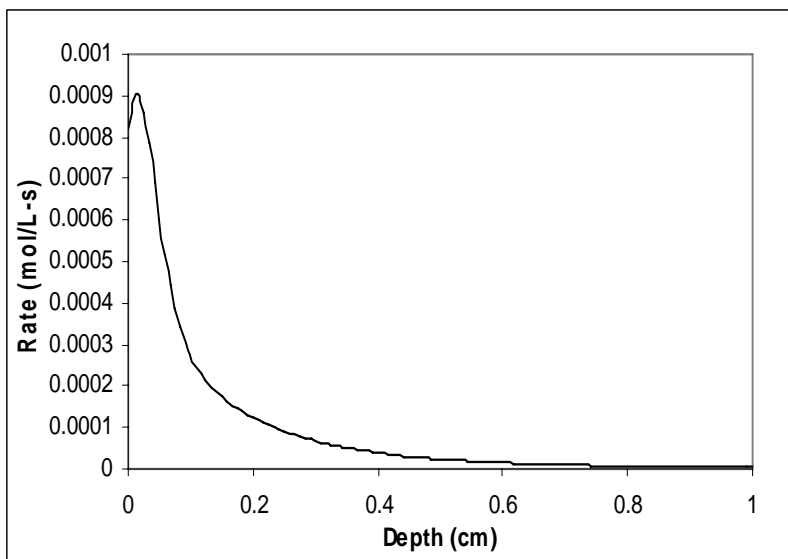
Figure 5.4. Photoinitiation rate profiles after 100 seconds of illumination for three different cases: (a) equal photon flux, (b) λ_1 with twice the photon flux of λ_2 , and (c) λ_1 with three times the photon flux of λ_2 (2.9×10^{-4} Einsteins/ $\text{m}^2 \cdot \text{s}$).

The initiator molar absorptivity corresponding to λ_1 and λ_2 are 1,000 and 10,000 L/mol-cm, respectively. The initiator concentration is 0.012 mol/L, and $\epsilon_p = 0$ L/mol-cm for all cases.

Table 5.1. Values used for modeling a perfectly bleaching multi-wavelength illumination system including incident wavelength (λ); intensity (I_0); initiator quantum yield (Φ), and the Napierian molar absorptivities (ϵ_i).

| λ (nm) | I_0 mW/cm ² | Φ | ϵ_i (L/mol·cm) |
|-------------------|-----------------------------|--------|----------------------------|
| 303 | 15 | 0.2 | 4,100 |
| 313 | 30 | 0.2 | 3,300 |
| 334 | 4 | 0.2 | 1,000 |
| 365 | 40 | 0.2 | 600 |
| 405 | 11 | 0.2 | 200 |

5.5a. 10 seconds of illumination.



5.5b. 100 seconds of illumination.

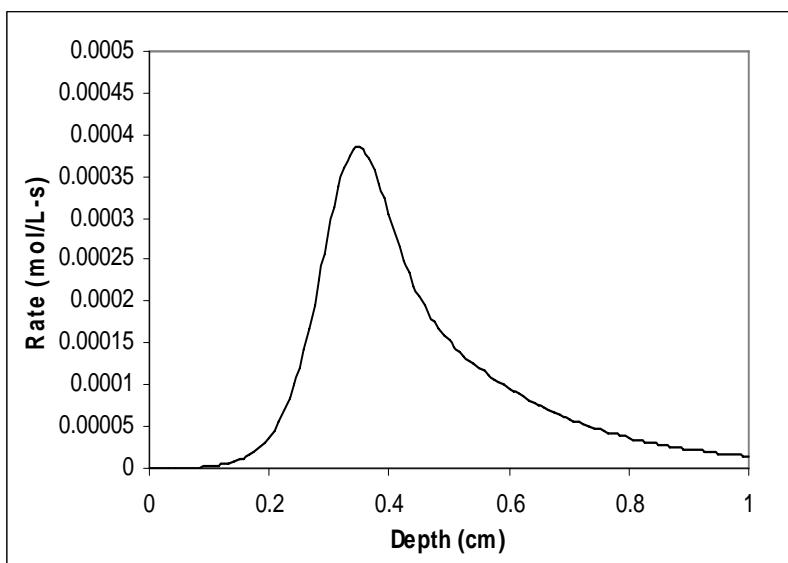
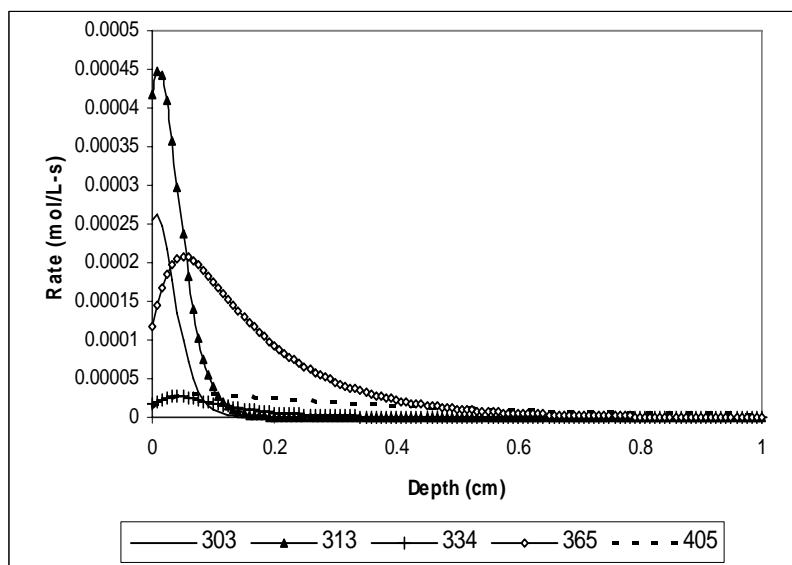


Figure 5.5. Photoinitiation rate profiles for simultaneous multi-wavelength illumination for the system described in Table 5.1.

The initiator concentration is 0.012 mol/L, and $\epsilon_p = 0$ L/mol-cm for all five wavelengths. The aggregate photoinitiation rate profiles at 10 and 100 seconds of illumination are shown in (a) and (b), respectively. The contributions of each wavelength at 10 and 100 seconds of illumination are illustrated in (c) and (d), respectively.

5.5c. 10 seconds of illumination.



5.5d. 100 seconds of illumination.

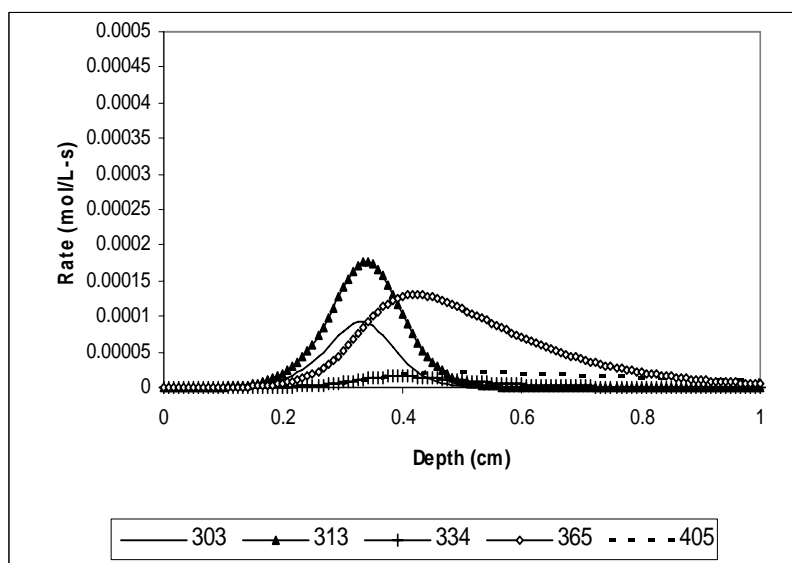
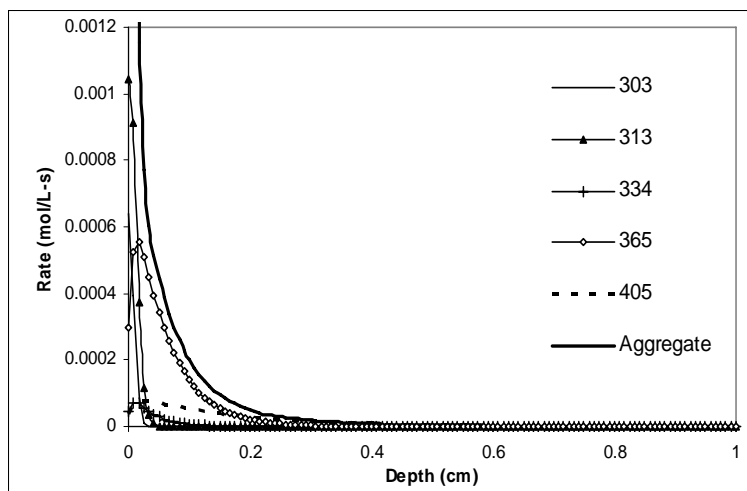


Figure 5.5. Continued.

5.6a. 10 seconds of illumination



5.6b. 100 seconds of illumination

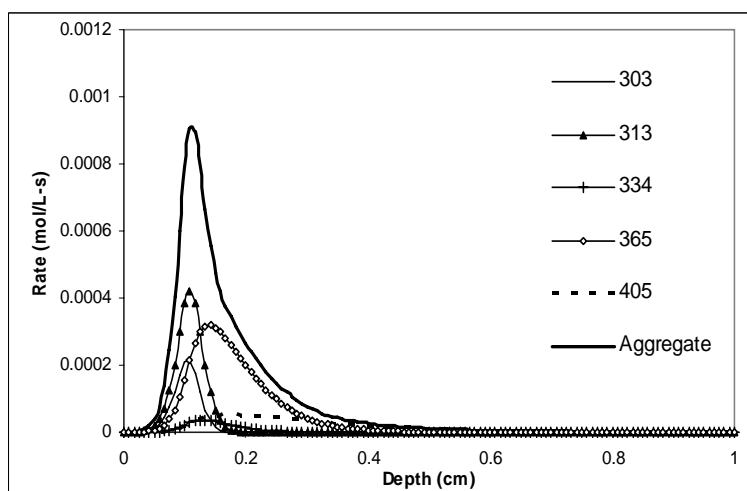


Figure 5.6. Photoinitiation rate profiles for simultaneous multi-wavelength illumination for the system described in Table 5.1.

The initiator concentration is 0.03 mol/L, and $\epsilon_p = 0$ L/mol-cm for all five wavelengths. The contributions of each wavelength and the aggregate photoinitiation rate are illustrated in (a) and (b) for 10 and 100 seconds of illumination, respectively.

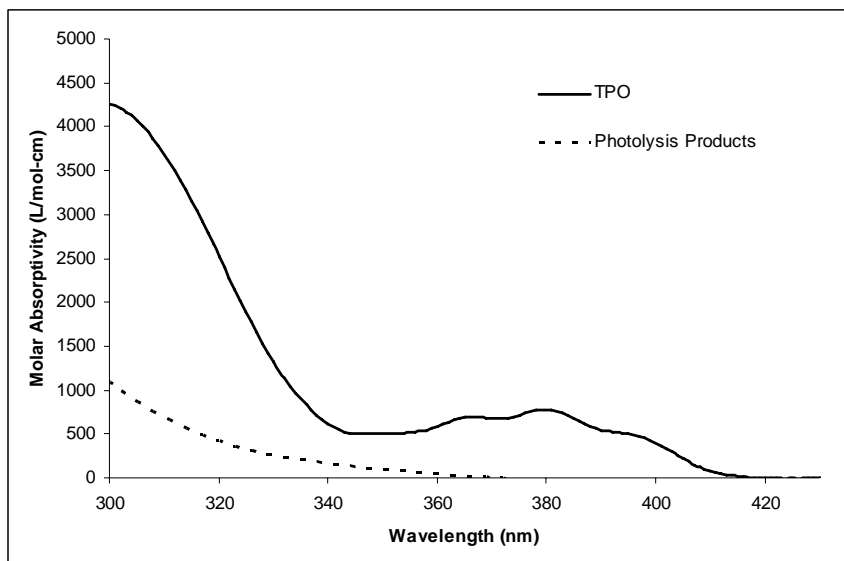
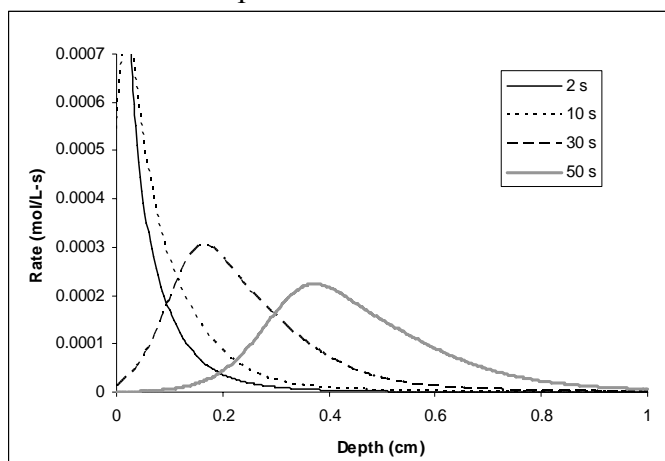
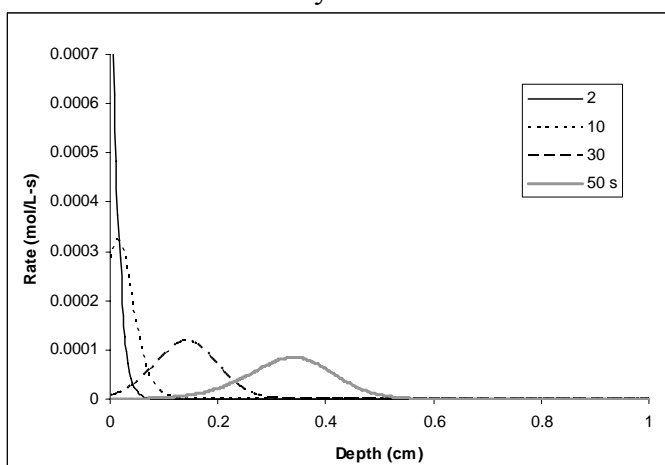


Figure 5.7. Molar Absorptivity of TPO (—) and its photolysis products (---), 0.013% in methanol.

5.8a. Composite Photoinitiation Rate



5.8b. Photoinitiation by 308-318 nm contribution



5.8c. Photoinitiation by 360-370 nm contribution

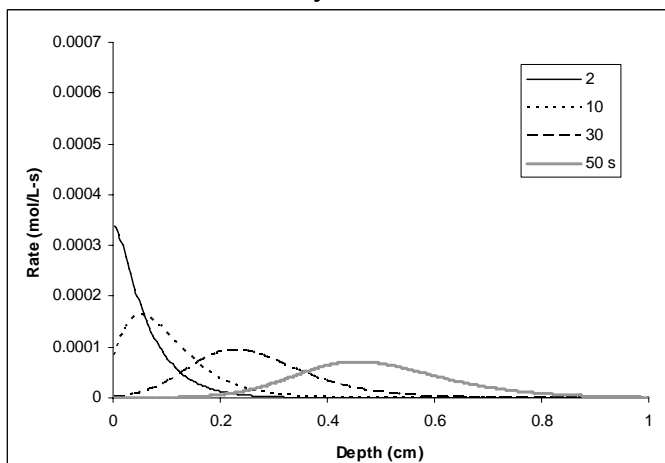
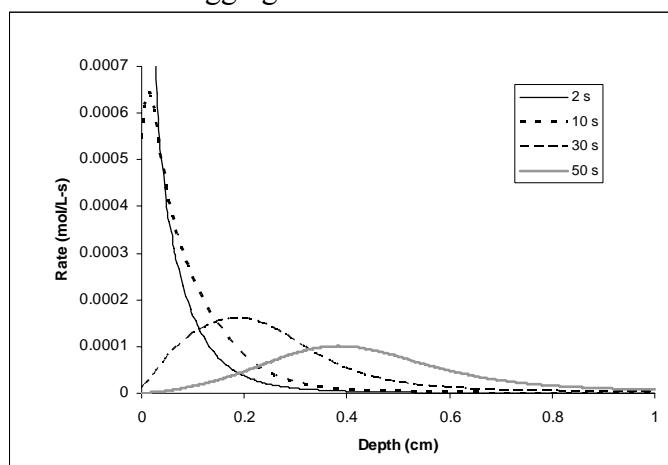


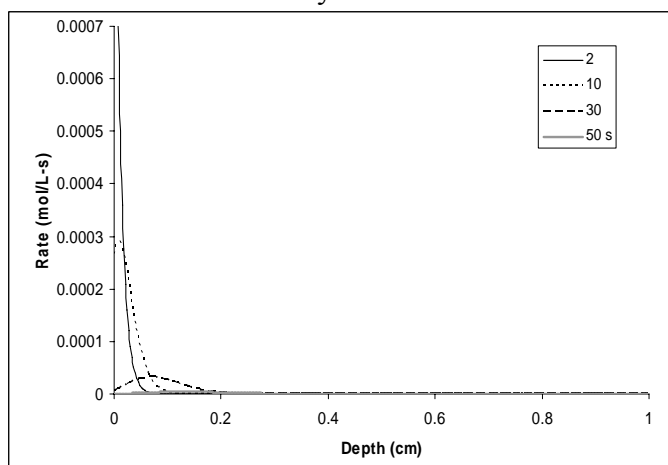
Figure 5.8. Photoinitiation of a system initiated with TPO using a medium pressure 200 W Hg-Xe arc lamp.

$I_0 = 94 \text{ mW/mm}^2$, $C_0 = 0.0268 \text{ mol/L}$, $\phi = 0.2$, ϵ_i as shown in Figure 5.7, $\epsilon_p = 0 \text{ L/mol-cm}$.

5.9a. Aggregate Photoinitiation Rate



5.9b. Photoinitiation by 308-318 nm contribution



5.9c. Photoinitiation by 360-370 nm contribution

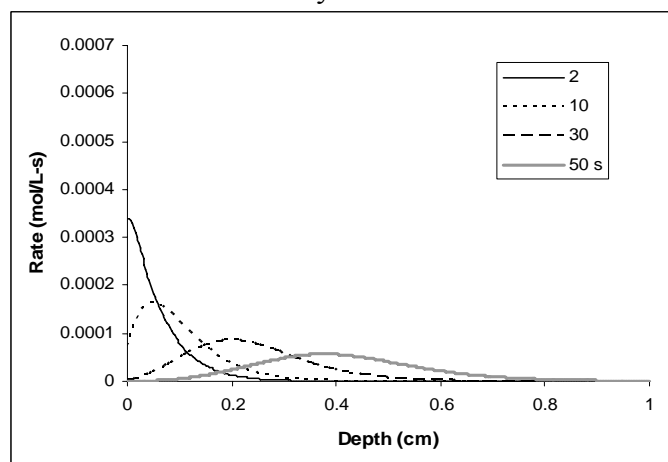


Figure 5.9. Photoinitiation of a system initiated with TPO using a medium pressure 200 W Hg-Xe arc lamp.

$I_0 = 94 \text{ mW/mm}^2$, $C_0 = 0.0268 \text{ mol/L}$, $\phi = 0.2$, ϵ_i and ϵ_p as shown in Figure 5.7.

CHAPTER 6

MODELING OF THE PHOTOINITIATION RATE IN REAL THICK POLYMER SYSTEMS ILLUMINATED WITH POLYCHROMATIC LIGHT

6.1. Introduction

In order to provide guidelines for the efficient and effective photoinitiation of thick polymer systems, a dimensionless, generalized description of the photoinitiation of thick systems would be convenient. Although this type of analysis may be interesting in the case of a perfectly bleaching photoinitiator illuminated with monochromatic light where the system can be described with a single value for initiator absorptivity as well as intensity of a single wavelength, a polychromatic system is not conducive to such a model. The separate initiator and product absorptivities and intensities at each wavelength are not additive properties, so a single value characterizing these properties would not describe the system accurately. Photoinitiation with polychromatic light is considerably more complicated than the monochromatic case because each incident wavelength has a unique intensity; also, the initiator absorbs each wavelength to a different degree and photobleaches to different extents. Additionally, the contribution of one wavelength on the resulting photoinitiation rate is influenced by the intensities at all other wavelengths (due to their effect on the initiator concentration as described in Chapter 5). Indeed, it is necessary to separately model each system of interest using an initiator's unique absorbance pattern and a light source's unique emission profile to adequately describe a particular system.

In this chapter, the effect of polychromatic illumination on the initiation of thick polymer systems (~1 cm) is examined by modeling several common photoinitiators and two common lamps. Since most photopolymerizations are performed using a light source that emits over a range of wavelengths, this chapter describes photoinitiation using the most common UV light sources, medium pressure mercury-xenon (Hg-Xe) arc lamps which have prominent emissions between 200-600 nm, and the emerging light-emitting diode (LED) sources, which typically emit with a significant (~40 nm) bandwidth. The analysis reveals that the photoinitiation rate profile obtained with polychromatic illumination is considerably different depending on the specific initiator. The governing set of coupled differential equations is first presented, followed by simulation results of polychromatic illumination from either a Hg-Xe lamp or an LED light source that accounts for every wavelength active for initiation, and initiated with one of five photoinitiators. The photoinitiation profiles of the photoinitiator/light source combinations are analyzed and compared to show the importance of selection of system components.

6.2. Governing Equations

The set of differential equations which govern the evolution of the light intensity gradient and initiator concentration gradient for multi-wavelength illumination are shown below.²⁹

$$\frac{\partial C_i(z, t)}{\partial t} = -\frac{C_i(z, t)}{N_A h} \sum_j \left(\frac{\epsilon_{ij} \phi_j I_j(z, t)}{\nu_j} \right) + D_i \frac{\partial^2 C_i(z, t)}{\partial z^2} \quad (1)$$

$$\frac{\partial C_p(z, t)}{\partial t} = \frac{C_i(z, t)}{N_A h} \sum_j \left(\frac{\varepsilon_{ij} \phi_j I_j(z, t)}{\nu_j} \right) + D_p \frac{\partial^2 C_p(z, t)}{\partial z^2} \quad (2)$$

$$\frac{\partial I_j(z, t)}{\partial z} = -[\varepsilon_{ij} C_i(z, t) + A_{mj} + \varepsilon_{pj} C_p(z, t)] I_j \quad (3)$$

Here, the subscript j is an index with a different value for each wavelength of light under consideration; $C_i(z, t)$ is the initiator molar concentration at depth z and time t ; $C_p(z, t)$ is the photolysis product molar concentration at depth z and time t ; $I_j(z, t)$ is the incident light intensity of a specific wavelength at depth z and time t with units of energy/(area*time); ε_i is the initiator Napierian molar absorptivity of a specific wavelength with units of volume/(length*mole); ε_p is the photolysis product Napierian molar absorptivity of a specific wavelength with units of volume/(length*mole); ϕ_i is the quantum yield of the initiator at a specific wavelength, defined as the fraction of absorbed photons that lead to fragmentation of the initiator; N_A is Avogadro's number; h is Plank's constant; ν is the frequency of light in units of inverse seconds; D_i is the diffusion coefficient of the initiator in units of length²/time; D_p is the diffusion coefficient of the photolysis products; and A_m is the absorption coefficient of the monomer and the polymer repeat unit with units of inverse length. Note that in this paper we have adopted the Napierian molar absorptivity because it is most natural for the differential version of the absorption equation (equation 3). In the literature the decadic (base 10) molar absorptivity is commonly reported and should be converted to the Napierian value before using the model.

Comparison of equations 1 and 2 to those used in single wavelength descriptions¹⁷ reveals that, in the polychromatic case, the absorbance terms must be summed over all incident wavelengths. Therefore, the description of the change in

initiator concentration with respect to time at a given time and depth (equation 1) contains an absorbance term for each of the “ j ” distinct wavelengths (these terms are negative since the initiator is consumed) plus the term that accounts for diffusion of initiator against the gradient created by the previous consumption of the photoinitiator. As in the monochromatic case, equation 2 (dependence of the photolysis product concentration on illumination time at a specific time and depth) resembles equation 1, with the exception of the opposite sign on the absorbance terms since the photolysis products are created when the initiator is consumed.

For an accurate description of initiation with polychromatic illumination, the light intensity gradient of each incident wavelength must be individually described. As shown in equation 3, the intensity of an individual wavelength is attenuated by absorption of the initiator, monomer and polymer repeat units, and the photolysis product. Since the local initiator concentration depends upon all of the incident wavelengths, and the local light intensity of each wavelength depends upon the initiator concentration, the time-evolution of all of the light intensities are coupled to one another, and therefore the complete set of differential equations must be solved simultaneously. Therefore, the wavelength dependence of the intensity considerably increases the complexity of the model; for description of n wavelengths of incident light, $n+2$ equations must be solved simultaneously (typically a 100 nm region of the spectrum is important, therefore in excess of 100 equations must be simultaneously solved).

The following initial and boundary conditions apply to this system:

$$C_i(z,0) = C_o \quad (4);$$

$$C_p(z,0) = 0 \quad (5);$$

$$\frac{\partial C_{i,p}}{\partial z} = 0 \text{ at } z = 0 \text{ and } z = z_{\max} \quad (6);$$

$$I(0, t) = I_o \quad (7).$$

Equation 4 states that the initial initiator concentration is uniform throughout the depth of the sample. Similarly, equation 5 indicates that the initial photolysis product concentration is zero. Equation 6 is the no-flux boundary condition indicating that there is no diffusion through the ends of the sample, and equation 7 states that at any time, the intensity on the surface of the sample where the light enters is equal to the initial intensity of the light source.

The rate of production of free radicals as a function of depth was also considered in this study and is defined by equation 8.

$$R_i(z,t) = 2C_i(z,t) \sum_j [I(z,t)]_j \phi_j \varepsilon_{ij} \quad (8)$$

This defines the instantaneous local rate of production of free radicals, $R_i(z,t)$, if two active centers are produced upon fragmentation of the initiator.

Solution of this set of equations by method of finite differences provides detailed information regarding the time-evolution of the light intensity gradient, the initiator concentration gradient, and the photoinitiation rate profile (rate of active center generation as a function of time and location). Once active centers are generated, the subsequent reaction events (propagation, termination, chain transfer, *etc*) are the same for either thick or thin polymerization systems and have been extensively investigated in literature.ⁱ⁻ⁱⁱⁱ

6.3. System Under Investigation: Selection of Photoinitiators and Light Sources

To investigate the photoinitiation rate profiles for thick systems using common photoinitiators and lamps, the following model scheme was selected: a thick polymerization system (typically 1 cm thick) of rectangular cross-section subject to uniform polychromatic illumination normal to the top surface. The model can be used with any combination of monomer, initiator, and light source as long as the absorption and emission properties are known. In this chapter the following commercially available initiators were considered: bis(2,4,6-trimethylbenzoyl)-phenylphosphineoxide (BAPO), 2-benzyl-2-(dimethylamino)-1-[4-(4-morpholinyl)phenyl]-1-butanone (BDMB), 2,2-dimethoxy-2-phenylacetophenone (DMPA), (all obtained from Ciba Specialty Chemicals), and diphenyl (2,4,6-trimethylbenzoyl)-phosphine oxide (TPO, BASF). Figure 6.1 shows the chemical structures of these four photoinitiators. The molar absorptivity of these initiators and their respective photolysis products were determined at one nanometer increments using an Agilent UV-Visible spectrometer, and these absorptivities are shown in Figure 6.2. These initiators were chosen because they absorb to different extents between 300 – 500 nm where one or both of the lamps emit light. The initiators can be compared by noting the relative strength to which the initiators absorb light, as well as how completely the initiators photobleach (i.e. how strongly the photolysis products absorb). The normalized emission spectra of the medium pressure 200W Hg-Xe arc lamp (Oriel) and LED lamp (Firefly) used in this chapter are illustrated in Figure 6.3. The relative emission intensities of the lamps were determined at one nanometer increments using an Ocean Optics spectrometer. For simulations of photopolymerizations initiated

using these light sources, an effective wavelength range of 300 to 500 nm was chosen since wavelengths shorter than 300 are generally removed by monomer absorbance (acrylate monomers generally absorb below 300 nm and recall that the monomer is ~1000 times more concentrated than the initiator), and wavelengths longer than 500 are not absorbed by the chosen photoinitiators. Figure 6.3 illustrates that the Hg-Xe light source has several emission peaks throughout the range of interest, while the LED source has a single large peak centered at 400 nm.

6.4. Results and Discussion

Chapter 5 illustrated that for each incident wavelength of light, at a given depth and time, the change in intensity with depth depends upon the local concentrations of the initiator, photolysis products, and any other light-absorbing components as well as the corresponding molar absorptivities at the wavelength under consideration. In addition, it was shown that the instantaneous rate of consumption of the photoinitiator depends upon the local initiator concentration as well as the local light intensity and initiator molar absorptivity at each of the incident wavelengths. As a consequence of these simultaneous differential relationships, the time evolution of the light intensity gradient at one incident wavelength is dependent on the light intensities and molar absorptivities of all incident wavelengths.

6.4.1. Initiation with BAPO

Figure 6.4 shows a series of photoinitiation rate profiles at four different times for a one centimeter sample illuminated with the medium pressure 200 W Hg-Xe arc

lamp (94 mW/cm^2) and initiated using BAPO. Figure 6.5 shows the same initiator illuminated with the LED lamp (94 mW/cm^2). Comparison of these figures reveals several interesting results. First, because the most prominent emission peaks of the Hg-Xe lamp (especially the 313 and 365 nm peaks) correspond to relatively high initiator molar absorptivities while BAPO has relatively low absorption in the range where the LED lamp emits, after 2 seconds of illumination, the photoinitiation rate wave front in the system illuminated by the LED has already begun to move into the sample while the corresponding front in the Hg-Xe system has not. This also allows the wave front to propagate further into the sample in the LED illumination case (the maximum rate after 50 seconds of illumination is at approximately 0.56 cm versus 0.32 cm in the Hg-Xe illumination case). Also, because BAPO more completely photobleaches in the LED emission range (that is, the photolysis products absorb to a lesser extent) than in the Hg-Xe wavelength range, the maximum rate decreases less in the former case (the maximum rate after 50 seconds of illumination with the LED lamp is about 45% of that after 2 seconds of illumination, versus 7% in the Hg-Xe illumination).

6.4.2. Initiation with TPO

Photoinitiation with TPO reveals similar results to that of initiation with BAPO. Figure 6.6 shows a series of photoinitiation rate profiles at four different times for a one centimeter sample illuminated with the medium pressure 200 W Hg-Xe arc lamp (94 mW/cm^2) and initiated using TPO. Figure 6.7 shows the same initiator illuminated with the LED lamp (94 mW/cm^2). Comparison of the

absorptivities of BAPO and TPO (Figure 6.2a and 6.2d, respectively) shows that although the overall molar absorptivity of TPO is less than BAPO, the two initiators have similar initiator absorptivity patterns and degrees of photobleaching. Indeed, the maximum rate after 50 seconds of illumination has moved through the entire depth of the sample in the system illuminated with the LED lamp, while it is only 0.42 cm into the sample in the system illuminated with the Hg-Xe lamp. The maximum rate is also decreased less with the LED lamp than with the Hg-Xe light source; the maximum rate after 30 seconds of illumination is 22% the rate after 2 seconds of illumination in the former case, and 6% in the latter.

Comparison of the photoinitiation rate profiles for BAPO, Figures 6.4 and 6.5, to those of TPO, 6.6 and 6.7, shows that the overall lower absorptivity for TPO leads to a broader wave front that moves through the sample more quickly. The overall values of photoinitiation rates are generally lower for TPO than BAPO. These trends are examined in depth in Chapter 5.

6.4.3. Initiation with BDMB

While the absorptivities of the photolysis products of both BAPO and TPO (Figures 6.2a and 6.2d, respectively) were considerably less at all wavelengths of interest, those of BDMB (Figure 6.2b) are only considerably less in a very small wavelength range (around 340 – 350 nm) and are equal to or greater than the initiator in other regions. Figure 6.8 shows the photoinitiation rate profiles at two different times for a one centimeter sample illuminated with the medium pressure 200 W Hg-Xe arc lamp (94 mW/cm^2) and initiated using BDMB. Figure 6.9 shows the same

initiator illuminated with the LED lamp (94 mW/cm^2). Figure 6.8 illustrates that a significant photoinitiation rate is generated after 2 seconds of illumination, but that this rate is not sustained even after 10 seconds of illumination. In both Figures 6.8 and 6.9, the wave front is quickly diminished since neither lamp has a strong emission peak between 340 – 350 nm, and this region is the only one in which the initiator is able to preferentially absorb light. Figure 6.9 shows that the overall rate is much lower and decreases much more rapidly when the system is illuminated with the LED lamp than when it is illuminated with the Hg-Xe lamp. Comparison of the initiator and photolysis product absorptivities in Figure 6.2b and the lamp emission spectra in 6.3 reveals that there the initiator absorptivities corresponding to the emission peaks of the Hg-Xe lamp are higher than those corresponding to the wavelengths emitted by the LED lamp. Additionally, while some amount of photobleaching occurs over the wavelength range of the Hg-Xe lamp, little to none occurs over the wavelengths of the LED lamp, and some wavelengths actually anti-bleach (that is, the products absorb to a greater extent than the initiator). This leads to very ineffective photoinitiation.

6.4.4. Initiation with DMPA

DMPA has an attractive initiator molar absorptivity spectrum, but analysis of the corresponding photolysis product molar absorptivity reveals that there is a significant amount of anti-bleaching, and very little photobleaching, as shown in Figure 6.2c. Indeed, as Figure 6.10 illustrates, the maximum photoinitiation rate of DMPA illuminated with the Hg-Xe lamp stays at or near the illuminated surface until the initiator concentration at that point is consumed to a great enough extent to allow

the maximum rate to shift slightly into the depth of the sample after 50 seconds of illumination. The light is never able to penetrate deeply in the sample, and the competing absorbance of the photolysis products will cause the initiation rate to continually decrease until there is virtually no rate at all.

Comparison of Figures 6.10 and 6.11 (illumination of DMPA with the LED lamp) shows that the overall lower initiator molar absorptivities corresponding to the wavelength range emitted by the LED lamp leads to much lower overall photoinitiation rates. The latter case of illumination by the LED source also leads to photoinitiation profiles which extend all the way through the depth of the sample, which can also be attributed to the low values of initiator absorptivity. Much like the case shown in Figure 6.10, the maximum rate in Figure 6.11 stays at or near the surface for the illumination times shown, while the rate continually decreases for all depths with increasing illumination time.

6.5. Conclusions

This chapter has illustrated how the complete, polychromatic description of photoinitiation can be applied to any combination of monomer, initiator, and light source as long as the absorption and emission properties are known. A dimensionless, generalized description of photoinitiation in thick systems illuminated with polychromatic light is not possible because a given light source is described by a possible infinite number of wavelengths, and the initiator and photolysis products (along with any other absorbing species) are described by the same number of corresponding absorptivities. Additionally, the model is complicated by the coupling

of the light intensity gradients through the initiator concentration gradient. Therefore, the ability to model a specific monomer, initiator, and light source combination is of great importance and may provide an invaluable tool for design of these systems.

In this chapter, four common photoinitiators that absorb in the 300 – 500 nm region of the light spectrum were modeled with either a common medium pressure 200 W mercury/xenon arc lamp or with an LED lamp that emits at high intensity band centered at 400 nm \pm 20 nm. The first two initiators modeled, BAPO and TPO, showed similar photoinitiation behavior. Both initiators led to the classic wave front shape described in previous chapters. Because both are fairly effective photobleachers, the initiation rate was able to propagate into the depth of the sample. Indeed, it is critical for the absorbance of the photolysis products to be significantly lower than that of photoinitiator at all wavelengths that are absorbed by the initiator, especially those which correspond to wavelengths of higher intensity. This photobleaching behavior allows light to penetrate more deeply into the sample and is essential for photoinitiation in thick samples. Initiation of thick samples with poor photobleachers, such as BDMB or DMPA, is shown to be very ineffective. In these cases, the rate was only significant at or near the surface, and competing absorption by the photolysis products did not allow light, and thus initiation, to occur deeper in the sample.

Interestingly, in the cases of both BAPO and TPO, the LED lamp was a better match for the absorption characteristics of the initiators. More complete photobleaching in the wavelength region emitted by the LED lamp led to higher sustained photoinitiation rates. Depending on the critical requirement set for the

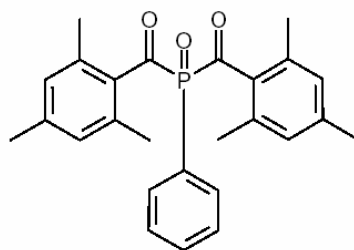
photopolymerization of a system (such as minimum number of active centers created or time for photoinitiation to occur throughout the depth), these initiators are an appropriate choice for use with this lamp. To optimize the selection of monomers, initiators, and light sources for thick photopolymerization systems, it is important to understand these effects described in the previous chapters.

This chapter again illustrates that photopolymerization initiated with polychromatic light is considerably more complex than the monochromatic case. Chapter 5 described how the relative contribution of an individual wavelength to the photoinitiation rate profile not only depends upon the incident intensity and the initiator molar absorptivity at that wavelength, it also depends upon the intensity and initiator molar absorptivity of all other incident wavelengths. Although a single value of initial initiator concentration was modeled, as well as a single value of total lamp intensity, the shape and attributes of the aggregate photoinitiation rate profile may change markedly if these variables are changed. Certainly the optimum initiator concentration is initiator dependent, and should be chosen accordingly. This reiterates the importance of separately modeling each system of interest in order to get an accurate picture of the photoinitiation behavior.

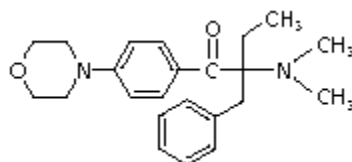
In this chapter, several real systems were modeled and compared by individually specifying the intensity at each wavelength, as well the initiator and photolysis product absorptivity at the corresponding wavelengths. The results clearly showed that initiator and light source combination is critical to the success of the photoinitiation. This complete and accurate description of the photoinitiation of thick

systems illuminated with polychromatic light will be a valuable tool for selection of effective and appropriate system components.

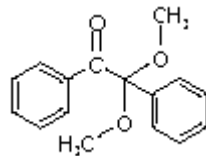
6.1a. BAPO



6.1b. BDMB



6.1c. DMPA



6.1d. TPO

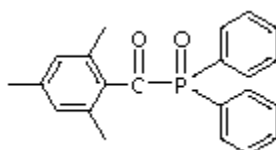
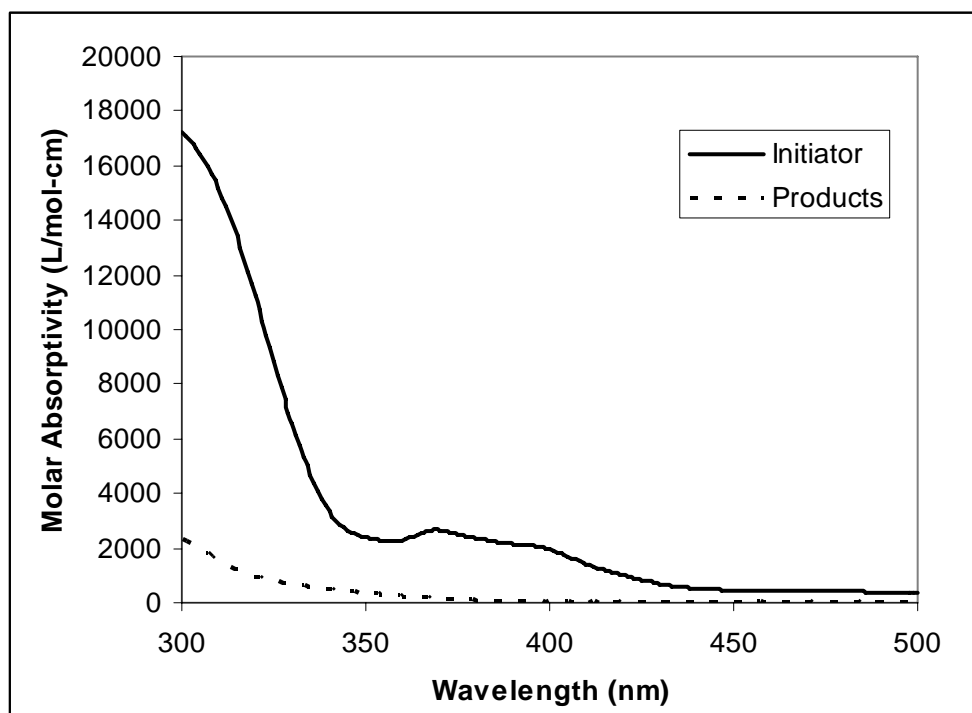


Figure 6.1. Chemical structures of photoinitiators modeled.

6.2a. BAPO



6.2b. BDMB

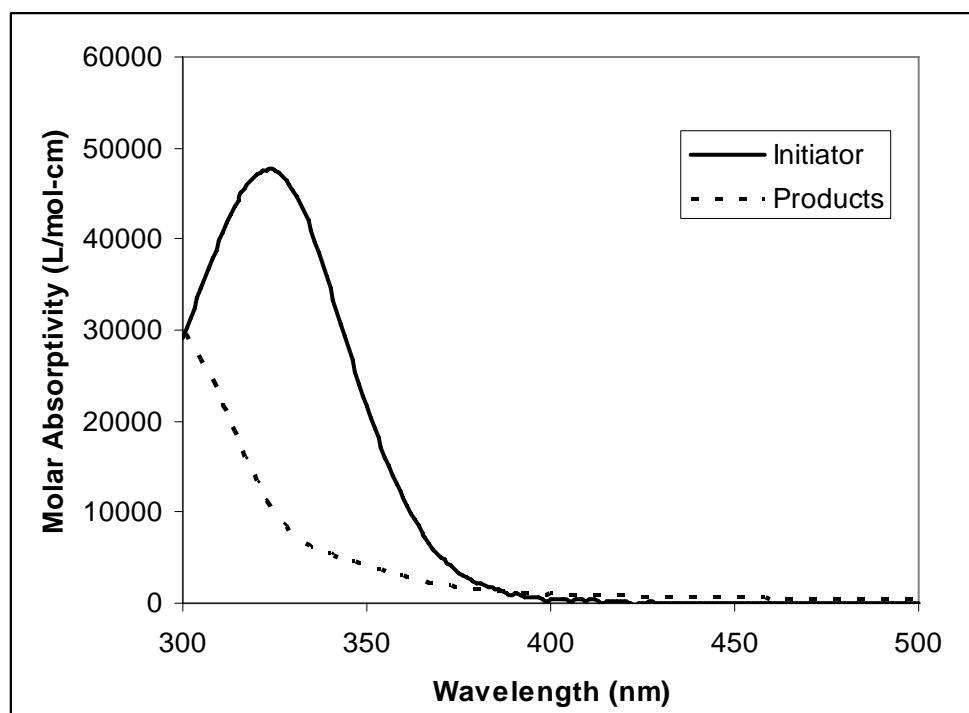
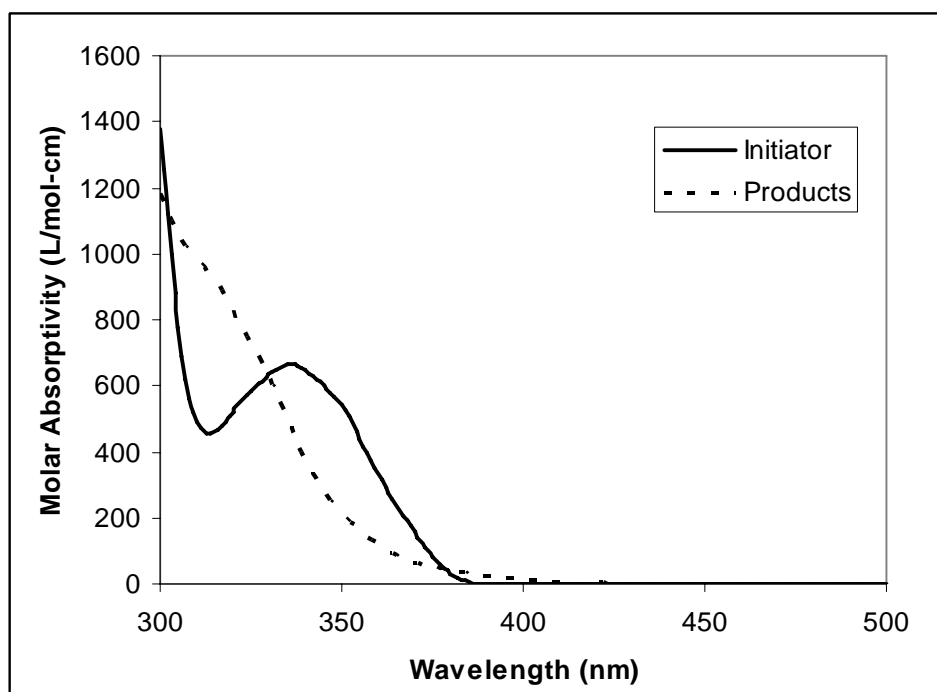


Figure 6.2. Napierian molar absorptivity of initiator (—) and its respective photolysis products (---), 0.013% in methanol.

6.2c. DMPA



6.2d. TPO

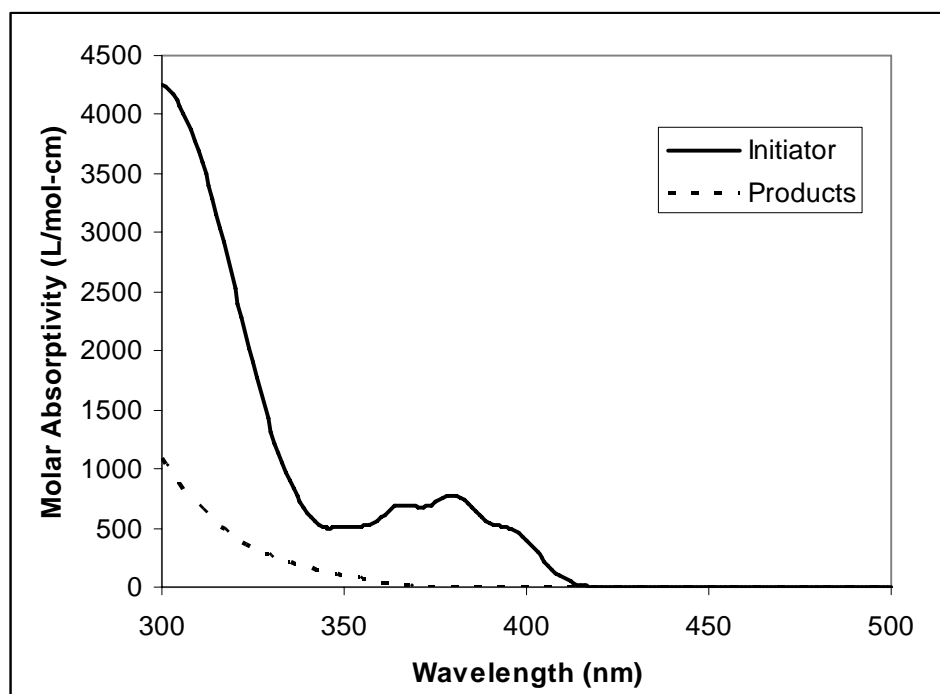


Figure 6.2. Continued.

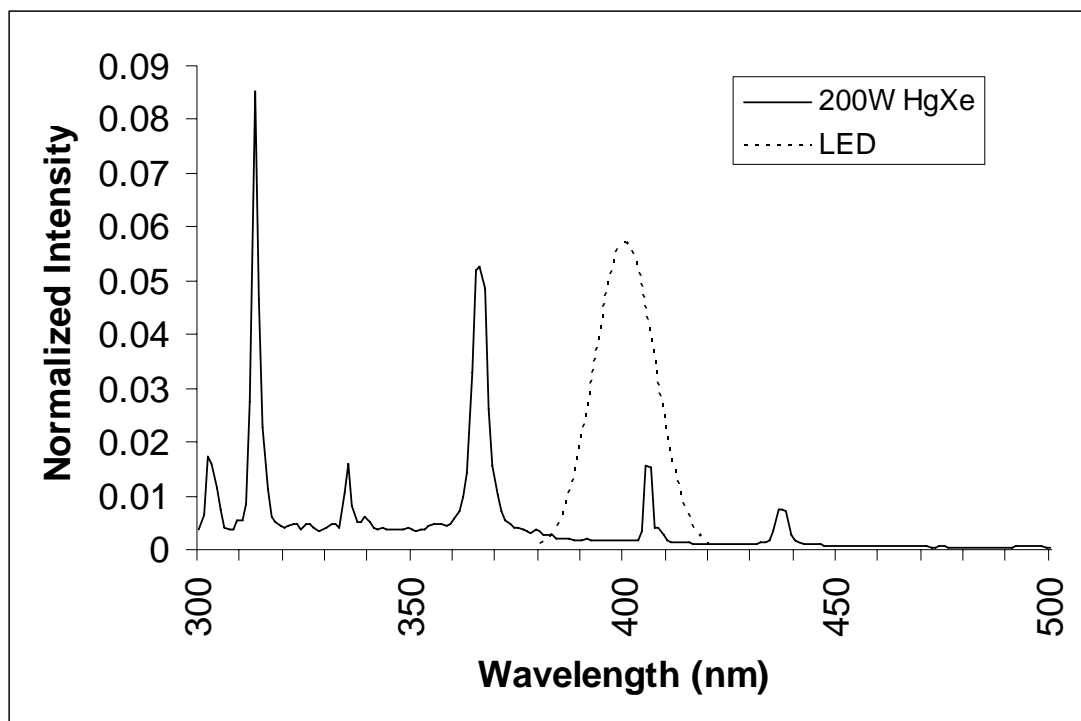


Figure 6.3. Normalized intensity as a function of wavelength for a medium pressure 200W Hg-Xe arc lamp and an LED lamp with emission centered around 400 nm.

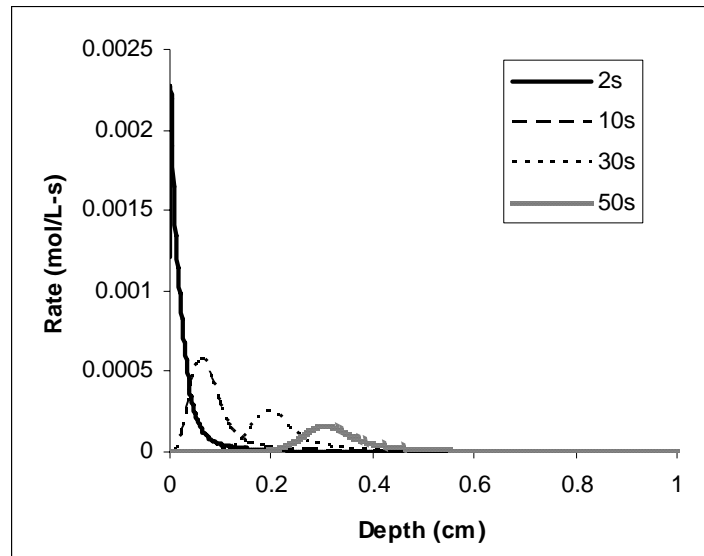


Figure 6.4. Photoinitiation of a system initiated with BAPO using a medium pressure 200 W Hg-Xe arc lamp.

$I_0 = 94 \text{ mW/mm}^2$, $C_0 = 0.0268 \text{ mol/L}$, $\phi = 0.2$, ϵ_i and ϵ_p as shown in Figure 6.2a.

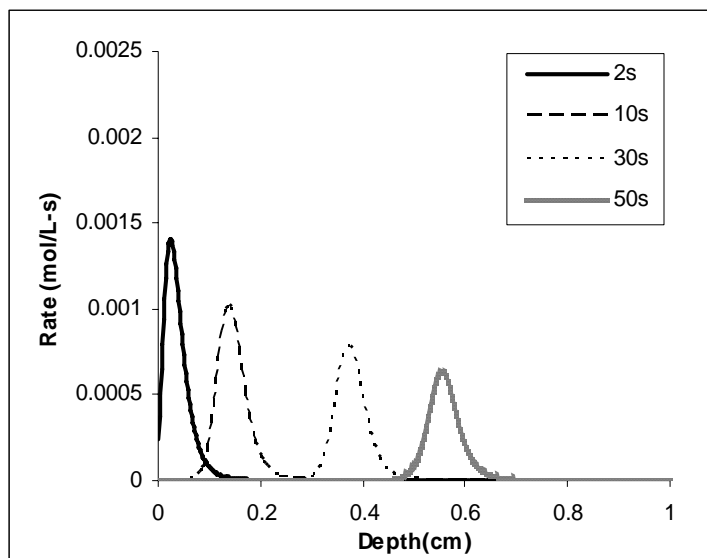


Figure 6.5. Photoinitiation of a system initiated with BAPO using the LED light source.

$I_0 = 94 \text{ mW/mm}^2$, $C_0 = 0.0268 \text{ mol/L}$, $\phi = 0.2$, ϵ_i and ϵ_p as shown in Figure 6.2a.

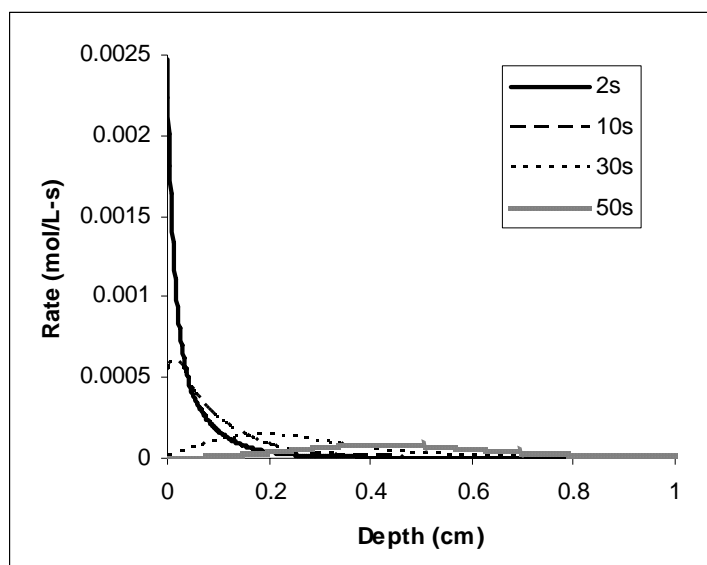


Figure 6.6. Photoinitiation of a system initiated with TPO using a medium pressure 200 W Hg-Xe arc lamp.

$I_0 = 94 \text{ mW/mm}^2$, $C_0 = 0.0268 \text{ mol/L}$, $\phi = 0.2$, ϵ_i and ϵ_p as shown in Figure 6.2d.

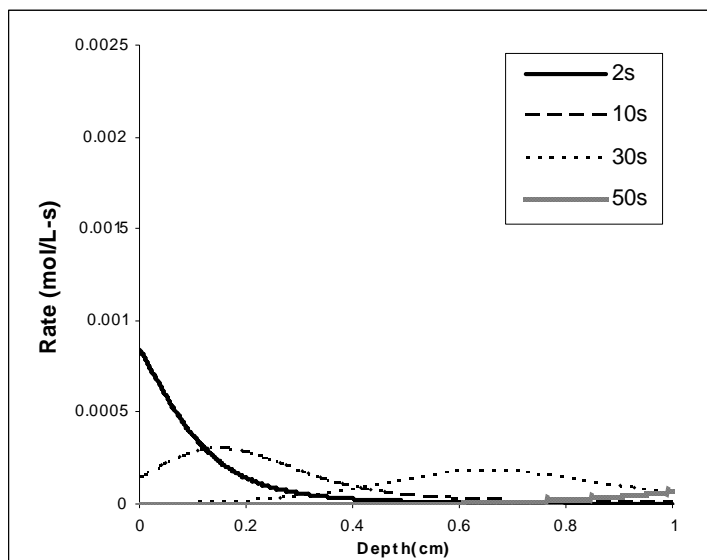


Figure 6.7. Photoinitiation of a system initiated with TPO using the LED light source.

$I_0 = 94 \text{ mW/mm}^2$, $C_0 = 0.0268 \text{ mol/L}$, $\phi = 0.2$, ϵ_i and ϵ_p as shown in Figure 6.2d.

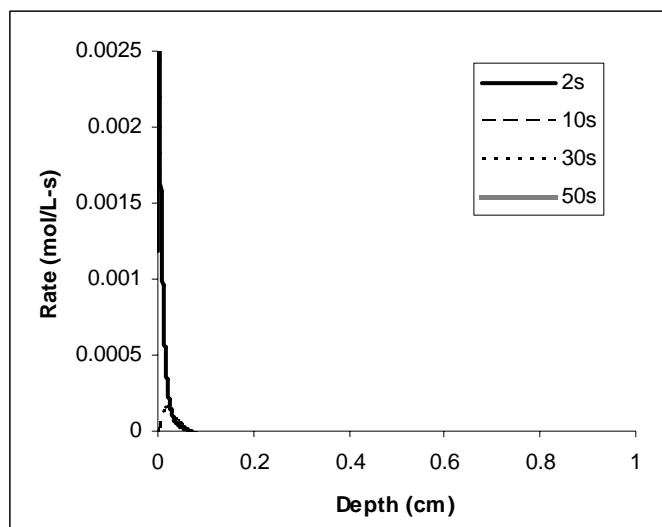


Figure 6.8. Photoinitiation of a system initiated with BDMB using a medium pressure 200 W Hg-Xe arc lamp.

$I_0 = 94 \text{ mW/mm}^2$, $C_0 = 0.0268 \text{ mol/L}$, $\phi = 0.2$, ϵ_i and ϵ_p as shown in Figure 6.2b.

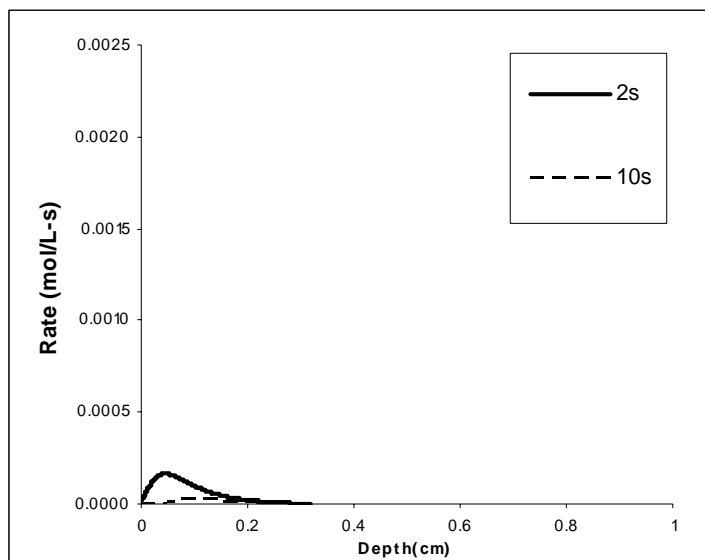


Figure 6.9. Photoinitiation of a system initiated with BDMB using the LED light source.

$I_0 = 94 \text{ mW/mm}^2$, $C_0 = 0.0268 \text{ mol/L}$, $\phi = 0.2$, ϵ_i and ϵ_p as shown in Figure 6.2b.

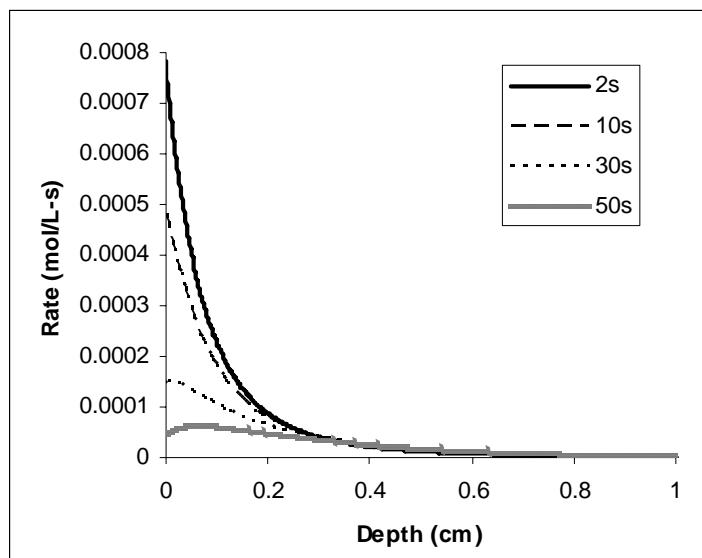


Figure 6.10. Photoinitiation of a system initiated with DMPA using a medium pressure 200 W Hg-Xe arc lamp.

$I_0 = 94 \text{ mW/mm}^2$, $C_0 = 0.0268 \text{ mol/L}$, $\phi = 0.2$, ϵ_i and ϵ_p as shown in Figure 6.2c.

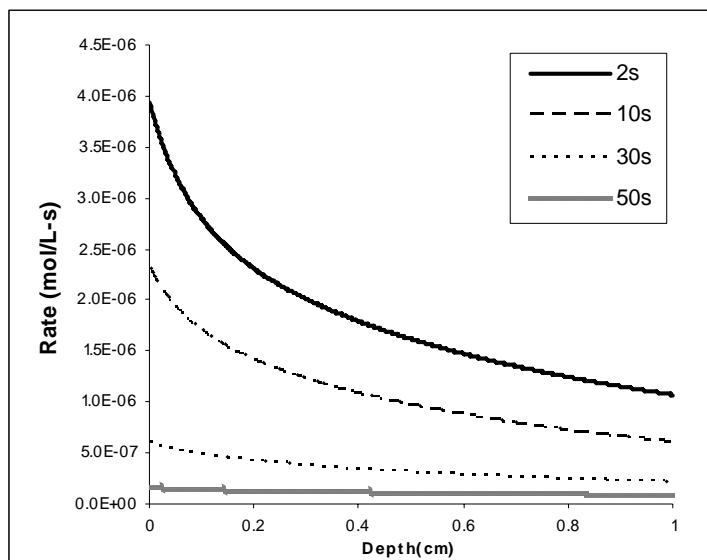


Figure 6.11. Photoinitiation of a system initiated with DMPA using the LED light source.

$I_0 = 94 \text{ mW/mm}^2$, $C_0 = 0.0268 \text{ mol/L}$, $\phi = 0.2$, ϵ_i and ϵ_p as shown in Figure 6.2c.

CHAPTER 7 CONCLUSIONS AND FUTURE RECOMMENDATIONS

7.1 Summary of Research

This work has explored the photoinitiation behavior in thick polymer systems. The recent flurry of research in this area demonstrates the interest and need for a comprehensive model describing photoinitiation. In this project, a set of differential equations describing the spatial and temporal evolution of the light intensity gradient, photoinitiator concentration gradient, and the photoinitiation rate profile have been developed for a thick polymer system. Unlike any of the models reported previously in the literature (which focus on monochromatic illumination of perfectly bleaching systems which contain no other absorbing components), the model presented here can account for polychromatic illumination as well as the absorptivity of any system component (initiator, photolysis products, monomer, additives, etc). Therefore, this research has contributed substantially to the understanding of the complex photoinitiation behavior in thick systems. This component makes it possible to model real initiation systems, and is beneficial to the scientific community interested in these reaction systems. An overview of some important conclusions is provided below.

In this thesis, successive chapters deal with systems of increasing complexity, and interesting results for the simplest case of modeling monochromatic illumination of thick films are presented first (Chapter 3). This investigation illustrated that there is an optimum concentration of initiator that results in both high initiation rates as well as efficient progression of the initiation wave front throughout the sample. As in thicker systems, for thick films with complete photobleaching, increasing the initiator

concentration leads to an increase in both the photoinitiation rate and the time required to cure throughout the depth of the sample. Also demonstrated was that an initiator with a high molar absorptivity leads to a narrowing of the initiation rate profile which moves as a sharp front from the illumination surface toward the center of the sample. Increasing the molar absorptivity also increases the maximum photoinitiation rate. Additionally it was shown that increasing the intensity has a positive effect on both the maximum rate of photoinitiation, as well as the rate at which the wave front moves through the sample, however, other considerations such as energy costs may prevent this from being a practical implementation.

The model was then expanded (Chapter 4) to include illumination from two separate light sources. Due to the variation in light intensity with depth in the sample, the placement of the lamp is important, and the photoinitiation profile may be markedly affected by addition of a second light source. Simulation results revealed that when two lamps of equal intensity are used, the spatial and temporal evolution of the photoinitiation rate profile is indeed highly non-uniform, but is always symmetric with respect to the center of the sample and follows a characteristic progression from a bimodal distribution, to a unimodal shape with a maximum in the center of the sample. At the instant of illumination the rate is highest at each of the illuminated surfaces, and exhibits a minimum rate at the center of the sample. For low to moderate values of molar absorptivity and initiator concentration, the light from each lamp penetrates past the middle of the sample and the light intensity profiles overlap, even at the instant of illumination. As time progresses, the initiation rate at the two illuminated surfaces of the sample decreases due to the consumption of initiator, and a symmetric, bimodal

photoinitiation rate profile is established. When the peaks of the initiation wave fronts meet in the center of the sample, the overall photoinitiation rate profile becomes unimodal, and the rate in the center reaches its maximum. From this time on, the maximum photoinitiation rate occurs at the center of the sample, and at all depths the rate decreases as the initiator is consumed. For some applications, the uniformity of the photoinitiation as a function of depth may be an important consideration and examination of the two-sided illumination cases presented illustrates that a considerably more uniform photoinitiation rate can be achieved throughout the sample.

Initiator concentration is of particular interest in thick photopolymerization, because it has a pronounced impact on the photoinitiation rate profile. For single-sided illumination of thick systems with complete photobleaching, increasing the initiator concentration leads to an increase in both the photoinitiation rate and the time required to cure throughout the depth of the sample. For two-sided illumination, the situation is more complex due to the addition of the second light source. For high initiator concentrations, each light source may lead to a sharp photoinitiation front that moves from the illumination surface toward the center of the sample, independent of each other. In contrast, for low initiator concentrations, the light intensity gradients from the two lamps may overlap immediately upon illumination, leading to more uniform initiation rate profiles and a less frontal behavior.

An initiator with a high molar absorptivity leads to a narrowing of the initiation rate profile which moves as a sharp front from the illumination surface toward the center of the sample. For two-sided illumination, two sharp peaks moving from the illuminated surfaces toward the center will ultimately meet in the middle and initiation will be

complete. While this condition leads to an inherently non-uniform photoinitiation profiles (indeed the percent variation is 100% at all times), there are situations in which a sharp initiation front is desired, such as in the production of flexographic printing plates where backside illumination may be used to create a substrate of specific depth, and topside illumination through a mask may be used to create defined surface features.

Since the monomer is the predominant component in most photopolymerization systems (typically more than 90% of the total system), it is important for the monomer absorption coefficient to be as small as possible at the effective initiation wavelength. This is especially true for photoinitiation of thick samples since even a relatively small value of the molar absorptivity will significantly attenuate the incident light. In general, absorption by the monomer leads to reduced penetration of light into the sample and therefore reduces the photoinitiation rate at a given depth and slows the rate at which the photoinitiation profile evolves. When the monomer absorbs on the scale of the initiator, the photoinitiation rate remains zero in the center and the initiation rate closer to the illumination surfaces continuously decreases until it approaches zero. This phenomenon shows why choosing an initiator/monomer/light source combination is critical to thick photopolymerizations.

A special case of two-sided illumination is a reflective boundary condition in which the sample is illuminated on only one side with a lamp, but any light that reaches the back surface is reflected back into the sample. In this case, the intensity of reflected light is initially low (typically zero) but increases with time as the initiator is consumed and more light is able to penetrate through the sample. With increasing time, the reflective boundary leads to an increased light intensity at the back side of the sample

which in turn leads to an increase in the rate at which the photoinitiator is consumed in this location. The added light intensity from the reflection eventually causes the initiation rate to increase. Indeed, a reflective surface can be beneficial in thick systems, especially by increasing the initiation rate in the deep portion of the sample.

Illumination of two perpendicular sides of a sample was also investigated, and simulation results revealed that a photoinitiation rate wave front will progress from the doubly-illuminated corner across the sample towards the dark corner. This model begins to explore the possibility of modeling more specific, complex sample geometries.

Evaluation of two-sided illumination has shown that either a uniform or very sharp initiation rate front can be achieved in a thick sample if the parameters of the illumination scheme are chosen appropriately for the desired initiation behavior. Many different illumination schemes can be imagined, and this model illustrates that with independently controlled light sources, as well as properly suited system variables (such as concentration and molar initiator absorptivity), a desirable initiation rate profile can be attained.

The complexity of the model was next increased to account for polychromatic illumination (Chapter 5). The simulations show that the photoinitiation rate profile for polychromatic illumination is much different than in systems illuminated by monochromatic light. Moreover, the results are complicated by the coupling of the light intensity gradients through the initiator concentration gradient. For this reason, we continually increase the complexity of the model from two-wavelength illumination, to five-wavelength illumination, and finally to continuous spectrum illumination in order to

fully demonstrate the effects of polychromatic illumination on the resulting photoinitiation rate profile.

Illumination with two wavelengths (high and low initiator molar absorptivity) can synergistically cause both a high rate of surface initiation and active center production in the deep portions of the sample. The presence of one incident wavelength affects all other incident wavelengths by altering the initiator concentration gradient. These simulations also illustrate that changes in either the relative and absolute incident intensities affect the relative importance of a particular wavelength to the aggregate photoinitiation profile.

The complexity of the model was further increased to include five incident wavelengths broadened the overall photoinitiation rate profile into a single, unified wave front. Wavelengths corresponding to high intensities had the largest impact on the shape of the overall rate profile, while contributions from wavelengths corresponding to similar initiator molar absorptivities essentially combined with one another. The initiator concentration has a marked effect on contributions of each wavelength to the overall photoinitiation rate profile. High initiator concentrations allow less light, regardless of absorptivity, to penetrate into the system, causing less active center generation in the deep portions of the sample, while low concentrations do not produce high rates of active center production at any depth or time.

The final model presented is a complete and accurate description of photoinitiation using polychromatic light in which each wavelength within the region active for initiation was considered (300-420 nm) and the incident intensity and initiator molar absorptivity at each wavelength could be independently specified. Inclusion of the continuous spectrum of incident wavelengths broadened and flattened the photoinitiation

rate profile, and absorption by the photolysis products effectively filtered some incident wavelengths.

For polychromatic light, the shape and attributes of the aggregate photoinitiation rate profile may change markedly if any of a number of variables are changed, including the relative intensities, the absolute intensity, initiator concentration, degree of photobleaching, *etc.* To optimize the selection of monomers, initiators, and light sources for thick photopolymerization systems, it is important to understand these effects.

In chapter 6, the complete, polychromatic description of photoinitiation presented can be applied to any combination of monomer, initiator, and light source as long as the absorption and emission properties are known, and may provide an invaluable tool for design of these systems. Four common photoinitiators that absorb in the 300 – 500 nm region of the light spectrum were modeled with either a common medium pressure 200 W mercury/xenon arc lamp or with an LED lamp that emits at high intensity band centered at 400 nm \pm 20 nm. The first two initiators modeled, BAPO and TPO, showed similar photoinitiation behavior. Both initiators led to the classic wave front shape described in previous chapters. Because both are fairly effective photobleachers, the initiation rate was able to propagate into the depth of the sample. Indeed, it is critical for the absorbance of the photolysis products to be significantly lower than that of photoinitiator at all wavelengths that are absorbed by the initiator, especially those which correspond to wavelengths of higher intensity. This photobleaching behavior allows light to penetrate more deeply into the sample and is essential for photoinitiation in thick samples. Initiation of thick samples with poor photobleachers, such as BDMB or DMPA, is shown to be very ineffective. In these cases, the rate was only significant at or near the

surface, and competing absorption by the photolysis products did not allow light, and thus initiation, to occur deeper in the sample.

Interestingly, in the cases of both BAPO and TPO, the LED lamp was a better match for the absorption characteristics of the initiators. More complete photobleaching in the wavelength region emitted by the LED lamp led to higher sustained photoinitiation rates. Depending on the critical requirement set for the photopolymerization of a system (such as minimum number of active centers created or time for photoinitiation to occur throughout the depth), these initiators are an appropriate choice for use with this lamp. To optimize the selection of monomers, initiators, and light sources for thick photopolymerization systems, it is important to understand these effects described throughout this thesis.

7.2 Recommendations for Future Work

Photoinitiation of thick systems is an important emerging technology that continues to become more widely implemented. With this research work in place, future work is recommended to further enhance the understanding of photoinitiation in thick systems. There are many different directions in which this research could be expanded. For example, with the polychromatic model well developed, it would be beneficial to study a wider range of photoinitiators, monomers, additives, and light sources. Each monomer, initiator, and additive should each be characterized for their absorption properties, and degree of photobleaching. Interesting additives, such as dyes, pigments, and inert bleaching and anti-bleaching compounds could also be included. The latter of

these could be used to control depth of initiation or to produce stratified polymers. In addition, the model could be expanded to account for light scattering.

There are also many trends in light sources, and this is an area of active research due to the desire get away from mercury lamps (because of mercury vapor and UV emissions). Reduction of power consumption is also always a goal in the photopolymerization industry. One current trend discussed in this thesis is LEDs, but other interesting possibilities may emerge including visible sources and novel technologies such as chemi-luminescence.

This work has looked at the more complex design variable of placement of illumination sources using monochromatic light. Expanding this research to polychromatic light would be of interest, as the resulting photoinitiation rate profiles may change markedly in shape. This study would provide more understanding of how the placement of lamps can achieve different photoinitiation profiles. The placement of lamps is a step towards expanding the model to model specific complex shapes, but as each shape is unique, a separate model would need to be created for each.

APPENDIX A

A Short Tutorial

What this program does:

It takes information about the photoinitiator, light source, and other surrounding variables and runs it through a series of finite differential equations to determine the rate of photoinitiation with respect to depth and time.

What information does this program exactly need?

About Photoinitiator

- Initial concentration of the photoinitiator in mol/L
- Quantum yield of the photoinitiator (maximum of one)
- The number of radicals the photoinitiator generates (fragments)
- Extinction coefficient of the photoinitiator on 1nm increments in mol/ L cm
 - Program will convert decadic to Napierian values from UV-Vis absorbance data
- Extinction coefficient of the photoinitiator products on 1nm increments in mol/L cm

About Light Source

- Normalized intensity of spectral irradiance on 1nm increments
- Total intensity of specific spectral region of interest in mW/cm²

Additional

- Spectral region of interest (eg. 350nm-450nm)
 - Large regions can use up immense amounts of computer power
- Depth of sample (cm)
- Total time of illumination (sec)
- Mesh sizes for depth and time
 - Both have a large effect on the stability of the program

Where does this information go into the program?

- Core input variables
- Mesh variables
- Excel file reference to photoinitiator, light source, product absorptivity, and solvent absorptivity

How do the M\$ Excel files work?

It would be best to see the sample files. Each file has a separate tab for each photoinitiator that all link to a master tab for ease of use. The simulation first looks for

the location of the Excel file and then for the tab of interest. It is this tab name that tells the simulation which photoinitiator to use.

How do I plot results?

For the most detailed information search the help file for plotting tools. Typically the Cmatrix, sumI_{tot}, and Rate_ovr variables are the most useful for representation of the system.

Troubleshooting

A search of the help file is the best troubleshooting tool.

Equation Sheet for Matlab Multi-wavelength Simulation

Equation for light intensity gradient with respect to depth and time

$$\frac{\partial I_j(z, t)}{\partial z} = -[\varepsilon_{ij} C_i(z, t) + A_{mj} + \varepsilon_{pj} C_p(z, t)] I_j \quad (1)$$

Matlab finite element equation

$$I(t, z, j) = I(t, z - 1, j) - I(t, z - 1, j) \{ \varepsilon_{ij} C_i(t - 1, z) + A_{mj} + \varepsilon_{pj} [C_o - C_i(t - 1, z)] \} \times \text{Depth increment} \quad (2)$$

Gamma equation used to consolidate constants

$$\gamma_j = \left(\frac{\varepsilon_{ij} \phi_j}{v_j N_A h} \right) = \left(\frac{\varepsilon_{ij} \phi_j \lambda_j}{c N_A h} \right) \quad (3)$$

Equation for Concentration of photoinitiator with respect to depth and time

$$\frac{\partial C_i(z, t)}{\partial t} = - \frac{C_i(z, t)}{N_A h} \sum_j \left(\frac{\varepsilon_{ij} \phi_j I_j(z, t)}{v_j} \right) + D_i \frac{\partial^2 C_i(z, t)}{\partial z^2} \quad (4)$$

Matlab finite element equation

$$C_i(t, z) = C_i(t - 1, z) - \left[\sum_j \gamma_j I(t, z, j) \right] C_i(t - 1, z) \times \text{Time increment} \quad (5)$$

Equation for rate of photoinitiation

$$R_i(z,t) = 2C_i(z,t) \sum_j [I(z,t)]_j \phi_j \epsilon_{ij} \quad (6)$$

$$R(t,z) = (\# \text{ of fragments}) C_i(t,z) \left[\sum_j \gamma_j I(t,z,j) \right] \quad (7)$$

Boundary Conditions

At time zero

$$C_i(0,z) = C_o \quad (8)$$

$$C_p(0,z) = 0 \quad (9)$$

$$I(0,t) = I_o \quad (10)$$

And initial light intensity gradient through the thickness of the sample immediately after illumination

Matlab Script for Polychromatic Illumination

```

%This is the main script that will combine all the functions
% Note that this script can now run alone.
% This script needs to be able to access external MS Excel files
% Only sections marked with [USER INPUT] need to be changed
% [...] indicates transition to next line

clear; %clears the workspace

%---Core Input Variables---[USER INPUT]-----
-----
C0 = 0.003787158; % the initial concentration of
photoinitiator in mol/L
phi = .2; % initiator efficiency (quantum yield)
frgmnt = 2; % Number of Fragments by initiator
waveStart = 300; % wavelengths of interest in nm
waveEnd = 500; %range 200:800nm
total_intensity = 65; %mW/cm2 - total intensity of lamp in that
range

%---mesh variables---[USER INPUT]-----
depth = 1; %depth of the sample, cm
depint = .005; %depth increment, Stay between 0.025 and 0.001 for
stability
fulltime = 100; %total time of illumination, sec
timeint = 1; %time increment, 1 is the usual value

```

```

%---define the number of data point for time and depth-----
-
time = 0:timeint:fulltime;
z = 0:depint:depth;
lt = length(time);
lz = length(z);

%-Read in constants from excel worksheet in format
'file.xls','worksheet'--
% See Excel file for proper setup
% Files must be in pointed to by Matlab current directory
waveread = xlsread('Table_of_Lamps_Normalized.xls','Wave');
% Inputs all Wavelengths 190-1100
I0read =
total_intensity*xlsread('Table_of_Lamps_Normalized.xls','FireFly');
Kiread = 2.303*xlsread('Table_of_Initiators.xls','TPO');
% initiator absorptivity
prod_absread =
2.303*xlsread('Table_of_Product_Absorptivities.xls','TPO');
% Product absorptivity
% both adj for log10 base (2.303)
solv_absread =
xlsread('Table_of_Product_Absorptivities.xls','zero');
%solvent absorptivity

%---Chooses particular wavelengths of interest-----
--
wave = waveread(waveStart-189:waveEnd-189);
I0 = I0read(waveStart-189:waveEnd-189);
Ki = Kiread(waveStart-189:waveEnd-189);
prod_abs = prod_absread(waveStart-189:waveEnd-189);
solv_abs = solv_absread(waveStart-189:waveEnd-189);

% find length of data files - needed for for loops
lw = length(wave);

%---Compress data-----
save('compress.mat');
clear;
load('compress','lt','lz','lw');
Itot = zeros(lt, lz, lw);
Cmatrix = zeros(lt, lz);
Rate_ovr = zeros(lt, lz);
load('compress.mat');

%---Construct Gamma matrix-----
-----
% Takes care of constants, Avagrado, Plank's, speed of light,
quantum yield
% unit conversion, absorption of initiator at each particular
wavelength
for c = 1:lw
    G(c) = Ki(c)*wave(c)*10^-9*phi/((6.02*10^23)*(6.64*10^-
34)*300000000);
    % Equation 3 on Equation sheet
end

```

```

%{
-----At time ZERO -----
---
Total intensity I(t,z,wave)
these loops find the initial intensity immediatly after
illumination
(time zero) and sum them for all waves through the depth of the
sample
before returning through the loop for each time interval
%}
for xx = 1:lw % Boundry Condition, concentration uniform at
time zero
Cmatrix(1,xx) = C0; %Equation 8
end

for i = 1:lw % at time =0 for all waves
Itot(1,1,i) = I0(i); % Equation 10
for zz = 2:lw
Itot(1,zz,i) = Itot(1,zz-1,i)-Itot(1,zz-
1,i)*(solv_abs(i)+Ki(i)*C0 + prod_abs(i)*(C0-C0))*depint;
%Equation 2
%prod_abs(i)*(C0-C0) means no prod abs at time zero
end
end

%---Beyond time ZERO -----
--
for time_count = 2:lt

%---calculates depth the wavelength-----
for i = 1:lw
Itot(time_count,1,i) = I0(i);
for zzz = 2:lw
Itot(time_count,zzz,i) = Itot(time_count,zzz-1,i)-
Itot(time_count,zzz-1,i)*(solv_abs(i) + Ki(i)*...
Cmatrix(time_count-1,zzz) + prod_abs(i)*(C0-
Cmatrix(time_count-1,zzz)))*depint;
end
end

%---Sums the product of Gamma Intensity for each wavelength
%-----and then sums for use in the Concentration equation
for za = 1:lw
SumIandG = 0;
for l = 1:lw
N = Itot(time_count,za,l)*G(l);
SumIandG = N + SumIandG;
end
Cmatrix(time_count,za) = Cmatrix(time_count-1,za)-
SumIandG*Cmatrix(time_count-1,za)*timeint;
end
end

%---compress data-----
cwd = pwd;

```

```

        cd(tempdir);
        pack
        cd(cwd)

%-----Overall Rate Computation-----
for ttt = 1:lt
    for ddd = 1:lz
        SUMr = 0;
        for lll = 1:lw
            N = Itot(ttt,ddd,lll)*G(lll);
            SUMr = N + SUMr; % summation over total wavelengths
        end
        Rate_ovr(ttt,ddd) = frgmnt*Cmatrix(ttt,ddd)*SUMr; % rate
equation
    end
end

%-----Total Intensity with respect to depth and time-----
-----
totIntensity = sum(I0(:));
for t = 1:lt
    for z = 1:lz
        sumItot(t,z) = sum(Itot(t,z,1:lw));
    end
end
%-----file output-----
z = 0:depint:depth;
clear Itot; % done to reduce memory stress on computer

```


REFERENCES

1. Fouassier, J.P.; Allonas, X.; Burget, D. Photopolymerization reactions under visible light: principles, mechanisms and examples of applications. *Progress in Organic Coatings* 2003, 47, 16-36.
2. Cook, D. Kinetics and Properties of Photopolymerized Dimethacrylate Oligomer. *Journal of Applied Polymer Science* 1991, 42, 2209-2222.
3. Burdick, JA, Philpott, LM, and Anseth, KS, Synthesis and characterization of tetrafunctional lactic acid oligomers: A potential in situ forming degradable orthopaedic biomaterial. *Journal of Polymer Science Part A: Polymer Chemistry* 39:683–692 (2001).
4. Kim, BS, Hrkach, JS, and Langer, R, Synthesis and characterization of novel degradable photocrosslinked poly(ether-anhydride) networks. *Journal of Polymer Science Part A: Polymer Chemistry* 38:1277–1282 (2000).
5. Muh, E, Stieger, M, Klee, JE, Frey, H, and Mulhaupt, R, Organic-inorganic hybrid networks by the sol-gel process and subsequent photopolymerization. *Journal of Polymer Science Part A: Polymer Chemistry* 39:4274–4282 (2001).
6. Narayanan, V, and Scranton, AB, Photopolymerization of composites. *Trends in Polymer Science* 5:415–419 (1997).
7. Decker, C, The use of UV irradiation in polymerization. *Polym Int* 45:133-141 (1998).
8. Kaur, M, and Srivastava, AK, Photopolymerization: A review. *J Macromol Sci, Polym Rev* C42:481-512 (2002).
9. Baikerikar, KK, and Scranton, AB, Photopolymerizable liquid encapsulants for microelectronic devices. *Polymer* 42: 431–441 (2001).
10. Baikerikar, KK, and Scranton, AB, Photopolymerizable liquid encapsulants for microelectronic devices: Thermal and mechanical properties of systems with reduced in-mold cure times. *Journal of Applied Polymer Science* 81:3449–3461 (2001).
11. Coons, LS, Rangarajan, B, Godshall, D, and Scranton, AB, Photopolymerizations of vinyl ester: Glass fiber composites. *Photopolymerization ACS Symposium Series* 673:203–218 (1997).
12. Crivello, JV, and Dietliker, K. *Photoinitiators for Free Radical and Cationic Photopolymerisation*. Wiley: New York, 1998.

13. Fouassier, JP. Photoinitiation Photopolymerization and Photocuring. Hanser: Cincinnati, OH, 1995.
14. Crivello, JV, and Sangermano, M, Visible and long-wavelength photoinitiated cationic polymerization. *Journal of Polymer Science Part A: Polymer Chemistry* 39:343–356 (2001).
15. Terrones, G.; Pearlstein A.J. Effects of Optical Attenuation and Consumption of a Photobleaching Initiator on Local Initiation Rates in Photopolymerizations. *Macromolecules* 2001, 34, 3195-3204.
16. Ivanov, V.; Decker, C. Kinetic Study of Photoinitiated Frontal Polymerization. *Polymer International* 2001, 50, 113-118.
17. Miller, G.A.; Gou, L.; Narayanan, V; Scranton, A.B. Modeling of Photobleaching for the Photoinitiation of Thick Polymerization Systems. *Journal of Polymer Science* 2002, 40, 793-808.
18. Goodner, M.D.; Bowman, C.N. Development of a comprehensive free radical photopolymerization model incorporating heat and mass transfer effects in thick films. *Chemical Engineering Science* 2002, 57, 887-900.
19. Terrones, G.; Pearlstein, A.J. Effects of Kinetics and Optical Attenuation on the Completeness, Uniformity, and Dynamics of Monomer Conversion in Free-Radical Photopolymerization. *Macromolecules* 2001, 34, 8894-8906.
20. Terrones, G.; Pearlstein, A.J. Nonuniformity of Chain-Length Distributions in Photopolymerized Layers. *Macromolecules* 2003, 36, 6346-6358.
21. Cramer, N.B.; Davies, T.; O'Brien A.K.; Bowman, C.N. Mechanism and Modeling of a Thiol-Ene Photopolymerization. *Macromolecules* 2003, 36, 4631-4636
22. Cramer, N.B.; Reddy, S.K.; O'Brien, A.K.; Bowman, C.N. Thiol-Ene Photopolymerization Mechanism and Rate Limiting Step Changes for Various Vinyl Functional Group Chemistries. *Macromolecules* 2003, 36, 7964-7969.
23. Lovestead, T.M.; O'Brien, A.K.; Bowman, C.N. Models of Multivinyl Free Radical Photopolymerization Kinetics. *Journal of Photochemistry and Photobiology A: Chemistry* 2003, 159, 135-143.
24. Scranton, A. B.; Sipani, V.; Jain, K.; and El-Maazawi, M. Photopolymerization of Thick Polymer Systems. 30th Annual International Waterborne, High-Solids, and Powder Coatings Symposium 2003.
25. Cramer, NB, and Bowman, CN, Kinetics of thiol-ene and thiol-acrylate photopolymerizations with real-time Fourier transform infrared. *Journal of Polymer Science Part A: Polymer Chemistry* 39:3311–3319 (2001).

26. Padon, KS, and Scranton, AB, A mechanistic investigation of the three-component radical photoinitiator system eosin Y spirit soluble, N-methyldiethanolamine, and diphenyliodonium chloride. *Journal of Polymer Science Part A: Polymer Chemistry* 39:715–723 (2001).
27. Padon, KS, and Scranton, AB, The effect of oxygen on the three-component radical photoinitiator system: Methylene blue, N-methyldiethanolamine, and diphenyliodonium chloride. *Journal of Polymer Science Part A: Polymer Chemistry* 38:3336–3346 (2000).
28. Stephenson, N, Kriks, D, El-Maazawi, M, and Scranton, A, Spatial and temporal evolution of the photo initiation rate for thick polymer systems illuminated on both sides. *Polym Int* 54: 1429-1439 (2005).
29. Stephenson Kenning, N, Kriks, D, El-Maazawi, M, and Scranton, A, Spatial and temporal evolution of the photo initiation rate for thick polymer systems illuminated with polychromatic light. *Polym Int*, Accepted January 2006.
30. Odian, G, *Principles of Polymerization*, 2nd edition, Wiley, New York (1981).
31. Perry, MF, and Young, GW, A mathematical model for photopolymerization from a stationary laser light source. *Macromol Theory Simul* 14:26-39 (2005).